Development and Application of Light Sources for Biomedical Use

Thorhauge, Morten; Buchhave, Preben; Tidemand-Lichtenberg, Peter

Publication date:
2007

Document Version
Publisher's PDF, also known as Version of record

Ph.D. thesis:

Development and Application of Light Sources for Biomedical Use

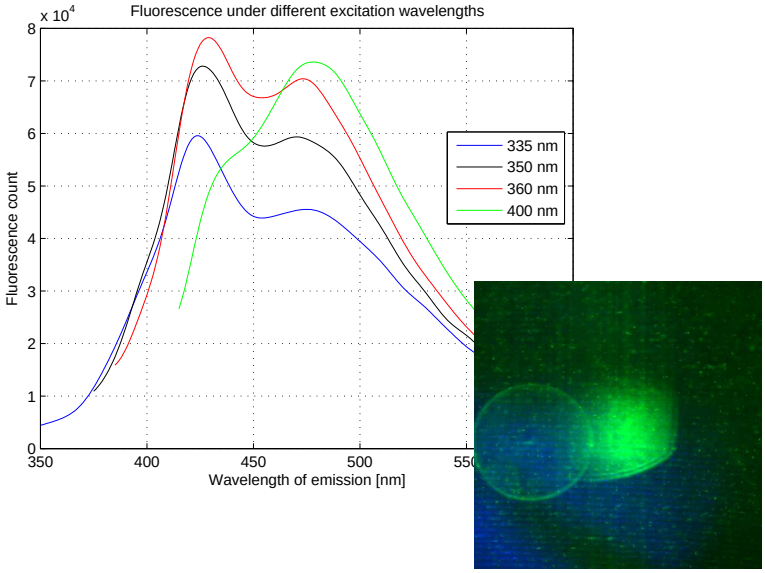

by

Morten Thorhauge, *M.Sc.*

Supervisors:

Peter Tidemand-Lichtenberg, FYS, DTU

Michael Larsen, Herlev Hospital

Preben Buchhave, FYS, DTU

Optics Group

Department of Physics

Technical University of Denmark

Fysik INSTITUT FOR FYSIK

DTU

Typeset in LaTeX 2_ε

Preface

This thesis is a partial fulfillment of the requirement for obtaining the Ph.D. degree at the Technical University of Denmark (DTU). The work has been carried out at the Department of Physics, FYS, DTU. My project started on the 1st of January 2003 and ended on the 1st of January 2006.

This report would not have been, had it not been for the assistance, help, involvement, support, motivation, and interest from several people. I would like to thank all of them. First of all my supervisors; Peter Tidemand-Lichtenberg, FYS, DTU, for always having the time for a talk, and allowing and encouraging me to plan my own time and investigations to a large extend; Professor Preben Buchhave, FYS, DTU, for being a competent and supportive head of the Optics Group; and Michael Larsen, Department of Ophthalmology, Herlev Hospital, for introducing me to eyes, cataract, and lasers in ophthalmology. Also, I would like to mention my co-student Jesper Liltorp Mortensen, FYS, to whom I am grateful for his practical and theoretical help and advices regarding my research; Line Kessel, Herlev Hospital, for answering questions regarding ophthalmology; Doktorand Linus Ryderfors and Professor Emad Mukhtar, Department of Physical Chemistry, University of Uppsala, Sweden, for giving me access to their laboratory, time, and support during my three week-long trips to their department; and finally our technician Søren Hjort, our laboratory assistant Line Groth-Andersen, the rest of my group, my family and friends + whoever I have forgotten for moral and general support.

Morten Thorhauge
Kgs. Lyngby
7th of November, 2006

Abstract

This report has its background in work performed at Herlev Hospital, under the guidance of Dr.Med. Michael Larsen. For some time research has been performed at this facility in the area of non-invasive cataract treatment. The proposed novel treatment consists of bleaching by light the chromophores causing cataract. During this research it has been found that the chromophores may readily be bleached by light in the UV part of the electromagnetic spectrum. However it is not practical to use UV light in a clinical treatment of cataract due to both the phototoxicity of UV light as well as the high absorbance of light in the outer layers of the eye in this wavelength region. Therefore it was suggested that a two-photon process could cause similar bleaching in the lens without the problems associated with UV light.

This report describes the results of work in the possibility of TPE bleaching of the chromophores causing cataract in the lens of the eye. It is the first step towards proof-of-concept for this treatment scheme. To establish proof-of-concept it was necessary to look into bleaching of chromophores of a kind similar to those in cataractous lenses. First it was necessary to develop a UV laser having a wavelength approximately half of what a TPE bleaching scheme would use. Then this laser was applied on a cataract assay. The data from these UV bleaching experiments were then analysed to establish an approximate bleaching rate for a TPE bleaching scheme. This report presents results from the steps mentioned above.

Two main topics are treated in this work. One, generation of blue-to-UVA light through frequency doubling of a Ti:Sapphire laser, as well as investigation, and two, bleaching of a potential candidate for an assay for cataract.

A CW frequency doubled Ti:Sapphire laser system was investigated as a UVA light source . The relative new material BiBO was investigated as nonlinear medium. Tools needed for a mathematical investigation of the utilised laser designs were derived. Subsequently, Ti:Sapphire lasers were set up and investigated in the laboratory. Finally the frequency doubled laser was developed. Several good results were obtained. 53 mW of light at 392 nm and 100 mW of light at 405 nm were generated, which to the best of my knowledge is a new record for a intracavity doubled CW Ti:Sapphire laser utilising BiBO as the nonlinear medium. In addition broad tunability – 8 nm FWHM centred around 392 nm – and low temperature dependence were shown.

Development of cataract is a very slow process, and therefore fully developed cataract is only found in humans and animals with comparable lifetime. It is thus not possible to use easily available animal lenses – such as from slaughtered pigs or cattle – for studies on cataract. It is possible to acquire cataractous lenses from diseased humans, but this is not only very expensive but also ethically problematic. And finally there are so many types of cataract and factors involved in the formation of the condition, that for study purposes it is easier and more predictable to work with a model system – a cataract assay. A potential candidate for a model system for cataract was developed and investigated. Glycated lysine was chosen as model molecule. It was shown that this molecule exhibits several of the spectral and fluorescence characteristics found for cataractous lenses. TPE fluorescence was found to have same spectral characteristics as SPE fluorescence. Bleaching of the assay was investigated utilising

the developed UVA light source. Quantum efficiency for the bleaching was calculated using a numerical method. The quantum efficiency for bleaching was measured to be $2.70 \cdot 10^{-3}$ at 392 nm, and $2.51 \cdot 10^{-3}$ at 405 nm. Based on the values found a theoretical estimate for TPE bleaching of cataractous lenses in-vivo was calculated. This showed that the proposed bleaching of cataractous lenses by a two-photon process is not practical in a clinical implementation.

During the work on this project several novel results were achieved, partly in the area of laser technology, partly in the area of bleaching of human-like chromophores. Some of these results were published, while some – in the area of bleaching – were not. The latter due to a need to keep the found data non-disclosed for later, possible patenting opportunities.

Dansk sammendrag

Denne rapport er udarbejdet som en del af kravet for at opnå Ph.D. graden ved Institut for Fysik, Danmarks Tekniske Universitet.

To hovedemner er blevet gennemgået i projektets løb, generering af blåt-til-UVA lys ved en frekvensfordobling af en infrarød laser, samt undersøgelse og blegning af et potentielt assay for grå stær.

Som UVA lyskilde blev valgt en frekvensfordoblet Ti:Safir laser. For det ikke-lineære medie blev det besluttet at prøve det forholdsvist nye krystalmateriale BiBO. Først blev de nødvendige matematiske værktøjer til beregning på laseren udledt. Dernæst blev Ti:Safir lasere afprøvet i laboratoriet. Endelig blev den frekvensfordoblede laser udviklet. Flere gode resultater blev opnået med denne, og arbejdet resulterede i et antal publikationer. 100 mW blåt lys ved 405 nm og 53 mW ved 392 nm blev målt, og det er til mit bedste kendskab ny rekord for en CW intrakavitet-frekvensfordoblet Ti:Safir laser med BiBO som det ikke-lineære mediet. Herudover blev det vist, at temperaturafhængigheden for den valgte implementation er lav, mens tunbarheden af det genererede lys er god – 8 nm FWHM omkring 392 nm.

Et assay til brug for undersøgelse af potentiel mulighed for blegning af grå stær blev udviklet. Det blev valgt at benytte glykeret lysin som assay. Assayet blev undersøgt grundigt, og det blev vist at det besidder flere af de egenskaber vedrørende absorbtion-, emission-, og ekscitationsspektre som også findes for humane linser med grå stær. Det blev vist, at en og to-foton eksciteret fluorescens udviser samme karakteristika. Blegning af assayet blev undersøgt ved anvendelse af den udviklede UVA kilde. Kvanteeffektiviteter for blegning blev udledt ved en numerisk metode, og fundet til at være $2.70 \cdot 10^{-3}$ for blegning ved 392 nm, og $2.51 \cdot 10^{-3}$ ved 405 nm. Endelig blev opnåede resultater benyttet til et teoretisk overslag over muligheden for at blege grå stær in-vivo ved hjælp af to-foton eksciteret blegning. Det blev fundet, at den foreslåede behandlingsmetode sandsynligvis vil være for langsom til, at det kan anvendes i klinisk praksis.

Acronyms and symbols

Acronyms

AFM	Atomic force microscopy
BRF	Birefringent filter
CW	Continuous wave
FWHM	Full width at half maximum
LSM	Laser scanning microscope
NIR	Near infra-red
NUV	Near ultra-violet
RPE	Retinal pigment epithelium
SHG	Second harmonic generation
SPE	Single-photon excitation
TCSPC	Time correlated single photon counting
TPE	Two-photon excitation
UV	Ultra-violet
UVA	UV range A (315-400 nm)

Symbols

c	Speed of light – $2.99792458 \cdot 10^8\ m \cdot s^{-1}$
C	Temperature – degrees Celsius
h	Planck's constant – $6.626068 \cdot 10^{-34}\ m^2 \cdot kg \cdot s^{-1}$
I	Flux or photons per second – $s^{-1} \cdot cm^{-2}$ or s^{-1}
I_0	Initial flux or photons per second – $s^{-1} \cdot cm^{-2}$ or s^{-1}
l	Path length in cuvette (in general, path length) – cm
M	Molarity – $mol \cdot litre^{-1}$
n	Concentration – measured in cm^{-3} or $mol \cdot litre^{-1}$
W_{mol}	Size of molecular orbital – m
ζ	Quantum efficiency for bleaching
σ_{2P}	Two-photon absorption cross section – $m^4 s$
σ_{abs}	Absorption cross section – cm^2
σ_{mol}	Molar absorbtivity – $mM^{-1} \cdot cm^{-1}$
σ_{SPA}	Single photon absorption cross section – m^2
$\sigma_{SPA\,max}$	Single photon absorption cross section at band-edge – m^2
$\sigma_{transitional}$	Transitional cross section in cascaded TPE absorption – m^2

Contents

1 Introduction 1

I Lasers for studies of bleaching 7

2 Laser basics 9
2.1 Selection of laser system 10
2.1.1 Selecting laser type for bleaching experiments 11
2.1.2 Other blue laser light sources 11
2.2 Simple Ti:Sapphire laser 12
2.2.1 Matrix laser theory 12
2.2.2 Ti:Sapphire laser 12
2.2.3 Measurements on the simple Ti:Sapphire laser 15
2.3 Summary on the simple Ti:Sapphire laser 16

3 BiBO for SHG 19
3.1 Introduction 19
3.2 Set-up 21
3.2.1 Acceptance parameters 22
3.3 Results 23
3.3.1 392 nm BiBO 24
3.3.2 404 nm BiBO 28
3.3.3 Comparison of 392 nm and 405 nm generation 31
3.4 Blue output spot 32
3.5 Coating problems 33
3.6 Summary of results obtained for BiBO for UV-SHG 36

II Bleaching 39

4 Eyes, lenses and cataract 41
4.1 Formation of cataract 41
4.2 The human eye 42
4.2.1 The lens of the human eye 43
4.3 Pigs eye 44
4.3.1 TPE fluorescence images of lens tissue 44
4.4 Summary: Eyes 45

5 Investigation of model **49**
5.1 Selection of model 50
5.1.1 Maillard reaction 50
5.2 Evaluation of glycated lysine compounds 51
5.2.1 Preparing the mixtures 51
5.2.2 Test for pH dependence 52
5.2.3 Temperature dependence 52
5.2.4 Incubation time 53
5.2.5 Influence of non-reacted glucose and lysine 54
5.2.6 Selecting the model system incubation parameters 54
5.3 Test for rest sugar content 55
5.3.1 Filter factor 57
5.3.2 Setting the scale and results 57
5.4 Incubation of glucose 59
5.5 Calculation of chromophore cross section 60
5.6 Glycated lysine measurements 63
5.6.1 Sample preparation 63
5.6.2 Fluorescence spectra 64
5.7 TPE 66
5.7.1 TPE fluorescence spectra 68
5.8 TCSPC measurements on glycated lysine 69
5.9 Summary on model system 70

6 Bleaching by UVA **73**
6.1 Bleach Bleach Bleach! 73
6.1.1 Measurement set-up 74
6.1.2 Sample preparation for bleaching 74
6.1.3 Cuvette loss 75
6.1.4 Calculation of bleaching quantum efficiency 76
6.1.5 Bleaching results 77
6.1.6 Fluorescence spectra after bleaching 82
6.1.7 Bleaching of pure glucose at 392 nm 83
6.2 Bleaching on human eyes 84
6.3 Summary on bleaching 84

7 Bleaching – two-photon **87**
7.1 TPE 88
7.1.1 Two photon absorption cross section 88
7.1.2 Evaluating the TPE cross section 89
7.2 Photobleaching in the eye – an estimate 90
7.2.1 Photo-bleaching by TPE 94
7.3 Summary on TPE bleaching 95

8 Conclusion **99**
8.0.1 Future work 100
8.1 Final remarks and comments 101

A Matrices **103**
A.0.1 Oblique incidence on mirrors 103
A.1 The oblique slab 104
A.1.1 Diffraction at slab interface – Huygens construction . . . 104
A.1.2 Out of the slab 107
A.1.3 Travelling through the slab 107
A.1.4 The slab – ABCD-matrix, horizontal 108
A.1.5 Lensing in the crystal 109

B Theoretical SHG estimates **113**
B.1 Theoretical model for SHG 113
B.2 Theoretical results for SHG 114

C Eye pictures and lens scans **117**

D Preparation of glycated lysine **119**

E Gels and browned porcine collagen **121**
E.1 Browned porcine collagen "Husblas" 121
E.1.1 Preparation of samples and results 121
E.1.2 Summary on browned porcine gel 122
E.2 Gelling of samples 122

F Code **125**

G Articles and conference submissions **127**

List of Figures

2.1 Energy band structure in Ti:Sapphire 13
2.2 Fluorescence from Ti:Sapphire laser crystal 14
2.3 Cavity design for a simple Ti:Sapphire laser 14
2.4 Power-slope measurement of Ti:Sapphire laser 15
2.5 Tunability of a Ti:Sapphire cavity 16
2.6 Line widths of a Ti:Sapphire laser 16

3.1 Laser cavity for experiments with BiBO crystal 21
3.2 Beam waist size in resonator 22
3.3 Angle sensitivity in ϕ-plane of BiBO crystal 23
3.4 Angle sensitivity in θ-plane of BiBO crystal 23
3.5 Sensitivity to wavelength for BiBO crystal 23
3.6 Temperature dependence of SHG 25
3.7 Temperature dependence of SHG – conversion efficiency 25
3.8 Slope efficiency of SHG 26
3.9 Wavelength tunability of blue light 26
3.10 IR intracavity spectrum 27
3.11 Blue output spectrum 27
3.12 Stability of blue output 28
3.13 Temperature dependence of SHG 29
3.14 Temperature dependence of SHG – conversion efficiency 29
3.15 Temperature dependence of SHG 29
3.16 Temperature dependence of SHG – conversion efficiency 29
3.17 Sensitivity to wavelength for BiBO crystal 30
3.18 Stability of blue output 31
3.19 Image of facet on BiBO crystal showing damages 34
3.20 Image of facet on BiBO crystal showing damages 34
3.21 Image of facet on BiBO crystal showing damages 34
3.22 Image of facet on BiBO crystal showing damages 34
3.23 AFM height plots of damages on BiBO crystal 35
3.24 3D AFM image of damages on BiBO crystal 36

4.1 A cut-through sketch of the eye 42
4.2 A sketch of the lens of the eye 43
4.3 Pictures of a dissected porcine eye 45
4.4 Lens from porcine eye 46
4.5 Y-sutur lines in lens 46
4.6 Fluorescence images of porcine lens 46

5.1 Comparing different glycated lysine mixtures 52
5.2 Comparing different temperatures for incubation 53
5.3 Wavelength dependence of different incubation temperatures . . 54
5.4 Transmission curves for glycated lysine 55
5.5 Transmission through pure glucose and lysine 55
5.6 Transmission of 48 hours incubated 0.1M glucose samples 60
5.7 Plot of absorption cross sections 62
5.8 0.2 M sample and 0.1 M sample comparison 64
5.9 SPE fluorescence emission spectra of glycated lysine 65
5.10 SPE fluorescence spectra of glycated lysine 66
5.11 Emission spectra of cataractous lens 66
5.12 Excitation spectra of cataractous lens 66
5.13 SPE and TPE in Jabłoński diagram 67
5.14 SPE and TPE fluorescence of glycated lysine 68
5.15 TCSPC on glycated lysine 69

6.1 Set-up for bleaching 74
6.2 Glycated lysine sample bleached at 392 nm 79
6.3 Sample bleached 2 hours with 405 nm light 80
6.4 Wavelength dependent change in transmission 81
6.5 Fluorescence spectra under 392 nm excitation 82
6.6 0.1 M pure glucose incubated 72 hours 83

A.1 Beam incident on oblique slab 105
A.2 Different lengths in a slab 107

C.1 Additional pictures of a dissected pigs eye 117
C.2 Images of lens fibres 118
C.3 Images of the lens epithelium 118

E.1 Glucated porcine collagen gel 122
E.2 SPE bleached line in gellified sample 123

List of Tables

2.1 Useable laser crystals 11
2.2 Comparison of laser crystals 13
2.3 Thresholds and efficiencies for different OCs 15

3.1 Coefficients for some nonlinear crystals 20
3.2 Properties of the crystals 21
3.3 Ellipticity of red and blue output spots 32

5.1 Glucose Lysine test batches 51
5.2 Glucose gauge measurements 57
5.3 Filter factors for glycated lysine 57
5.4 Comparison of rest glucose concentrations 58
5.5 Incubated pure glucose 59
5.6 Cross sections for interesting wavelengths 62
5.7 Transmission coefficients for glycated lysine samples 62
5.8 Cross section comparison 64

6.1 Transmission values for cuvettes 75
6.2 Data for the second 392 nm bleaching 79
6.3 Quantum efficiencies for bleaching 80

7.1 Two-photon cross sections at 785 nm and 810 nm 90

B.1 Theoretical SHG results 114

Chapter 1

Introduction

> Doth not wisdom cry?
> and understanding put forth her voice?
>
> Proverbs 8. 1.

One of the most blinding eye diseases – or conditions – worldwide is cataract. According to WHO it is the most blinding condition in all but the most developed countries, being responsible for 47.8% of all cases of total blindness on a world wide basis[1]. In addition, it is a condition, on which large sums annually are spent on treatment procedures. In the US more than 3.8 billion USD is spent every year on cataract treatment[1]. Thus the drive for developing novel, faster, cheaper treatments is enforced both from a medical and a financial point of view.

Cataract is an opacity in the crystalline lens of the eye, or an opacity in the envelope of the lens. The name is derived from the Latin word for waterfall – *cataracta*[2]. Factors such as overexposure to ionising radiation, smoking, diabetes and physical injuries to the eye may cause or be a prohibitor for the development of cataract, but usually cataract is simply age related. The opacity is caused by a breakdown of proteins in the lens or envelope. However, the mechanism – or mechanisms – behind are still relatively uncertain. Cataract treatment has to date been intra-ocular surgery; dating back to the roman age a technique known as couching was used, in which a thin, sharp item was used to scratch away the opaque parts. Later treatments removed the entire lens, but leaving most of the lens envelope still in place to avoid the vitreous body falling into the front of the eye. Today the normal procedure is to "chew" the lens to bits using an ultra-sonic probe and then suck out the liquified lens using a combination of water injection and suction. This technique is called phacoemulsification, and is the least invasive of the known treatments – "only" needing a few holes to be punctured in the eye. It is commonplace to install a plastic lens in place of the removed lens, so the patient may see normally without glasses – albeit only with a fixed focus.

Invasive procedures are both painful and potentially dangerous – as all invasive surgery. Therefore it would be ideal if a cheap, non-invasive treatment

[1] http://www.v2020.org/news/documents/FactsheetBlindness-101204.pdf
[2] Cataract, Wikipedia – www.wikipedia.org

could be developed. A novel drug would be a comfortable choice, but unfortunately the metabolism of the lens is extremely slow, meaning the infusion of a drug into the lens would be very inefficient. Another kind of treatment could be based on the transparency of the eye to light in the visual or Near-IR range, utilising light in this wavelength range to non-invasively reach the cataractous parts.

The project

The project, of which this report is a part of, is based on utilising light to bleach the chromophores often found in cataractous lenses. Bleaching of chromophores by UV light is commonly known, and is usually considered a problem – such as in paints and inks for pressed or printed materials or clothing, or the bleaching of laser dyes in dye laser systems. However, it may be utilised in the treatment of cataract. Unfortunately, UV light is not usable in clinical treatments due to its inherent photo-toxicity and poor penetration in tissue. Thus it was suggested to utilise a two-photon process using NIR or IR light instead.

Two-photon processes are processes where two photons interact with the medium literally at the same time. The combined effect of the two photons are then similar to the effect of a single photon of twice the energy. It is a statistical process – it is proportional to the square of the flux, and to get any noticeable two-photon effects a very high flux rate is needed. This calls for the use of femtosecond lasers, which may deliver very short pulses with a high peak power. In addition, due to the required high density of photons two-photon effects on take place in the focal volume of the laser beam. This may be utilised to make 3D confinement of the reaction. When the two-photon effect is used to excite a molecule or atom the process is called TPE.

To be able to use a TPE scheme it is first and foremost necessary to investigate the speed and efficiency of the bleaching – if it is high enough to allow efficient bleaching in clinically acceptable time spans. In addition it is necessary to check for adversary effects from the bleaching, which could – if hazardous – render the scheme unacceptable.

In this work the focus was on estimating the possible speed of the bleaching. Utilising data found for the cross section for single photon bleaching of "cataract-like" chromophores, the TPE bleaching was estimated semi-empirically. The estimated bleaching speed is an important step in the process towards a proof-of-concept experiment. Or rather, it is an important aspect to take into consideration, when the feasibility of the TPE bleaching scheme is evaluated.

The report

The aim of the work described in this thesis was to do initial research regarding the feasibility of utilising ultra-short pulses for bleaching of cataract in the lens of the human eye through a process known as TPE. The initial research presented deals with finding a useable assay – a model system – for cataract, and study the bleaching of this by a SPE process. The applicability of using TPE bleaching for clinical treatment of cataract is discussed based on the obtained results.

It is to be said that the report focuses as much on the development of the light source for the initial measurements of bleaching speed, as on finding a useable assay. Thus there is no laser physics in the report for the sake of laser

physics, nor is there any chemistry for the sake of chemistry itself. It is – in short – a work of applied science.

- To obtain the fluency and wavelengths needed for a careful study of the wavelength dependence of bleaching, a frequency doubled laser source is needed. This device provides high-power light in the NUV region where bleaching may take place. In chapter 2 the selection of a suitable laser system for doubling is discussed, and results for a simple Ti:Sapphire system presented. In addition in the appendix chapter A various matrices not commonly found in the literature, but necessary for calculations on the laser system, are derived and presented.

- SHG is a process, through which it is possible to reach the wavelengths needed for bleaching. Although NUV lasers do exist, they are in general based on excited gas as the laser medium, and do not have the advantages of the solid-state lasers. The latter type is characterised by high efficiency, compact design and stable operation. A Ti:Sapphire based laser design was chosen, as this is an interesting laser giving a broad tuning range in the near infra-red region. It allows for reaching NUV to UV wavelengths through SHG. Description of research and results from investigations of a novel nonlinear crystal for SHG generation of the Ti:Sapphire laser emission is presented in chapter 3.

- Cataract and the human eye are briefly dealt with in chapter 4.

- For the initial research on bleaching of cataract a model system is needed. A process known as non-enzymatic browning is suspected to be one of the causes for cataract formation, and thus a model based on this reaction may give some of the characteristics of cataract. As a possible model glucose incubated with lysine is investigated in chapter 5.

- Bleaching of cataract in the eye can unfortunately not be done with NUV light, as the absorption in the outer layers of the eye is high. In addition light in this wavelength range may induce cellular damages. The TPE process gives the same response as SPE, but at twice the wavelength. Thus for basic research on bleaching of the model chromophores, NUV light in a SPE process may be utilised. Bleaching of the model chromophores by such a process is studied in chapter 6.

- The results from investigations on the model system may be used to give an idea of the useability of TPE bleaching of cataract in the human eye. This is discussed in chapter 7.

The next logical step after the initial investigations would be to advance to TPE bleaching. This was tried on a small scale in the course of this research project, but a full scale investigation was not initiated – in particular due to equipment costs and the time available. However, the presented research should give a good indication of the possibility of utilising TPE bleaching for treatment of cataract.

Bibliography

[1] *Vision Problems in the U.S.* (Prevent Blindness America, 2002)

Part I

Lasers for studies of bleaching

Chapter 2

Laser basics

> A child of five would understand this. Send someone to fetch a child of five.
>
> (Julius Henry) Groucho Marx.
> *American comedian (1890-1977)*

To obtain the desired data on bleaching of chromophores it was necessary to build a custom laser system, capable of generating light in the blue-to-UVA region of the spectrum. Hence the first task was to decide on what kind of system would be most suitable for the job. In this chapter I will go through some possible ways of generating monochromatic (laser) light in the required wavelength range, together with a discussion of advantages and disadvantages – leading to the selection of the system. In addition to the discussion on laser systems in the present chapter, a derivation and presentation of several much-needed matrices for laser components is included in the Appendix A. Most of the laser theory applied in my project is known material and may be found in the literature – recommended source for this is reference [7]. Commonly known material will not be dealt with in this report. However, during the project it was found that some areas were not sufficiently described in the literature, such as ABCD-matrices. ABCD-matrices are well-known, but, as it sometimes happens, the matrices you really need, prove impossible to find anywhere. In particular the matrices for oblique incidence on mirrors and slabs, as well as crystals with lensing. The chapter is structured in the following way:

- For selecting the laser system to be used in the bleaching experiments a number of expected requirements for a final (clinically applicable) system were set up. From these the laser system to be used in this project was decided upon. Discussion of this selection is found in section 2.1.
- The initial foray into the Ti:Sapphire laser territory was made on a simple design to investigate its basic behaviour, operational parameters, and what could be expected in terms of stability, line-width and power delivery. And – perhaps most importantly – to gain knowledge and skills for setting up such a system. All this presented on page 12 and following pages – in section 2.2.
- Summary is presented in section 2.3 on page 16.

2.1 Selection of laser system

The selection of the particular laser system for the bleaching experiments was based on the expected final characteristics of a potential clinical system for bleaching of cataract. A number of expected requirements may be set up for the specifications of the final, clinically applicable laser system:

- Transparency of the eye. Transparency of the eye is strongly connected to transparency of water. Between the lens and the outside comes first a thin tissue layer (the cornea), which is transparent to visible and near infra-red light. Between the cornea and the lens is a fluid filled chamber (the anterior chamber), basically with transmission properties like water. Water has an absorption coefficient of less than 0.1 cm^{-1} in the range 200 to 1000 nm, with a minimum around 400 nm[1].

- Bleaching wavelength. In order to get an effective bleaching of the chromophores, the "effective" bleaching wavelength should lie in the UVA to near-UV (deep blue) wavelength region. However, due to the high absorption of UV light in the cornea and the photo-toxicity of light in the UV region, it is preferable to utilise a TPE scheme with fundamental light of twice the wavelength. In addition TPE gives a 3-dimensional confinement of interaction, as this only takes place in the focal volume of the laser beam.

- Selection of fundamental wavelength. In order to get an effective bleaching the fundamental light should thus lie in the near-IR region – around 700-800 nm. Light in this wavelength range has the additional advantages of low scattering in tissue – giving larger penetration depth in a scattering lens environment, and a low possibility of photo-induced damages to the retina (not taking thermal damages into consideration).

- Candidates for laser system for clinical use. As the bleaching is to utilise a TPE-effect, the required laser system must be able to produce pulses in the femtosecond range. Longer pulses will also lead to two-photon effects, but the efficiency of the process scales roughly inversely with the pulse length squared. The selection of gain materials having sufficient bandwidth to produce femtosecond pulses in the near-IR region are practically limited to Ti:Sapphire, and the chromium doped colquiriite crystal -LiSGaF, and -LiCAF. A possible alternative is the chromium doped alexandrite crystal.

The possible crystal gain materials are shown in table 2.1.

Of the gain materials only Ti:Sapphire based lasers are widely commercially available in mode-locked configurations. Alexandrite is widely used in Q-switched lasers, but few sources have reported on mode-locked configurations; in [2] the authors achieve only 7 mW average power and 35 ps pulses without compensation for dispersion – with a centre wavelength of 750 nm. Very little research seems to have been performed on mode-locked Alexandrite systems. To the best of my knowledge no Alexandrite based mode-locked laser systems have to date been marketed.

[1] http://www.lsbu.ac.uk/water/vibrat.html

Crystal	λ_{center}	Pump source
Ti:Sapphire	795 nm	Laser, 500-550 nm
Cr:LiCAF	763 nm	Laser diode, 635-660 nm
Alexandrite	755 nm	Laser diode, 680 nm

Table 2.1: *Comparison of commercially available gain materials capable of generating femtosecond laser pulses in the 700-800 nm wavelength range. Data from [10] for Ti:Sapphire, [4] for Cr:LiCAF, and [5, 6] for Alexandrite.*

The chromium doped colquiriite family is mostly known for Cr:LiSAF, which unfortunately has a emission wavelength span centred around 825 nm [3] – slightly too long for efficient TPE bleaching. Of the two remaining colquiriite hosts Cr:LiSGaF has an emission maximum around 835 nm[4], which leaves us only with Cr:LiCAF as a useable gain material. However, commercially available mode-locked laser systems based on Cr:LiCAF have to the best of my knowledge yet to be seen. In this respect it makes sense to assume the currently best suited system for a clinically applicable system would be based on a Ti:Sapphire laser oscillator, of which there are many commercial systems on the market to choose from.

2.1.1 Selecting laser type for bleaching experiments

The decision on the laser gain material to be used in the bleaching experiments was based partially on the discussion above on what type would likely be the preferred choice for a clinical system. And partially because the Ti:Sapphire material may give a broad tunability of the fundamental.

A CW laser was chosen, as this was more interesting in scientific terms – little have been published on intracavity CW lasers frequency doubled utilising the chosen nonlinear material BiBO, a discussion regarding the choice of nonlinear crystal follows in chapter 3.

Requirements for the laser

The laser for the bleaching experiments should be able to provide stable light in the blue-UV region. Preferably the output power should be in the 50-100 mW range, although on forehand nothing could be said about the required (for bleaching within reasonable time) power level. In addition the laser should be "reasonably tuneable", in order to investigate the effect of the wavelength on bleaching. The laser should be stable enough to be useable for bleaching experiments of several hours.

2.1.2 Other blue laser light sources

Other types of laser sources may provide light in the blue-to-UV region. However, in the wavelength range 375-400 nm, which is interesting with respect to a clinical system configuration utilising Ti:Sapphire as the laser source – there are only a very limited number of choices. In general the solid-state lasers only become important in the near-IR region and upwards. Second harmonic generation (SHG) of solid-state lasers, besides the types mentioned previously,

generally lie from the blue-green wavelength region and upwards – the important Nd-doped laser materials can only give SHG light from around 455 nm[2] and upwards. Excimer lasers lie further down in the UV region; longest generated wavelength is found with the Xenon Fluoride excimer laser type at 351 nm. With the exception of a Krypton-ion laser line at 416 nm none of the common types of gas lasers have lines in the range in question. Finally it is possible to frequency-tripling lasers, but the most suitable types for this – the Nd-doped gain materials – don't have lines around 1200 nm. One promising type of laser near 400 nm is the diode laser, of which Gallium Nitride diodes generating tens of milliwatts around 405 nm have been demonstrated, and are commercially available (such as the Sanyo DL-LS5017 giving 60 mW at 405 nm). However this has only recently become available, and there are no alternative wavelengths available besides 405 nm currently. Thus laser diodes were not an option for this work.

2.2 Simple Ti:Sapphire laser

A simple Ti:Sapphire laser system was set up for initial investigations on frequency doubling and for the initial bleaching experiments. A CW blue laser may be built for a reasonably low budget, and it was expected that a positive outcome from the initial bleaching experiments would result in funding and opportunities for either acquiring or borrowing a commercial femtosecond laser system for further studies.

2.2.1 Matrix laser theory

The parameters selected for the cavity design of the laser system were based on ABCD-matrix calculations. Most of the matrices may be found in the literature [7, 8], but some are not found although they are needed. In the appendix chapter A I have gone through the matrices needed for the Ti:Sapphire laser – including derivations of matrices not readily found in the common literature.

In general a dedicated matrix system was not needed for calculating laser designs. This was instead done using the excellent program Intarsia [3]. In some cases, however, ad-hoc matrix systems where used when a certain parameter was needed or some plot required of a parameter depending on a variable of the system. Laser calculations of this kind were performed mainly in Matlab, a few in Fortran. Responsible for most of the Matlab programming was J.L. Mortensen, FYS, DTU.

2.2.2 Ti:Sapphire laser

Ti:Sapphire crystals are Sapphire – or Al_2O_3 – crystals where Titanium is substituting some of the Al-atoms. The Ti:Sapphire laser crystal was first used in lasers around the early eighties [9, 10, 11], and first used in mode-locked configurations a few years later – acousto-optically active mode-locked first in 1987 [12], later kerr-lens mediated self-mode-locking was discovered [13].

[2] From doubling of the 909 nm line of Nd:YLF.

[3] http://www.intarsiaoptics.dk

Crystal	λ_{Laser} [nm]	λ_{Pump} [nm]	σ_{em} [cm^2]	τ_{Fluo} [μs]
Ti:Sapphire	650-1100	400-600	$4.9 \cdot 10^{-20}$ (795 nm)	3.2
Nd:YVO_4	1064	808	$2.5 \cdot 10^{-18}$	90

Table 2.2: *Comparison of laser crystals. Data taken from references [14] (Ti:Sapphire data) and the web pages of the crystal manufacturer Foctek (Nd:YVO). For Ti:Sapphire peak absorption is around 480 nm, while peak laser emission is around 795 nm.*

The Ti:Sapphire laser crystal is attractive in that it has a broad gain spectrum, making it useable not only for making ultra short pulsed mode-locked lasers, but also making a broadly tuneable CW laser source. Another advantage is its emission spectrum lying in the important near infrared range (NIR) for microscopic and biomedical applications. Tunability is in the range 650-1100 nm. It is useable for making (tunable) UV lasers in the near UV range 350-450 nm by frequency doubling. The disadvantages are the need for pumping in the blue-green region, and the short fluorescence lifetime and small cross section for stimulated emission – see data for Ti:Al_2O_3 in table 2.2. Ti:Sapphire lasers are usually pumped by doubled Neodymium-doped (Nd:Host) solid-state laser, which are relatively expensive systems. In table 2.2 is a comparison between Ti:Sapphire, and one of the most efficient laser lines, 1064 nm from Neodymium doped Ytterbium Orthovanadate – Nd:YVO_4.

The cause for the large tunability of the Ti:Sapphire crystal is that it is a so-called 4-level vibronic laser crystal [15]. The energies of the states in this type of crystal are dependent on the conformal structure. Each band is in addition "curved", where the energy is dependent on the inter-atomic distance in the crystal (for Ti:Sapphire the bond between Titanium atoms and Oxygen atoms). In the transition from ground state to excited state a conformal change takes place, causing the lowest edge of the excited band to be shifted to a larger Ti-O atom separation than for lowest edge of the ground state energy band. This is responsible for the broad, smooth, splittet absorption and emission spectra. For a sketch of the bands in ground state and under excitation see figure 2.1.

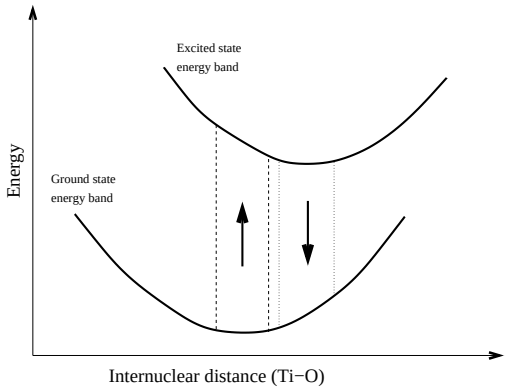

Figure 2.1: *Sketch of the band structure in Ti:Sapphire. The boxed regions indicate excitation ("up"-arrow) and emission ("down"-arrow).*

The fluorescence spectrum of Titanium-doped Sapphire is shown in figure 2.2. The fluorescence was recorded with a fibre-coupled spectrometer (Avantes

AvaSpec 2048). Peak fluorescence emission was at 725 nm. The fluorescence emission curve is not the same as the laser emission curve, which peaks around 785 nm. The reason in the difference between fluorescence and gain is mainly due to gain quenching from the self absorption at the short wavelength side. The sharp dips at 635 nm and 695 nm may be due to impurity absorption lines.

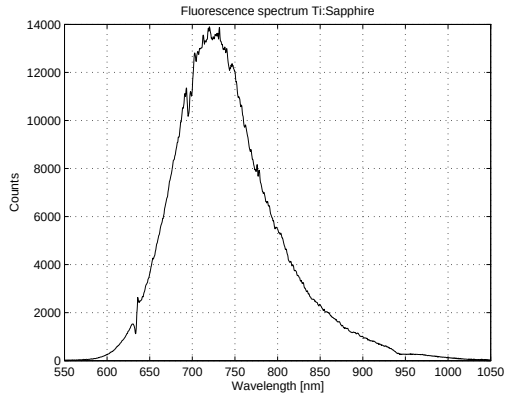

Figure 2.2: *Fluorescence from Ti:Sapphire laser crystal under pumping with 5.5 W 532 nm light. The curve is not smoothed for noise hence the spiky look at especially the peak fluorescence.*

To make initial experiments with simple Ti:Sapphire lasers a simple cavity design was made. This is shown in figure 2.3. Mirrors used were M1: highly reflecting 680–880 nm, flat; M2 and M3: highly reflecting at 680–880 nm and anti reflecting at 532 nm, both radius of curvature -100 mm; M4 was the output coupling mirror, partially reflecting at 680–880 nm with transmission coefficients of 3%, 5%, and 10%, flat. The laser crystal was a 10 mm long, 3x3 mm^2 cross section 0.15% doped and Brewster-cut Ti:Sapphire laser crystal (bought from Foctek). Pumping was by our 5.5 W CW 532 nm laser (Coherent Verdi V-5). Tuning was obtained by a Brewster-angle single plate BRF with a free spectral range of approximately 160 nm. The cavity had a beam waist inside the laser crystal of approximately 60 μm, and pumping was through a 80 mm focal length achromate lens – mounted on a xyz-axis translation stage for alignment of mode overlap between pump beam and cavity mode.

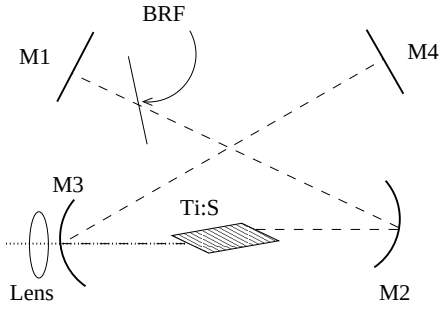

Figure 2.3: *The cavity design for the simple Ti:Sapphire laser used for the initial experimentation on Ti:Sapphire based lasers. The BRF tuning element was optional.*

Note on adjusting a Ti:Sapphire laser

Due to its short fluorescence lifetime and relative small emission cross section the Ti:Sapphire laser is not so easy to set-up and align (as an Nd:YVO laser for instance). The procedure is to use a sensitive detector(Newport Corporation

835), placed after the out-coupler M4, then carefully align all mirrors, as well as the pump focussing lens and its translation stage, to maximise fluorescence. This is best done with the pump laser turned up to full power (5.5 W in this case), and the BRF removed. After some fine tuning lasing is achieved. Then laser output is maximised by adjusting all mirrors and components again. Cooling water to the laser crystal must be turned on at all time, as the laser crystal otherwise quickly runs hot.

2.2.3 Measurements on the simple Ti:Sapphire laser

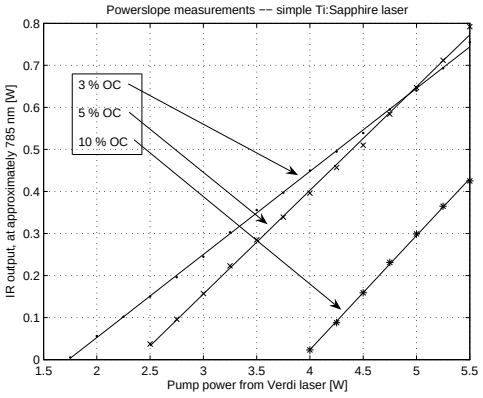

Figure 2.4: *Power-slope measurement of the simple Ti:Sapphire laser. Centre wavelength was 785 nm. Pump power is as indicated on the pump laser.*

In figure 2.4 a power-slope measurement is shown. This was recorded by adjusting the laser for maximum power at a pump power of 5.5 W. The pump was then gradually turned down 0.25 W a step and the laser output after the output-coupler M4 was recorded. Power-slopes were measured without the BRF element inserted, and the laser was running "freely" at its peak lasing wavelength of about 785 nm. This was not dependent on the output coupler used. In table 2.3 the pump-to-NIR conversion efficiencies are shown, together with thresholds for lasing, where threshold is the actual absorbed power. Single-pass pump absorption in the crystal was approximately 65%.

Output coupler	3 %	5 %	10 %
Conversion efficiency	19.76 %	24.66 %	27.14 %
Threshold – absorbed power	1.12 W	1.54 W	2.54 W

Table 2.3: *Different output couplers – thresholds and conversion efficiencies found from linear fitting of the measured data. Crystal absorption is approximately 65%.*

After measuring power-slopes the single-plate BRF was inserted, and tunability was recorded. This is shown in figure 2.5. The tunability is limited by the filter. When this was tuned beyond the curve shown in the figure, the laser would jump to run at the other edge of the curve, indicating a free spectral range for the filter in the order 160 nm. The precise material and thickness of the filter were not known.

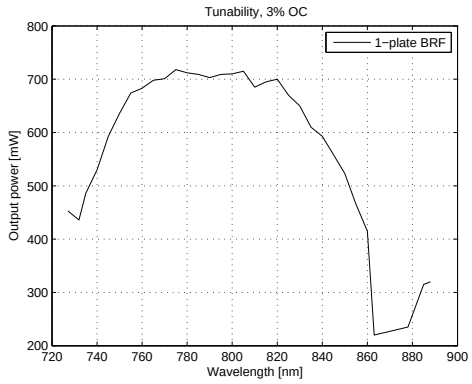

Figure 2.5: *Tunability of the simple Ti:Sapphire cavity utilising a BRF as tuning element. Measured with a 3% output-coupler.*

The line width of the laser mode was recorded with a rotating grating spectrometer (Reese Instruments). Later a three-plate BRF was tested, and the line width utilising this filter was also recorded. The results are shown in figures 2.6 left (single-plate) and right (three-plate). Line widths are approximately 0.69 nm FWHM with the single plate filter, 0.24 nm FWHM with the three plate filter. The latter result is close to the resolution of the spectrometer (0.25-0.3 nm), so the actual line width might be smaller. Centre wavelengths are 785 nm. Unfortunately, the three plate filter was not available when the BiBO experiments were done – see chapter 3.

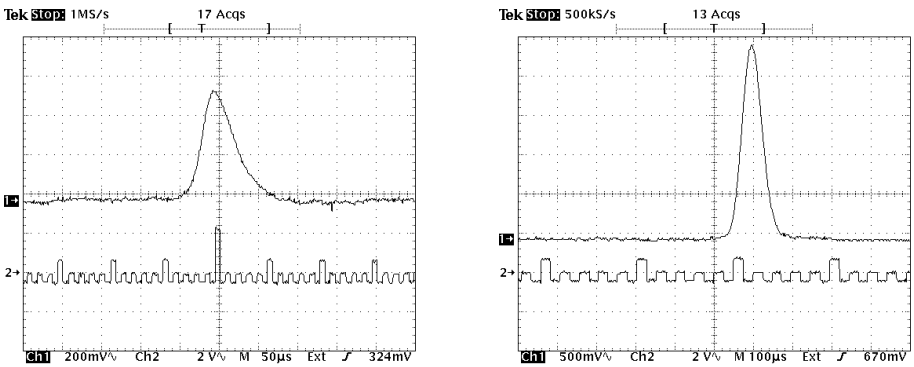

Figure 2.6: *Line widths of the simple Ti:Sapphire laser using different BRF elements. Single plate filter to the left, three plate filter to the right.*

2.3 Summary on the simple Ti:Sapphire laser

A simple Ti:Sapphire laser was build. It was found to require considerable care to align properly; the necessary skills for this being acquired during experimenting with this simple laser. Measurements on it showed that up to 800 mW could be extracted using 5.5 W of pump and 5 % output coupling. The laser could be tuned 160 nm around 785 nm utilising a single-plate BRF as tuning element. The line width was found to be 0.69 nm with the single-plate BRF – as used in the BiBO-experiments.

Bibliography

[1] D. Kopf, K.J. Weingarten, G. Zhang, M. Moser, M.A. Emanuel, R.J. Beach, J.A. Skidmore, and U. Keller, "High-average-power diodepumped femtosecond Cr:LiSAF lasers"; Appl. Phys. B – Lasers and Opt., vol. 65, pp. 235-243; 1997.

[2] R. Frey, F. de Rougemont, and C.H. Lee, "An actively mode-locked continuous wave Alexandrite laser"; Op. Comm., vol. 73, pp. 234-236; 1989

[3] S.A. Payne, L.L. Chase, and L.K. Smith, "Laser performance of LiSrAlF6:Cr3+"; J. Appl. Phys., vol. 66, pp. 1051-1056; 1989

[4] A. Cassanho, and H. Jenssen, "LiSGaF offers performance edge over LiSAF"; Laser Focus World, vol. 33, pp. 169-173; 1997

[5] J.C. Walling, D.F. Heller, H. Samelson, D.J. Harter, J.A. Pete, and R.C. Morris, "Tunable Alexandrite Lasers: Development and Performance"; IEEE J. Quant. Elect., vol. QE-21, pp. 1568-1581; 1985

[6] R. Scheps, B.M. Gately, and J.F. Myers, "Alexandrite laser pumped by semiconductor lasers"; Applied Phys. Lett., vol. 56, pp. 2288-2290; 1990

[7] T. Skettrup, *Laserteknik* 5. udg. (Polyteknisk Forlag, 1993)

[8] A. Yariv *Optical Electronics* Fourth Edition (Saunders College Publishing/HBJ, 1991)

[9] P. Moulton, "Recent advances in transition-metal-doped lasers"; *Tunable solid-state lasers, Proc. First Int. Conf.* La Jolla, CA, USA, June 13-15, 1984; P. Hammerling, A.B. Budgor, and A. Pinto, *eds.* (Springer-Verlag, 1985)

[10] P.F. Moulton, "Spectroscopic and laser characteristics of Ti:Al_2O_3"; J. Opt. Soc. Amer. B, vol. 3, pp. 125-133; 1986

[11] G.F. Albrecht, J.M. Eggelston, and J.J. Ewing, "Measurements of Ti:Al_2O_3 as lasing material"; Op. Comm., vol. 52, pp. 401-404; 1985

[12] R. Roy, P.A. Schultz, and A. Walther, "Acousto-optic modulator as an electronically selectable unidirectional device in a ring laser"; Op. Lett., vol. 12, pp. 672-674; 1987

[13] D.E. Spence, P.N. Kean, and W. Sibbett, "60-fsec pulse generation from a self-mode-locked Ti:Sapphire laser"; Op. Lett., vol. 16, pp. 42-44; 1991

[14] "Titanium-Sapphire Doped Laser Crystals", Data sheet;
Saint-Gobain Crystals `http://www.photonic.saint-gobain.com`

[15] W. Demtröder, *Laser Spectroscopy – Basic Concepts and Instrumentation* Second Enlarged Edition (Springer Verlag, 1996)

Chapter 3

BiBO for SHG

> The really fascinating thing about research is the new science, but to get to it, you have to get past that first level.
>
> Walter Gilbert.
> *American zoologist (1906-1974)*

A central point in this research project was to develop a narrow band light source that could be used in the bleaching of chromophores. I chose to investigate a NUV laser based on a frequency-doubled Ti:Sapphire laser. The crystal for the nonlinear process was chosen to be the novel nonlinear material BiB_3O_6.

This chapter presents the results from the investigations on this laser:

- A brief introduction to the area and previous research results by other groups is given in section 3.1, together with the motivation for choosing BiBO as nonlinear material.
- The set-up is described in detail in section 3.2 on page 21.
- Section 3.3 on page 23 presents results for the frequency doubled Ti:Sapphire laser. Results for 392 nm and 405 nm generation are compared.
- The blue output spot was found to be elliptical. This is being discussed on page 32 in section 3.4.
- Section 3.5 on page 33 discusses the coating problems encountered, and presents results obtained by light microscopy and AFM scanning.
- Finally on page 36 in section 3.6 the summary wraps up the chapter.

3.1 Introduction

There is a great demand from many applications for coherent light sources in the blue (400-450 nm) to UVA (320-400 nm) spectral region. For instance microscopy, where many intrinsic and extrinsic fluorophores are excited at these wavelengths. Other applications include semiconductor processing and medico technical equipment. Today, this spectral region is usually addressed by frequency tripled Nd:YAG lasers, excimer lasers, or gas lasers. However these

options only cover a limited number of colours, and it would be preferable to increase the wavelengths available. Currently, the research goes towards developing frequency doubled CW solid-state lasers for the blue-UVA region. One of the options are doubling Ti:Sapphire lasers, with the possibility of spanning wavelengths from around 325 nm to 525 nm.

For my project I chose to build and test frequency doubling of a Ti:Sapphire laser. The motivation for this choice was that such a source has the possibility of spanning a broad wavelength range in the most interesting blue-to-UV region, which would allow for testing tunable SHG in this region. In addition it would be relatively easy to change to a different wavelength in case the first tested would not be giving the desired bleaching effects. A CW laser was chosen as this was quicker and easier to set-up and manage, ant the scientific novelty value of characterising such a system is higher, than for a pulsed/mode-locked system.

It was decided to test the novel nonlinear crystal BiB_3O_6 – hereafter referred to as BiBO – in conjunction with frequency doubling of Ti:Sapphire lasers. The BiBO crystal excels in having high nonlinear coefficient – higher than most commonly used bulk crystals for frequency doubling to the UV region [1], see table 3.1 for a comparison of LBO, BBO, and BiBO. BiBO shows good transmission characteristics down to around 286 nm [2] – unlike KTP for instance. BiBO may be cut for Type I phase matching for the target wavelengths, which is preferable to Type II due to no walk-off between the fundamental field(-s). Fundamental field walk-off may increase losses in a system with tight focussing – such as the system designed for this work. Type I phase matching also does not have an inherent wave-plate effect, which otherwise needs careful temperature stabilisation of the nonlinear crystal.

To the best of my knowledge there has been no published references prior to this work on intracavity doubling of CW Ti:Sapphire laser systems utilising BiBO crystal as the nonlinear frequency conversion medium. Thus, the main motivation for utilising BiBO in this project is – besides its good properties – the prospects for important, novel scientific work with this crystal in the specified set-up.

Until now frequency doubling in BiBO crystal has either been utilised in extra-cavity doubling of Ti:Sapphire femtosecond lasers [3, 4, 5], or for intracavity doubling of CW laser systems at longer wavelengths – SHG of 1064 nm [6, 7], or SHG of 946 nm [8]. In reference [9] BiBO has been utilised for CW SHG of 768 nm in a locked external cavity.

	LBO	BBO	BiBO
d_{eff} [pm/V]	0.74	1.99	3.75
Transparency cut-off [nm]	160	185	286
Walk-off [mrad]	17.0	69.0	61.1
Acceptance bw. [nm/cm]	25.8	16.41	7.33

Table 3.1: *Coefficients for crystals commonly used in frequency doubling to the UV-blue region. Data calculated for Type I phase match of SHG of 785 nm at 23 C. Walk-off, acceptance bandwidth and d_{eff} is computed with the free software/database SNLO, which is also the reference for transparency cut-off.*

3.2 Set-up

To determine the design parameters for frequency doubling utilising our BiBO crystals the optimal beam waist in the nonlinear crystal was estimated using the Boyd-Kleinmann equations [10, 11]. The optimum beam waist was calculated to be in the order of 12-16 μm, see table 3.2. As this was smaller than practical for maintaining a sufficiently stable set-up, the cavity was designed to give a beam waist of 25μm in the nonlinear crystal. Walk-off was calculated using SNLO [1]. Estimates for optimum beamwaist and walk-off as well as crystal data are given in table 3.2.

Crystal	λ_{SHG}	L×W×H	θ	ϕ	ρ	w_{Opt}
1	392.5 nm	3×3×3 mm^3	149.9°	90°	61.0 mrad	12.2 μm
2	404 nm	5×3×3 mm^3	151.9°	90°	58.1 mrad	16.0 μm

Table 3.2: *Properties of the crystals. L×W×H are dimensions in length along the light propagation axis times width times height. θ and ϕ are the propagation direction angles for phase match at λ_{SHG}. ρ is the theoretical walk-off angle. Phase match temperature for both crystals was specified to be 23.5 C. The crystals were cut for Type I phase matching. Crystals were purchased Foctek.*

To achieve the needed small beam waist size at the nonlinear crystal, and a beam waist in the laser crystal of around 60 μm, a 5-mirror W-type cavity as shown in figure 3.1 was designed.

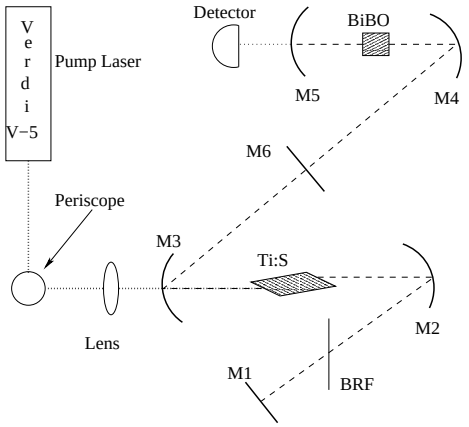

Figure 3.1: *The laser cavity utilised in the experiments with the BiBO nonlinear crystal.*

M1 was a plane mirror, highly reflecting between 680–880 nm and anti reflecting at 532 nm. M2 and M3 had coatings similar to M1, but were concave with a radius of curvature of -100 mm. M4 and M5 were highly reflecting between 750–850 nm, and anti reflecting between 375-425 nm, being concave with a radius of curvature of -50 mm. Between M1 and M2 a single plate BRF was

[1] SNLO – Free software package © Sandia National Laboratory, http://www.sandia.gov

placed for giving tunability. Between M2 and M3 a beam waist (V×H 56 μm × 65 μm) was formed, wherein the Ti:Sapphire laser crystal was positioned in a water cooled mount. Between M4 and M5 a smaller waist was formed, in which the nonlinear crystal was placed. By translating mirror M5 the beam waist in the nonlinear crystal could be adjusted. The beam waists at the nonlinear crystal position depicted in figure 3.2 were calculated as a function of the length between mirrors M4 and M5.

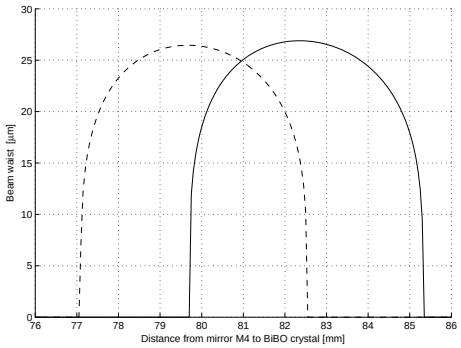

Figure 3.2: *The calculated beam waist between mirrors M4 and M5 as a function of the distance between these mirrors. Black curve is waist in horizontal plane, dashed curve is vertical plane. Plot based on ABCD matrix calculations assuming no lensing in the Ti:Sapphire crystal.*

The nonlinear BiBO crystal was mounted in a temperature controlled holder on a XYZ-$\phi\theta$ translation stage between mirrors M4 and M5. The Ti:Sapphire crystal was pumped by a 532 nm laser – Coherent Verdi V-5, maximum pump power 5.5 W – through mirror M3. The pump laser was focussed in the laser crystal by a lens with focal length 100 mm. To ease the initial alignment an extra plane mirror M6 (partially reflecting between 680-880 nm, transmission 3 %) was placed between mirrors M3 and M4, making a shorter, more easily aligned cavity. The output from this shorter cavity was then used to visually align the mirrors M4 and M5. M4 and M5 were aligned up to the point of a round trip of the beam from M6 to M4 to M5 and back to M6. It was not necessary to spend too much time aligning M4 and M5 this way, as the beam anyway shifted slightly going through the substrate of M6. After this aligning M6 was removed and (M4 and) M5 were adjusted (no nonlinear crystal inserted yet) until lasing occurred.

3.2.1 Acceptance parameters

Utilising a proprietary Matlab-based program [2] phase matching as function of angle for a 3 mm long BiBO crystal for Type I frequency doubling of 785 nm was calculated. To get an idea of the sensitivity to angle misalignments curves over the relative conversion efficiency as function of angle around the calculated phase match angles were plotted – figures 3.3 and 3.4. The θ-plane is sensitive to adjustments around the phase matching angle of 149.9°, which is seen as a narrow peak around this angle in the θ-plane. In the other plane – ϕ-plane – the angle is not sensitive to minor (mis-)adjustments. FWHM for the two curves are 8.36° and 0.186° for the ϕ-plane and θ-plane respectively. Theoretically a delta function is assumed for the spectrum in the calculations.[3]

[2] Inhouse development; © J.L. Mortensen, Department of Physics, Technical University of Denmark

[3] It may be noted that not only the chosen cutting angles provide phase matching. ϕ is chosen (at 90°) so the direction of propagation is as close as possible to a principal axis in

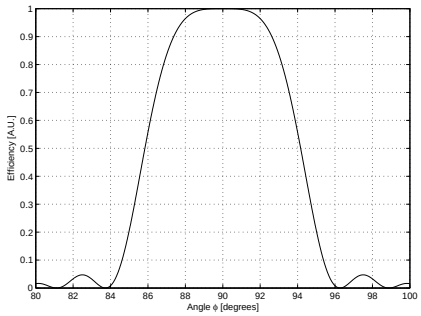

Figure 3.3: *Tuning the crystal around the design angle in the ϕ-plane, with the θ-angle fixed at the design angle. A sinc-curve is the result.*

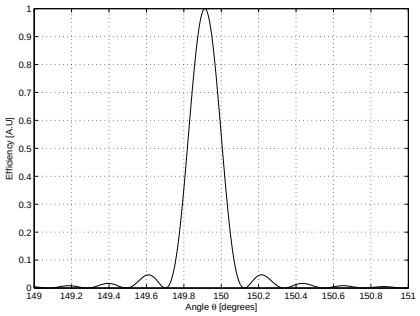

Figure 3.4: *Now tuning in the θ-plane. This is seen to be much more sensitive to perturbations than in the ϕ-plane.*

The sensitivity to changes in the fundamental wavelength for this crystal was calculated assuming angles and temperature fixed at the design parameters for SHG of 785 nm. This wavelength acceptance curve may be seen in figure 3.5. FWHM is found to be 2.1 nm. This may be compared with the 0.69 nm line width for the intracavity field. Calculating the correction factor (G-factor) due to the IR line width gives a result of G=0.97.

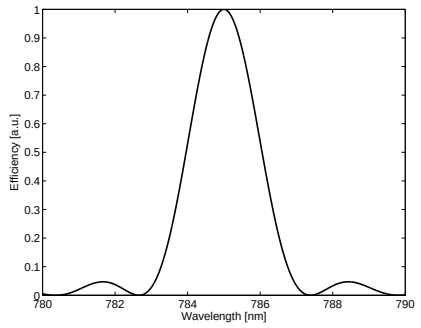

Figure 3.5: *Sensitivity to changes in fundamental wavelength for 3 mm crystal assuming fixed angles. FWHM is approximately 2.1 nm. Curve calculated utilising proprietary program, assuming incident field is a delta function.*

3.3 Results

Both BiBO crystals listed in table 3.2 were in turn used in the set-up shown in figure 3.1. The procedure for alignment was to get the set-up running without the BiBO crystal inserted in the beam. The insertion of the BiBO was then followed by a careful realignment of the cavity until the laser was optimised. Due the walk-off of the fundamental field in the crystal the mirrors around the crystal had to be adjusted. Finally, adjusting the crystal angles and the BiBO-arm mirrors was performed until blue output was generated and optimised. As

the crystal for least walk-off, whereas θ is chosen to give highest possible effective nonlinear coefficient, which is dependent on propagation direction in the crystal.

predicted in the calculation of acceptance parameters the SHG was sensitive to angular adjustments in the horizontal plane, while adjustments in the vertical plane did not influence conversion. Adjustments in the vertical plane were used as final fine tuning of the generated blue output power.

3.3.1 392 nm BiBO

The first crystal tested was the 3x3x3 mm sized BiBO. Measurements of generated blue light were only performed on the blue light generated in one direction, assuming the power in both directions was of equal level. Thus all data shown in the figures were multiplied by 2 – after correcting for filter transmission – before plotting, to give the full amount of generated blue output.

No attempt to direct all blue light out in the same direction was made. However, this may be achieved if the coating on the BiBO on one facet is also made HR to the generated blue light, or a special mirror HR@blue and AR@IR is inserted right after the crystal.

Utilising a blue filter (T=75% at 392 and 405 nm) to block any 785 nm light from reaching the detector, the blue generated power was measured after mirror M4. In all measurements besides the power-slope measurement the laser was run with the maximum available green pumping power (5.5 W).

With the laser tuned to 785 nm and adjusted for max power, a temperature scan of the nonlinear crystal was made. A thermal detector (Melles Griot 13PEM001) was placed after mirror M5. 240 samples were recorded, sampling time one second, then temperature was increased by 3 C, and the system was left to stabilise for one minute before next measurement. The result is depicted in figure 3.6. Within our "safe limit" of 20 to 75 C it was not possible to detect a sinc curve for the temperature dependence when measuring the absolute generated blue power. However, if the blue output is divided by the square of the red intracavity circulating field[4] – which specifically shows the conversion efficiency of red to blue – a more oscillatory temperature dependence is seen – see figure 3.7. Around the design temperature of 23 C the conversion efficiency is good, but there is also a second peak around 45 C, which is equally good. Between these peaks is a notable dip in the efficiency. This indicates that although the conversion efficiency drops around 30 C, the circulating field must increase, cancelling the effect of the lower conversion. There is a balance between generated blue power and intracavity circulating field – coupled through the intracavity loss for the circulating field, which leads to an increased intracavity field when the conversion efficiency drops, cancelling to some degree the influence of this drop. This only takes place for intracavity frequency doubling. Research supporting this may be found in the litterature [12]. At higher temperatures – like at the peak around 40 C, the overall blue output has dropped slightly. Above this the conversion efficiency and blue output both drops as phasematch is lost. The conversion efficiency is seen to lie around $6{\cdot}10^{-5}$ W^{-1} to $7{\cdot}10^{-5}$ W^{-1}. This may be compared to the theoretical estimate – see chapter B in the appendix – of $7.9{\cdot}10^{-5}$ W^{-1}. As seen the conversion efficiency in the laboratory lies close to the theoretical optimum.

[4]Calculated from the red leak, corrected for the mirror transmission at the wavelength in question, and for the transmission of the red bandpass filter blocking residual green pump light from reaching the detector. Red leak and blue output power were recorded simultaneously.

FWHM of the temperature dependence for blue power was found to be approximately 66 C – see figure 3.6.

The large spread in measurement points at a given temperature is due to an incomplete thermal stabilisation.

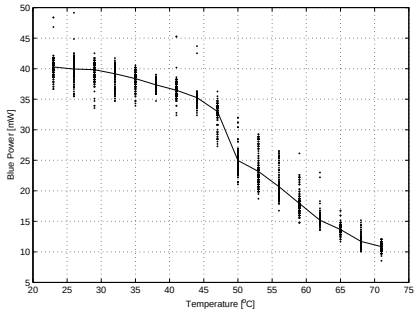

Figure 3.6: *The influence of temperature on the blue SHG power at 392 nm. Generated light is total for both directions.*

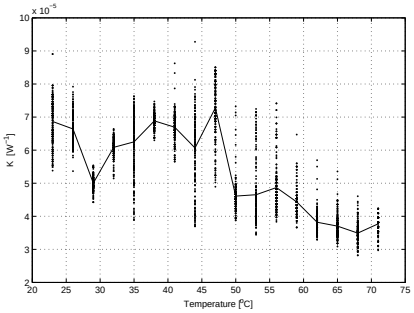

Figure 3.7: *The conversion efficiency from IR to blue. The large spread of measurement points leads to a quite low significance of the fit.*

After resetting the temperature of the BiBO crystal to its design temperature at 23.5 C a power-slope measurement was made. This was done by maximising the blue output at 5.5 W of green pump, and then turning down the pump laser, recording a data point for every 0.25 W steps of pump power from 5.5 W down to 2.5 W. Threshold for laser action (and blue generation) was approximately 2.25 W of green pump power. To eliminate influences from the operational characteristics of the Ti:Sapphire part of the laser the generated blue power was measured as a function of the leaking infrared 785 nm light. The intracavity IR leak was measured after M1, utilising a filter (transmission at 785 nm 81%) to block residual reflected pump light from reaching the detector. The transmission coefficient of the M1 mirror was measured to be 0.02% at 785 nm. This means 1 mW (corrected for filter transmission) of IR leak corresponds to approximately 5 W circulating field. In addition, it was also during this measurement the highest blue generated output at 392 nm was recorded at about 53 mW.

A tunability curve of the blue generated output was recorded by adjusting the BRF. For every measurement point the nonlinear crystal was adjusted for maximum SHG, the temperature was kept at 23.5 C. Subsequently, the cavity was readjusted as the adjustments made to the nonlinear crystal tended to mis-align the cavity. In figure 3.9 is seen the tunability of the laser with the crystal cut for frequency doubling of 785 nm light. The explanation for the dip around 390 nm is believed to be due to either a mode-hop or problems related to the BRF-effect of the Ti:Sapphire crystal. Tuning range was found to be approximately 8 nm, if the limits to tunability are set to where the generated power has droped to one-third of its peak value. This is in the range of what is found in reference [3], which reports a tunability of 375-435 nm. It should be noted that in reference [3] the experiment was done with a thin BiBO slice extra-cavity to a femtosecond laser and is thus not limited by alignment problems. In addition it is not clear what their lower cut-off criterion was set to.

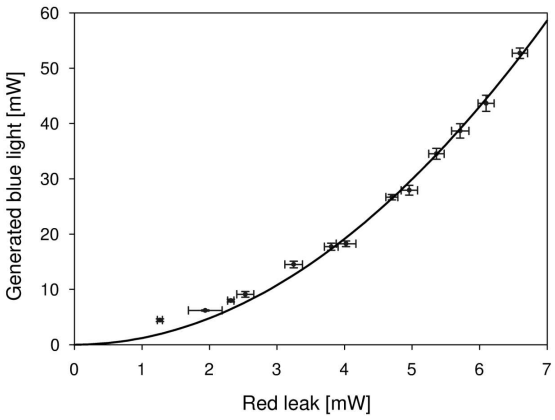

Figure 3.8: *Slope efficiency plot of the blue SHG output against leaked IR intracavity field. Corrected for transmission of red and blue filters. Fitting parameter for the curve fit* $a \cdot x^2$ *was* $a = 1.1956\, mW^{-1}$.

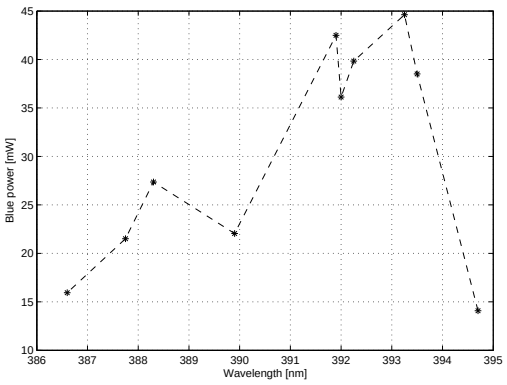

Figure 3.9: *Wavelength tunability of the generated blue light utilising the BiBO crystal optimised for doubling of 785nm.*

The spectra of the generated blue light as well as of the intracavity circulating IR field are narrow compared to the spectral acceptance of the BiBO crystal. Figures 3.10 and 3.11 shows the spectral widths for wavelengths around 782 nm and 391 nm respectively measured with a fibre-coupled spectrometer (Avantes AvaSpec 2048). For the 782 nm IR field a FWHM 0f 0.77 nm was measured. For the generated 391 nm output the line width was measured to 0.85 nm FWHM. In both cases limited by spectrometer resolution, which is about 0.7 nm FWHM at 700-800 nm, and slightly worse at shorter wavelengths. The line width of the 392 nm blue light should be narrower (FWHM) than the line width of the 782 nm fundamental by a factor of around 2. A previous measurement with a more precise Rees scanning grating spectrometer gave 0.69 nm line width for the fundamental field – see section 2.2.3, figure 2.6. Unfortunately, the more precise Rees scanning grating spectrometer did not work well at the SHG wavelengths, hence the use of the fibre-coupled spectrometer.

Some problems getting the laser to tune smoothly were experienced. This caused the wavelength of the intracavity field to jump in discreet steps of 2-3 nm when tuned. The reason is believed to be related to a BRF-effect of the Ti:Sapphire crystal. Hence the choice of 782 nm for measuring the line width, as 785 nm could not be selected for the particular cavity alignment.

Finally, the stability of the generated blue output was measured. To measure

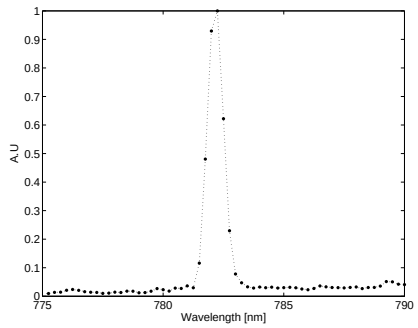

Figure 3.10: *Spectrum of the IR field at 782 nm.*

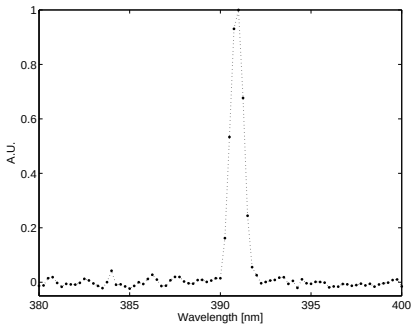

Figure 3.11: *Spectrum of the blue output at 391 nm.*

this the laser was left running for an hour, while a thermal detector (Melles Griot 13PEM001) coupled to a data recording computer sampled the blue power every two seconds. The first 300 measurement were discarded to allow the system to stabilise. Simultaneously a similar detector sampled the red leak through mirror M1. The data recorded are plotted in figure 3.12. Here the average generated blue power was down to 43.0 mW in total from the record 53 mW, due to problems with the coatings of the crystal. Also adjustments slightly below maximum blue power tended to be a bit more stable than maximum power adjustments. The standard deviation in the stability measurement was 3.23 mW – $\sim 8\%$. As seen the noise for the generated blue light increases over time, while the fundamental tends to get more stable over time. The latter due to thermal stabilisation of the laser crystal. As the detector has an integration time of about a second, the increasing blue noise is not due to "green noise" – occurring on a shorter time scale, but is believed to be related with slow breakdown of the coating of the BiBO crystal over time.

In addition to the power fluctuations "translational flickering" of the blue output spot was at times observed. The flickering moved the spot approximately a centimetre sideways 50 cm from mirror M5. This was mostly uncorrelated with the fluctuations in the blue output power level. The flickering was sensitive to the cavity alignment, where small adjustments could make the flickering stop without reducing or increasing the blue output power. The flickering is believed to be caused by photo refractivity in the BiBO – as reported by others [9], and a sensitive cavity alignment on the edge of stability. This may lead to mode-hopping of the laser between modes closer in wavelength than our spectrometer could resolve (no fluctuations in wavelength associated with this unstability could be seen).

Summary on 392 nm generation

We were able to make a maximum of 53 mW blue light with 5.5 W of green pump light. The standard deviation of the long time stability was about 8%, comparable to values found by the literature [6, 8]. Tunability FWHM was found to be about 8 nm with angle tuning of the crystal. The blue output was found to be rather temperature insensitive although the conversion efficiency showed os-

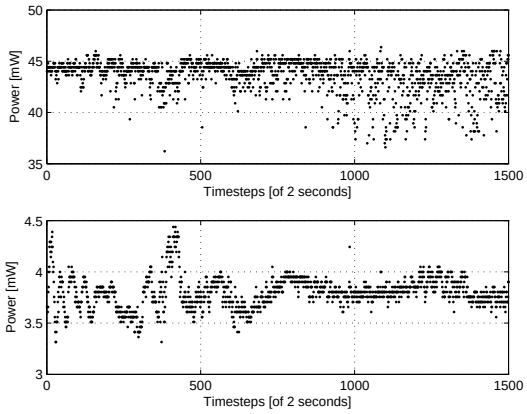

Figure 3.12: *Stability of the blue output (upper plot) and red leak (lower plot) for doubling of 782 nm. 1500 data points were recorded, every 2 seconds.*

cillatory behaviour as function of temperature. Maximum conversion efficiency was found to be around $6{\cdot}10^{-5}$ W^{-1} to $7{\cdot}10^{-5}$ W^{-1}. This may be compared to the theoretical estimate – see chapter B in the appendix – of $7.9{\cdot}10^{-5}$ W^{-1}. Possible cause for the difference between measured and theoretical estimate may be due to uncertainty in estimating the power of the circulating field; the HR mirror through which the leak was measured had a highly wavelength dependent behaviour in this region. The line width of the IR field has minimal influence due to the crystal being only 3 mm long – leading to a correction factor of 0.97.

3.3.2 404 nm BiBO

After measurements on 392 nm generation, the BiBO crystal was taken out and replaced by the BiBO crystal cut for 404 nm generation (crystal 2 in table 3.2). The BRF was adjusted accordingly.

First measurements done were temperature scans, performed in accordance with the procedure described under 392 nm generation; however, as the system tended to get unstable over long time spans only 30 samples of one second sampling time were taken at each temperature step. Initially the blue output was optimised at 23.5 C, as the crystal was cut for this temperature. In figures 3.14 and 3.13 the absolute generated blue output as function of temperature, and the conversion efficiency found by dividing the blue output by the square of the red intracavity field are shown.

From figure 3.14 it may be noted that the oscillatory behaviour of the conversion efficiency previously seen in the 392 nm SHG experiment also occurs here – though in the case for 404 nm generation even more pronounced. Again, as for the case of the 392 nm SHG crystal a second peak in efficiency may be seen, this time around 40 C. This peak is somewhat higher than the peak at 23.5 C, so it was decided to re-optimise the laser at 40 C.

Readjusting at a temperature of 40 C lead to the results shown in figures

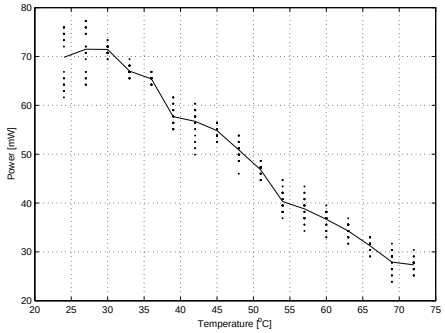

Figure 3.13: *Temperature scan, total generated blue output. The SHG process was optimised at 23.5 C.*

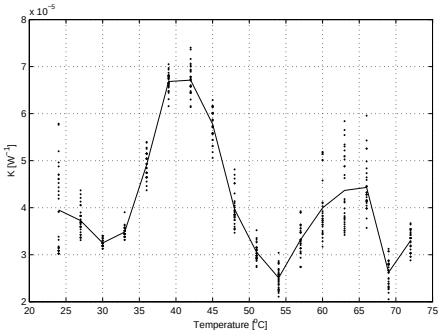

Figure 3.14: *Temperature scan, conversion efficiency. The SHG process was optimised at 23.5 C.*

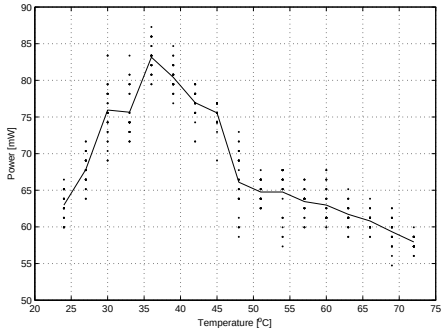

Figure 3.15: *Temperature scan, total generated blue output. SHG process optimised at 40 C.*

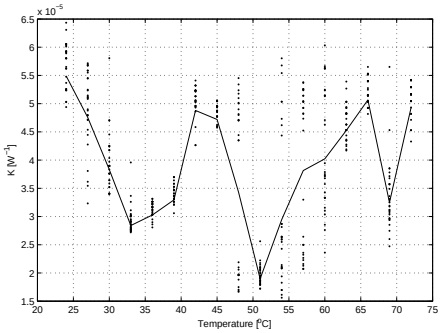

Figure 3.16: *Temperature scan, conversion efficiency. For this measurement series the SHG process was optimised at 40 C.*

3.16 and 3.15. As it may be seen from figure 3.15 the maximum achieved blue power was higher for the 40 C optimisation than for 23.5 C (figure 3.13). The optimum output was achieved at approximately 36 C. The conversion efficiency peaks around 42 C.

The higher efficiency and power output reached at 40 C optimisation rather than at 23.5 C is due to the fundamental field being 810 nm and not 808 nm, for which the crystal was designed, shifting the optimum phase match to a higher temperature. The fundamental wavelength was 810 nm, due to problems with tuning the laser smoothly, as described previously. The wavelength was 810 nm for both temperature scans (all four figures 3.14 to 3.15).

The FWHM of the temperature dependence curves for blue output generation optimised at BiBO-temperatures of 24 C and 40 C may be estimated from figures 3.13 and 3.15 to 64 C and more than 50 C, respectively. For the 40 C optimised curve the generation does not drop to half maximum within the scan range. These values may be compared with the result obtained in reference [6], where a 5 mm long BiBO was used to intracavity double a 1064 nm fundamental in a Type I phase matching scheme. In the reference the authors find the

FWHM of the temperature dependence to be about 6 C.

Both figures for the conversion efficiency versus temperature at 810 nm shows oscillatory behaviour. It is clear that the maximum power for one given alignment is reached close to the temperature, where the alignment took place.

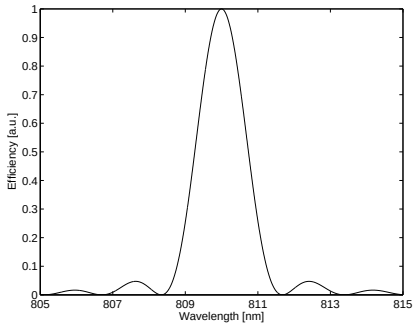

Figure 3.17: *Sensitivity to changes in fundamental wavelength for 5 mm crystal assuming fixed angles, calculated with a proprietary Matlab program. FWHM is approximately 1.5 nm.*

One thing to note is the apparent flipping between two regions as seen in figure 3.16 in the temperature range of approximately 45–60 C. A closer inspection of the raw data files showed that in general the conversion efficiency is periodically modulated with period in the 10-second range, rather than flipping randomly between the values. That the total generated blue output does not flip in value is due to the lower (detuned) conversion being offset by an increase in the IR field.

Normalising the top value of the conversion efficiency in the temperature range 40-60 C to 1 the efficiency relative to the peak value for the lowest measured value is then normalised to about 0.5. In figure 3.17 is shown wavelength dependence of conversion efficiency assuming fixed crystal angles for a 5 mm crystal cut for Type I phase matching at 810 nm. Peak value of the conversation efficiency is at 810 nm. A drop in relative efficiency to 0.5 corresponds to a change in fundamental field wavelength of about +/- 0.75 nm . An 0.75 nm jump in wavelength is just around the minimum, which may be resolved by our fibre coupled spectrometer. However, no jump in wavelength was detected. The wavelength of the IR field may have been jumping slightly due to thermal effects in the BiBO crystal. If the BiBO has been turned slightly around its optical axis it will act as a wave-plate for the circulating field, as the field gets split up in ordinary and ordinary waves. This will introduce a temperature dependent loss leading to a mode hop. The temperature of the BiBO crystal may drift slowly due to blue light absorption, creating a slow periodical modulation. Unfortunately, no temperature dependent Sellmeier equations may be found in the literature, so the temperature dependence of the modulation period can not be estimated theoretically.

After performing temperature scans, the BiBO crystal was optimised at 40 C and a stability measurement was performed, shown in figure 3.18. An average value of 93.3 mW was measured over the course of 60 minutes with a standard deviation of of 2.66 mW – $\sim$ 2.9%. The red leak had an average value of 0.70 mW.

The all-time highest recorded (stable) output for 405 nm light was measured to 100.3 mW – achieved at 36 C after careful fine tuning of the alignment.

Further measurements could not be made due to catastrophic failure problems with the coatings on the BiBO crystal.

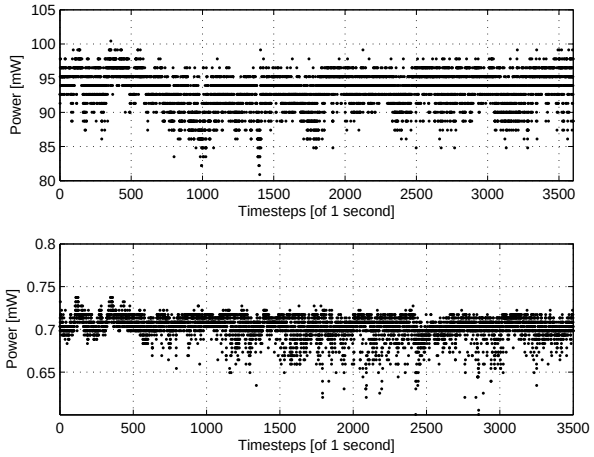

Figure 3.18: *Stability of the blue output at 405 nm (upper plot), and red leak (lower plot).*

3.3.3 Comparison of 392 nm and 405 nm generation

Comparing the results for temperature scans of 810 nm SHG with those of 785 nm SHG it may be seen that although the former gives higher blue output by almost a factor of two, the latter holds the highest conversion efficiency. Both blue wavelengths showed to be stable over longer time spans, where again doubling of 810 nm proved to be the superior performer.

Theoretical estimates were made for comparison – see Appendix B. The conversion efficiencies were calculated to $7.9{\cdot}10^{-5}$ W^{-1} and $20.0{\cdot}10^{-5}$ W^{-1} for frequency doubling of 785 nm and 810 nm respectively. Measured values were $6{\cdot}10^{-5}$ W^{-1} to $7{\cdot}10^{-5}$ W^{-1} for doubling of 785 nm, and $5.5{\cdot}10^{-5}$ W^{-1} to $6.7{\cdot}10^{-5}$ W^{-1} for doubling of 810 nm. Thus the measured and calculated values for the conversion efficiency are close for doubling of 785 nm, while the theoretical value for 810 nm doubling is about a factor of three larger than the measured value.

The theoretically and measured values for conversion efficiency may be compared to the values in reference [8]. In that reference the authors utilise a 10 mm long BiBO for intracavity doubling of a 946 nm Nd:YAG laser. They find a theoretical value for the conversion efficiency of $15.5{\cdot}10^{-5}$ W^{-1}, while their measured value is $5.4{\cdot}10^{-5}$ W^{-1}. Thus they also have a 1:3 factor between measured value and theoretical estimate. The results on conversion efficiency found in the presented are thus comparable to results from the literature.

Assuming a 33 W circulating field – estimated from measurements on the red leak – the theoretical estimate for 392 nm generation is 85 mW, while for 405 nm generation it is 217 mW. The "laboratory coefficient" Δ_{lab} – the goodness of the measured values as compared to the theoretical estimates – are (53/82 =) 64% for doubling of 785 nm, and (100/201 =) 50% for doubling of 810 nm – for both wavelengths the G-factors (0.97 at 785 nm, 0.93 at 810 nm) have been included. Thus the result for 392 nm generation is somewhat closer to the theoretical estimate than for 405 nm generation. Taking the rather poor

Arm length	Blue ellipticity	Red ellipticity
79.2 mm	0.20 V	0.46 V
80.0 mm	0.32 V	0.95 V
81.7 mm	0.35 V	0.32 H

Table 3.3: *Ellipticity of red and blue output spots measured after mirror M5. V indicates long axis is in the vertical plane, H that it lies in the horizontal plane.*

coatings on the crystal facets into consideration, achieving about half of the of theoretical power estimates is an acceptable result.

3.4 Blue output spot

The shape of the blue output spot was elliptical, with the long axis of the ellipse lying in the vertical plane – the ϕ plane as seen from the crystals point of view. This is not due to fundamental field walk-off, as walk-off for this set-up lies in the horizontal direction. To further investigate this the output spots in both red and blue were measured against length of the arm of BiBO crystal. Small changes in length of this arm had a drastic effect on the beam waist shape of the NIR intracavity field inside the BiBO. The testing was done with the 3 mm BiBO crystal inserted at a fundamental wavelength of 785 nm. First, the blue output at a given arm length was optimised. Then the blue output spot was drawn by means of eye and hand on a piece of paper 620 mm from the out coupling mirror M5 – in the far field. The laser was then tuned down in wavelength to around 740 nm, where the M5 mirror starts to lose its high reflectance. It was then possible to visually see the red output spot, which was also drawn on the paper. It is not possible to compare the actual blue and red spot sizes for different lengths of the BiBO arm, as the output power was dependent on this length – in turns influencing the visible spot size. What is possible to compare though, is the ellipticity of the spots. Measurements were done at three different arm lengths. For results see table 3.3

The ellipticity is given as the short axis divided by the long axis, so the result is always between 0 and 1. The V or H in table 3.3 indicates whether the long axis was in the vertical (V) direction or the horizontal (H) direction, the folding plane of the laser was in the horizontal plane. These results may be used to check the numerical predictions on the waist size inside the BiBO crystal. In figure 3.2 the numerical values for the beam waist in the BiBO crystal are given with no thermal lensing assumed in the Ti:Sapphire crystal. This was performed by trying different values for lensing in the ABCD-matrix for the Ti:Sapphire crystal, comparing the calculated values with the measured values. From this it was found a thermal induced lensing in the range 80-300 mm was needed in the Ti:Sapphire crystal to obtain an approximate circular beam waist with the given arm lengths and cavity folding angles.

It it believed the ellipticity of the blue output spot is due to the difference in the acceptance angle of the BiBO for the two planes (V and H) combined with the tight focussing of the infrared field inside the BiBO crystal. In the vertical

plane the broad angular acceptance means that phase matching will occur also for parts of the infrared field propagating with a considerable angle to the exact phase matching axis (the optical axis of the system). The angular acceptance being much more critical in the horizontal plane means the angle spread of the phase matchable part of the field is also much narrower. This causes the blue output spot to be elliptical.

Others [5] have mounted a similar BiBO crystal extra-cavity of a femtosecond laser, and found a similar elliptical blue spot with the laser focussed hard in the crystal, while a collimated pump beam lead to a circular blue spot, supporting the explanation presented above.

3.5 Coating problems

Problems were experienced with coatings of the BiBO crystals. After some time of use more and more scattering could be visually detected coming from the coatings. Following extraction of the crystals from the set-up, the coatings were inspected in a light reflection microscope. See figures 3.19-3.20 for pictures of a facet on the 392 nm SHG BiBO, and figures 3.21-3.22 for pictures a facet on the 405 nm SHG BiBO.

Several lines and pitting may be seen. The lines are interesting as they can only have been created in the few instances the crystal was translated transversally with the laser running. During these translations the laser (the red leak) would generally fluctuate in power. The lines are consisting of small micro pits in the surface, indicating the damage was only taking place whenever the alignment was "peaking", or where the coatings were spot wise "weak". However no more severe damaged areas are seen spot-wise, even though the laser was usually run for prolonged time with the crystal position fixed. This may be due to immediately occurring pitting of the surface creating a loss preventing the laser to reach an intra-cavity power high enough for causing further damage to the facets.

Others have reported probable damages to the crystal and/or coating [8], though they have not examined the crystal closer. An analysis of the damage threshold for BiBO crystals have been made [6], which states damages should not occur for powers lower than 400-600 MW/cm^2, depending on wavelength. As the used set-up lies comfortably below this limit (at 3-4 MW/cm^2 in/on the crystal with max focussing), the coatings must have been faulty or insufficient for the specified use[6].

[5] As my colleague J.L. Mortensen was told at a conference, however at the present time there seem to be no reference to this.

[6] As a comment to this, it may be noted that the supplier Foctek was contacted about their opinion on these problems. According to them the coatings were fault-free, but the crystals had been used at too high power for the used focussing, causing optical breakdown in the crystal itself. I believe, this is not the case, as based on measured data (see the section about AFM scans), and other published results making use of these crystals intra-cavity at a tighter focussing [9]. Foctek no longer markets BiBO crystals as of early 2006.

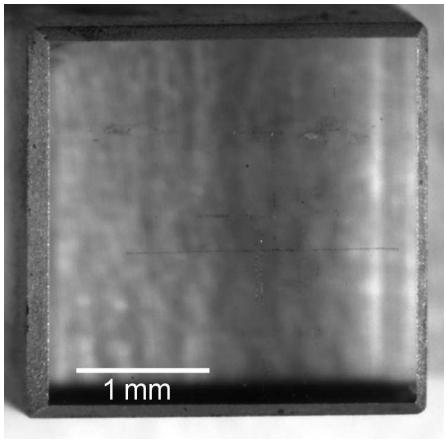

Figure 3.19: *Facet on the BiBO crystal for SHG of 785 nm. Several lines and pittings are seen. The damages appear black only due to shadow effects. The blurry background "pattern" is lens paper seen out of focus through the crystal.*

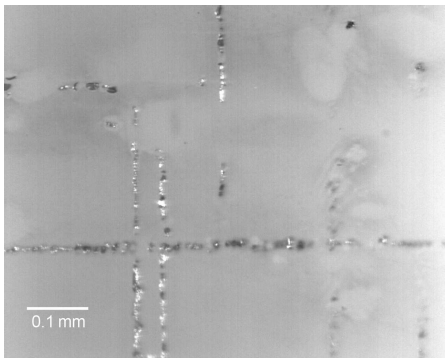

Figure 3.20: *Same facet as figure 3.19, zoomed in on some of the lines. The lines are not solid, but instead consists of a series of small spot-wise damages.*

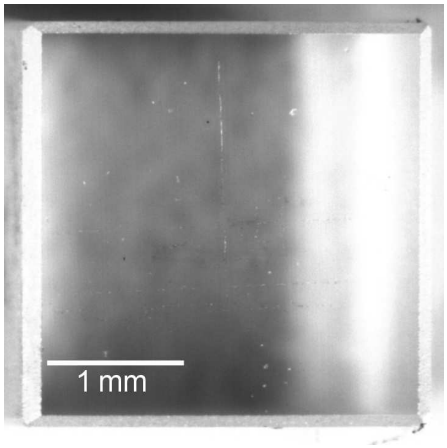

Figure 3.21: *Facet on the BiBO crystal for SHG of 810 nm. This crystal has slightly less damages than for the other BiBO crystal. This may be caused by the 810 nm doubling crystal being longer, and the facets therefore more out of focus than for the 785 nm doubling crystal.*

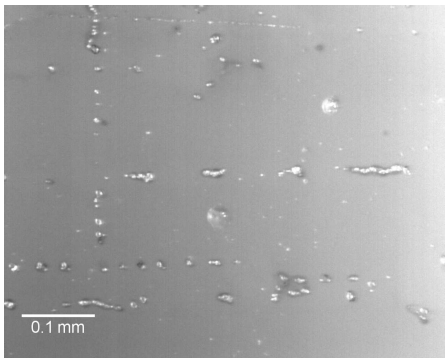

Figure 3.22: *Same facet as figure 3.21 zoomed on an area with line damages. Here it is very clear that the lines are not an unbroken damage, but consist of a string of widely spaced small dot-like individual damages.*

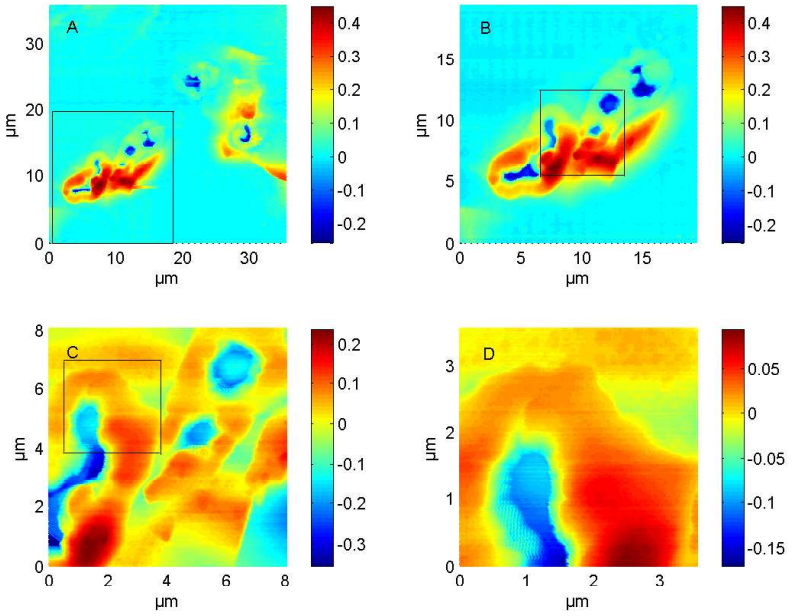

Figure 3.23: *AFM scanned 2-dimensional height plots of surface defects. B picture is a zoom of the boxed area on picture A, and so forth.*

AFM scans

To investigate the damages further an AFM investigation[7] was performed on one of the facets of the BiBO for 392 nm generation. AFM is able to give a precise measurement of surface structure and therefore useable in determining the nature and extent of coating damages. In figure 3.23 is shown 2-dimensional colour plots of a damaged area. The size of the individual defect spots may be seen to be half the size-range of the beamwaist in the BiBO – 10-20 μm. The details in the individual defects are of a much smaller scale – around 1 μm. The out of plane feature size is sub-micron, going from -200 nm to +400 nm relative to the undamaged coating surface as seen on plot A, figure 3.23. It is thus more a corrugation of the surface than deep pits or scratches.

3-dimensional visualisation of the surface is shown in figure 3.24. Here it clearly shows how the structure of the damages are "impact crater-like" with a crater surrounded by a cast-up ridge of material.

From the AFM scans it may be interpreted that the damages have been caused by a localised thermal overload in the coating or in the interface between coating and crystal. It certainly does not seem to be damages only related to the interior of the crystal. Thermal overload in the coating or in the interface between coating and crystal may cause the coating to "puff" or "explode" locally, as hinted by the corrugated defect spots seemingly having material pushed up above surface level – as well as pits in the surface. Thermal overload in the

[7]Equipment and training was kindly made available by Jakob Svagin at Nanoteket, Department of Physics, DTU.

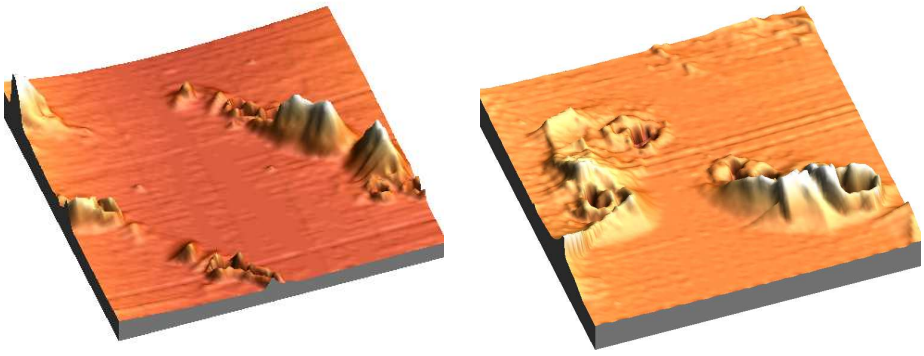

Figure 3.24: *3-dimensional visualisation of surface damage on the 392 nm BiBO. The slight curvature of the surface on the left picture is a measurement artifact. Scanned area is about 35 μm, with the height of the damages around 1 μm.*

coating may be caused if the coating is not sufficiently "hard", or gas/vapour has been trapped in coating micro cavities – porous coating. Thermal overload in the interface between crystal and coating may be caused by improper cleaning of the crystal facets prior to coating.

3.6 Summary of results obtained for BiBO for UV-SHG

The blue, BiBO-doubled Ti:Sapphire laser was central to this research project, and a lot of interesting knowledge and results were obtained and presented in this chapter. It was found that the BiBO-crystal is an excellent material for making SHG of Ti:Sapphire lasers. Two crystals were tested, one 3 mm long for doubling of 785 nm and one 5 mm long for doubling of 808 nm. The former gave a good 53 mW light at 393 nm while tunability was found to $\sim$ 8 nm. The latter crystal gave as maximum output excellent 100 mW of 405 nm light. Stability was measured over an hour and standard deviation of the power fluctuations were found to be 8% for the 3 mm crystal, 2.9% for the 5 mm. Temperature dependencies were low for both crystals. A comparison with theoretical estimates showed that 57 % of the theoretical value was achieved for the 810 nm case, an 80 % for the 785 nm doubling case.

Sensitivity to angular misalignment was computationally found to be sharp in one plane, while the other was very broad. Hands-on experience confirmed this.

Several problems occurred with the coatings of the crystals, and results from investigations of these were presented. It was found that the coatings suffered badly from catastrophic spot-wise failures. Likely the culprit was thermal overload from poorly made coatings.

Bibliography

[1] H. Hellwig, J. Liebertz, and L. Bohatý, "Exceptional Large Nonlinear Optical Coefficients in the Monoclinic Bismuth Borate BiB_3O_6 (BiBO)"; Solid State Comm., vol. 109, pp. 249-251; 1999

[2] H.Hellwig, J.Liebertz, and L.Bohatý, "Linear optical properties of the monoclinic bismuth borate BiB_3O_6"; J.Appl.Phys., vol. 88, pp 240-244; 2000

[3] M. Ghotbi, M. Ebrahim-Zadeh, A. Majchrowski, E. Michalski, and I.V. Kityk, "High-average-power femtosecond pulse generation in the blue using BiB_3O_6"; Op. Letters, vol. 29, pp. 2530-2532; 2004

[4] M. Ghotbi and M. Ebrahim-Zadeh, "Optical second harmonic generation properties of BiB_3O_6"; Op. Exp., vol. 12, pp. 6002-6018; 2004

[5] T. Harimoto, Y. Takeuchi, and M. Fujita, "Spectral properties of second-harmonic generation at 800 nm in a BiB_3O_6 crystal"; Op. Exp., vol. 12, pp. 811-816; 2004

[6] Z. Wang, C. Du, B. Teng, X. Xu, K. Fu, G. Xu, J. Wan, Z. Shao, and X. Yang, "Diode-laser-array end-pumped 1W CW Nd:YVO_4/BIBO green laser"; J. Mod. Optics, vol. 50, pp. 1253-1258; 2003

[7] A. Brenier, I.V. Kityk, and A. Majchrowski, "Evaluation of Nd^{3+}-doped BiB_3O_6 (BIBO) as a new potential self-frequency conversion laser crystal"; Op. Comm., vol. 203, pp. 125-132; 2002

[8] C. Czeranowsky, E. Heumann, and G. Huber, "All-solid-state continuous-wave frequency-doubled Nd:YAG-BiBO laser with 2.8-W output power at 473 nm"; Op. Letters, vol. 28, pp. 432-434; 2003

[9] V. Ruseva and J. Hald, "Generation of UV light by frequency doubling in BIBO"; Op. Comm., vol. 236, pp. 219-223; 2004

[10] GD. Boyd, and D.A. Kleinmann, "Parametric interaction of focussed Gaussian light beams"; J. Appl. Phys., vol. 39, pp. 3597-3639; 1968

[11] P.M. Petersen, and T. Skettrup, *Ulineær optik* 1. udgave (Polyteknisk Forlag, 1994)

[12] P. Buchhave, H. Abitan, and P. Tidemand-Lichtenberg, "Nonlinear frequency conversion in coupled ring cavities"; Op. Comm., vol. 200; pp. 359-368; 2001

Part II

Bleaching

Chapter 4

Eyes, lenses and cataract

> The light of the body is the eye;
> therefore when thine eye is single, thy whole body also is full of light;
> but when thine eye is evil, thy body also is full of darkness.
>
> Luke 11. 34.

The basic motivation for my Ph.D. project was to investigate the possibility of using laser pulses to bleach the discolourations in human eye lenses commonly known as cataract. To investigate this possible treatment on a model system as I did, it is necessary with a basic knowledge of cataract. In this chapter I have given a short overview of the (human) eye, cataract, and results from a research trip to Fraunhofer IBMT[1] on the microscopic structure of tissue in the eye. The latter is not related to cataract as such, but shows in details the structure of the tissue of the lens and cornea, which in itself are very interesting results.

- Cataract formation is briefly discussed based on published results in section 4.1. The motivation for choosing the glycated lysine as model system is discussed.
- Section 4.2 on page 42 gives a short introduction to eye and lenses.
- In Section 4.3 page 44 a pigs eye is dissected and pictures from this are presented. In addition LSM images of the lens from a porcine eye are presented, visualising the highly ordered structure of the lens.
- Finally section 4.4 on page 45 wraps up the chapter.

4.1 Formation of cataract

A brief introduction to cataract based on reference [1]. Natal native lenses are very clear but they quickly develop a yellowish hue. The chromophores responsible for this hue mainly absorbs light in the UV region, which is thought to be a protection mechanism protecting the retina from harmful UV exposure.

[1] Fraunhofer – Institut für Biomedizinische Technik, St. Ingbert, Germany; visit kindly made possible by Dr. Karsten König.

Later in life the colouring of the lens may become so deep that vision is impaired. Basically cataract may be characterised in two groups, based on their impact on – or hindering of – light transmission. One type of cataract is caused by scattering in the lens. This may be caused by the lens structure swelling or breaking down, thereby disrupting the highly structured short-range order of the lens making transparency possible. The other type of cataract may be described as a condition where light is absorbed. Responsible for the absorption is a number of chromophores. Many published results points toward advanced glycation end products – such as pentosidine – formed through nonenzymatic browning of lens proteins by a sugar being one of the components responsible for the yellowing of the lens [2, 3, 4, 5]. The nonenzymatic process, also known as the Maillard reaction, is a browning process taking place in the absence of enzymes; both glycation of lysine as well as caramelisation (oxidation) of sugars are possible pathways. The authors to reference [2] find that glycated lysine shows similar fluorescence peaks as pentosidine, making it a useable study molecule for cataract. In addition the authors suggest glycated lysine is one (possible) step in the formation of pentosidine in the lens. In light of the published results it makes good sense to use glycated lysine as a test model for studies and bleaching.

4.2 The human eye

In this section a short overview of the eye and the lens of the eye is given. For a more throughout description of eyes, lenses and diseases a text book such as [1] should be consulted. The discussion here is to a large part based on this book.

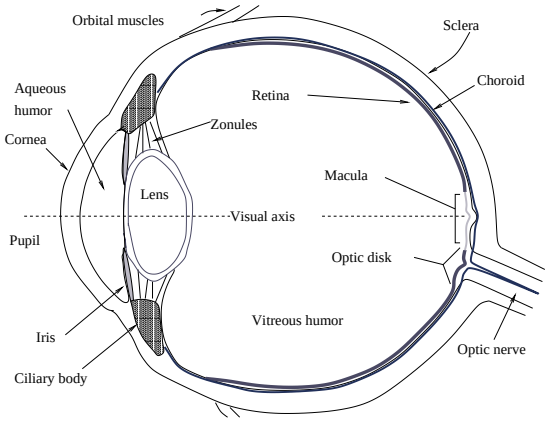

Figure 4.1: *A cut-through sketch of the eye.*

The eye is shown sketched in figure 4.1. It is a highly advanced vision system, which may be described as consisting of two parts, an optical focussing part – the anterior half, and a sensor part – the posterior half. The eye consists of (from the anterior to the posterior end) a fixed lens (the cornea) – also the entrance window to the interior of the eye, a light stop-down mechanism to avoid over-exposure of the retina (the iris), which also works as the limiting aperture, a flexible focussing lens (the lens – obviously) together with a bio-mechanical system (the ciliary muscles and the zonules) responsible for changing the shape of the lens, and an imaging light detector (the retina), which is connected to the

vision centre in the brain by the optical nerve. All encapsulated in a rugged, thick leather-like shell (the sclera), and equipped with a considerable "on-board" computing capacity – for contrast and line enhancement of the visual signal. The eye may be described as a sphere slightly flattened along its (optical) axis. The main refractive power actually does not stem from the lens but from the cornea, the lens mainly being responsible for the accommodation to different focal lengths – or totally about 20 % of the refractive power. The space between cornea and lens is fluid filled, while the space between lens and retina is filled with a clear gel-like substance – the vitreous humor.

Most important in this respect

What is important to consider regarding the eye in the context of lens photolytical surgery is the physical dimensions of the eye. The entrance pupil is of a limited size of approximately 1 cm across (fully dilated), which together with the distance from the cornea to the lens (centre) of approximately 5 mm limits the focussing numerical aperture for entering light beams. This has to be taken into account when designing a system for intra-lens light surgery, especially when some sort of scanning of the beam across the lens is needed. I will not deal further with the design restraints met here, as this is somewhat further down the line of system development, than I have dealt with.

4.2.1 The lens of the human eye

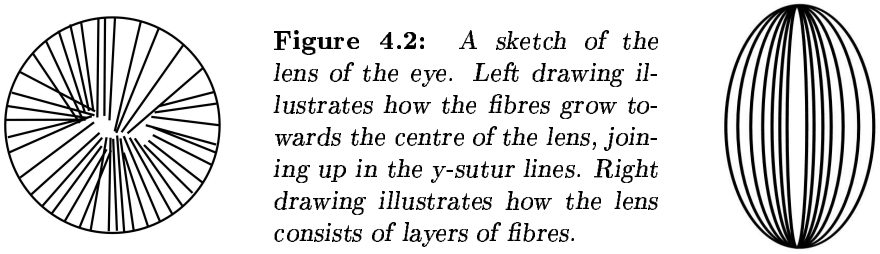

Figure 4.2: *A sketch of the lens of the eye. Left drawing illustrates how the fibres grow towards the centre of the lens, joining up in the y-sutur lines. Right drawing illustrates how the lens consists of layers of fibres.*

A brief introduction to the lens based on reference [1]. The lens is the centre of attention for this project as it deals with the possibility of treating cataract, which is a condition of the lens. The lens itself consists of an outer shell – or sack, a collagen structure. This shell is lined by an epithelial layer, which is responsible for a large part of the metabolism of the lens; metabolism also takes place in the equatorial rim of the lens. The lens itself is in virgin condition not hard but quite soft and gel-like. It has a very high protein content of about 35 %, which gives it an index of refraction of about 1.42 in average. The refractive index profile of the lens is not uniform. The outer edge of the lens has an index of 1.386, its centre – the nucleus – has an index of 1.46 [2]. It is approximately 10 mm in diameter and perfectly round normal to the optical axis, while lens shaped and approximately 4-5 mm thick along the optical axis – both dimensions for fully-grown adult lenses. The weight is about 200-250 mg. The lens can be characterised as crystalline as the structure is highly ordered. This is also the reason for its transparency and clarity – unlike any other tissue

[2] http://www.lhup.edu/ dsimanek/scenario/labman3/eye.htm

in the human body except for the cornea. The lens is made up of fibre bundles growing from the equatorial edge of the lens – the cortex, along the lens shell towards the centre (optical axis), where fibres from opposite sides meet. Fibres become hexagonal during the growth and are not cells in traditional sense, as they do not contain nuclei or mitochondria – or only traces of these.

A sketch is shown in figure 4.2. The growth of the lens fibres continues throughout the lifetime, which not only means the physical dimensions but also the density of the lens increase throughout life. The lens distinguish itself from other kinds of body tissues in that fibres – once formed – are not broken down, meaning the nucleus of the lens contains fibres as old as the person itself. This is a very important fact in the development of cataract.

4.3 Pigs eye

To give an impression of the size, consistency and composition of the eye I dissected a pigs eye[3]. From Roskilde Butcher School fresh, whole, unscalded eyes were purchased. It is important that they are not scalded as otherwise the corneas will be damaged. Eyes may be picked up just a few hours post mortem. The eyes were kept on cool until use. For storage the eyes were kept in autoclaved phosphate buffered saline solution (PBS, pH 7.2-7.4, Bie-Berntsen), with addition of cell culture medium 199 (Sigma-Aldrich, added 9.8 g/l) and a commercially available preservative (Atamon powder, Tørsleff, containing sodium benzoate, added 3.33 g/l). The whole eyes may be stored cold in this fluid for several days. The corneas will start to loose transparency within a day, but the lenses are very well preserved, as they are in a very protective, closed environment inside the (intact) eyeballs. In figure 4.3 pictures from the dissection is shown, showing in details the interior parts of the eye. Pictures 4.4 and 4.5 shows a porcine lens. Additional pictures may be found in the Appendix C.

4.3.1 TPE fluorescence images of lens tissue

During a research trip to FIBMT, Germany[4], I did several TPE fluorescence images of porcine lenses. The set-up utilised was an inverted confocal LSM (modified Zeiss Axiovert 100) coupled to a tunable femtosecond laser (Coherent Chameleon). The maximum depth reachable was about 150 μm, deeper than this and the signal-to-noise ratio became bad. Fluorescence mode microscopy did not only record the fluorescence but also the second harmonic signal. This was negligible for most tissues except collagen. In addition to fluorescence also "traditional" light microscopy images could be recorded – utilising the reflection from the sample rather than transmission. In figure 4.6 is shown a fluorescence image of the lens tissue in a depth of 25 μm from the surface of the lens.

The first 10-25 μm or so of the lens is the lens sack and epithelium, so the image is just into the crystalline lens material. On the picture the individual fibres are clearly seen. The white dots/marks seen in the fibres may be residuals from mitochondria or just highly fluorescent lumps of protein. The individual

[3]Pig lenses are very useable in this respect, as they are very close to human eyes in size, while practically identical in composition. After all, humans and pigs are – on organ level – quite close to each other.

[4]Visit kindly made possible by Dr. Karsten König.

Figure 4.3: Top left: *Eye of a pig seen from the front. The cornea is approximately 1.5 cm in diameter. The pink tissue on the sides are muscle attachments.* **Top right:** *The eye cut open. Cutting the sclera is difficult – it is very tough. The thickness of the sclera is about 1–2 mm. The black lining is the RPE. The grey sheet the tweezers are grabbing is the retina, its only loosely attached to the RPE, and seems more attached to the vitreous humor. The vitreous humor is difficult to see, but the light can be seen reflecting in it.* **Bottom left:** *The cornea. It is very clear but loses transparency when removed from the eye. Mechanical stretching as here further induces opacity.* **Bottom right:** *Close-up of the RPE, the sclera flipped inside out. Though it may seem brownish here, it is in fact very black and no details can be seen in it – it literally absorbs all incident light. The greyish retina is attached to the optical nerve coming out of the hole to the right of the centre – towards the snout.*

strains are approximately 5 μm across, with a spacing of a 2-3 μm. Additional images including a reflection image may be found in the appendix C.

4.4 Summary: Eyes

In this chapter the structures of the eye and lens have been described briefly. The lens was shown to be a highly ordered structure, consisting of hexagonal close-packed hexagonal fibres growing from the rim of the lens towards the centre. Cataract formation was briefly discussed and it was argued that glycated lysine may be a useable model system for studying cataract, as it shows the same spectroscopic characteristics as those of pentosidine and other advanced glycation end-products.

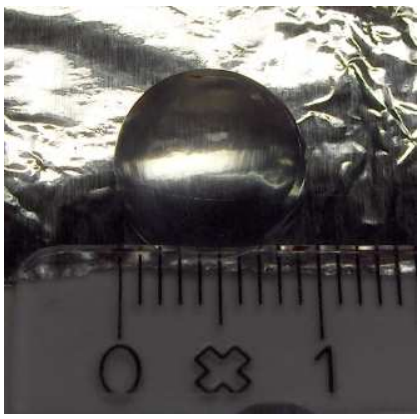

Figure 4.4: *Lens from a porcine eye seen along the optical axis. It is perfectly round normal to the optical axis.*

Figure 4.5: *Close up of a lens. The y-sutur lines may be seen on top of the lens.*

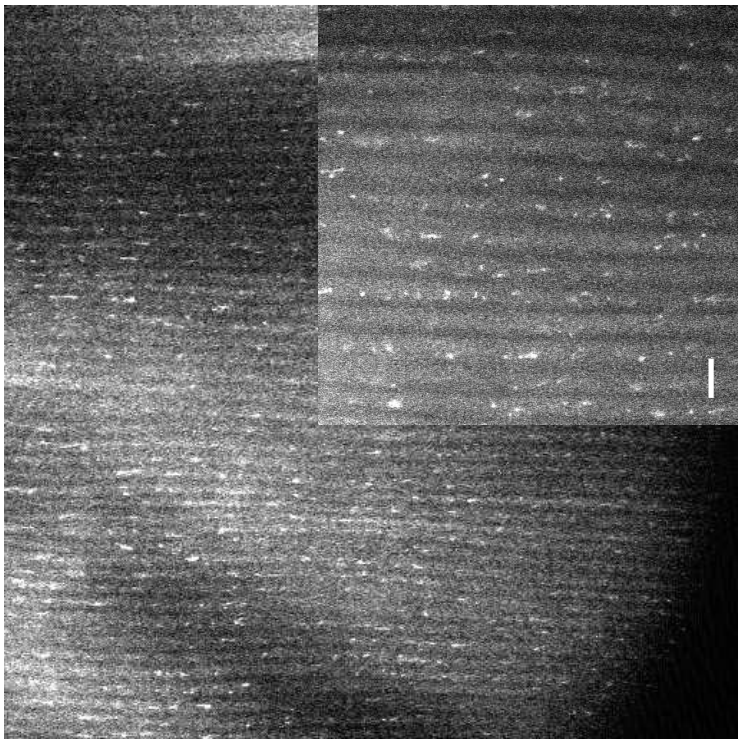

Figure 4.6: *Fluorescence LSM images of porcine lens, from a depth of about 25 μm, which is just into the crystalline lens structure, excitation wavelength 760 nm. Side length of the main image is 350 μm, on the insert the white bar is 10 μm. Individual fibres are easily seen.*

Bibliography

[1] C.A. Paterson and N.A. Delamere *The Lens*, Chapter 10, *Adler's Physiology of The Eye*; P.L. Kaufman, A. Alm, F.H. Adler, eds. (C.V. Mosby, 2002)

[2] S.K. Grandhee and V.M. Monnier, "Mechanism of Formation of the Maillard Protein Cross-link Pentosidine"; J. Biol. Chem., vol. 266, pp. 11649-11653; 1991

[3] L. Kessel, S. Kalinin, R.H. Nagaraj, M. Larsen, and L. B.-Å. Johansson, "Time-resolved and Steady-state Fluorescence of the Human Lens with Comparison to Argpyrimidine, Pentosidine and 3-OH-kynurenine"; Photochem. and Photobiol., vol. 76, pp. 549-554; 2002

[4] D.G. Dyer, J.A. Blackledge, S.R. Thorpet, and J.W. Baynes, "Formation of Pentosidine during Nonenzymatic Browning of Proteins by Glucose"; J. Biol. Chem., vol. 266, pp. 11654-11660; 1991

[5] V.M. Monnier and A. Cerami, "Nonenzymatic Browning in vivo: Possible Process for Aging of Long-Lived Proteins"; Science, vol. 211, pp. 491-493; 1981

Chapter 5

Investigation of model

> Models are to be used, not believed.
>
> Henri (Hans) Theil.
> "Principles of Econometrics"
> *Dutch economist (1924-2000)*

The first task to be completed after the initial literature studies of the eye and cataract was to find a useable model system for further studies. As the mechanisms causing cataract are not fully understood it is difficult to copy the natural process in the laboratory. Instead it was chosen to pursuit a "good guess" on one of the mechanisms involved in cataract – the glycation of lysine. As described in the previous chapter glycation of amino acids, or proteins, may be one of the main cataract forming reactions in the eye.

Following partially along the lines of the method used in reference [1] glycated lysine was investigated as the potential model system for studies of cataract bleaching. This chapter consists of results from these investigations:

- Section 5.1 briefly describes the possible reaction – Maillard and caramelisation – taking place in the sugar - amino acid mixtures. In addition results from literature studies are presented, which leads to the chosen model system (glucose and lysine).

- In section 5.2 on page 51 initial studies on browning of glucose-lysine mixture are presented. Studies include dependency of pH value on reaction speed. Transmission spectra, time and temperature dependency of chromophore yield were also investigated.

- Section 5.3 on page 55 comprehensively explains the method used for determining rest sugar content in the prepared samples. The found values are later used in the estimation of the chromophore cross section.

- Section 5.4 on page 59 presents results on caramelised glucose (incubated pure glucose mixture). Results regarding browning from this experiment is compared to the browning obtained through the Maillard reaction studied in sections 5.2 and 5.3.

- Section 5.5 on page 60 describes the method used for calculating the absorption cross section of the glycated lysine molecules, together with results hereon.
- In section 5.6 on page 63 are presented results on SPE fluorescence. Emission and excitation spectra are presented. Similarities between spectra from human eyes and glycated lysine compounds are discussed.
- Section 5.7 on page 66 present results on two-photon excited fluorescence spectra, together with a short introduction to TPE. TPE spectra are found to be similar to SPE spectra, although there are differences in detail.
- TCSPC was also performed for the glycated lysine, and results on this are presented in section 5.8 on page 69.
- Finally in section 5.9 on page 70 is a summary of the results presented in this chapter.

It should here be noted that my investigations were not meant to be a comparison between different possible model systems, as this was outside the scope of the project. Instead it was an investigation and characterisation of one possible, useable model system in order to estimate the (browning and bleaching) parameters to be used for estimating the bleaching efficiency.

5.1 Selection of model

From literature studies [1, 2] it was decided to select a model based on a non-enzymatic browning of sugars, as this is one of the proposed reactions leading to the discolouration of the lens. The non-enzymatic browning reactions, the Maillard reaction and caramelisation, are commonly studied in food science. It is responsible for the browning processes found in for instance such areas as brewing of beer and baking.

5.1.1 Maillard reaction

An introduction to the Maillard reaction and the effects of pH value may be found in the literature [3, 4]. The Maillard reaction links the carbonyl group of carbohydrates with the free amino group of amino acids, creating amongst other reaction products some highly brown compounds. Strongly absorbing compounds are created both in the intermediate stages of the reaction, as well as in the final, where the resulting polymeric compounds are also strongly absorbing and brown coloured. In a mixture of sugar and amino acid both the caramelisation and the Maillard reaction are responsible for producing brown reaction products. The speed of the individual reactions depends strongly on the type of amino acid added to the sugar solution, as well as on pH value. In reference [3] it is found that lysine is the amino acid forming most brown compound when added to glucose. In addition it was found that the degradation of glucose was lower when an amino acid was added – indicating the amino acid has some protective effect on the caramelisation of sugar. However the total absorption was higher in the case when an amino acid was added as when compared to the pure glucose incubated solutions. In both references [3, 4] it

was found that the reaction speed as well as the terminal level of browning were strongly depending on pH value, where the higher the pH the faster/stronger browning occured (in the tested pH-value range 4.0-12.0). It was also found that both the Maillard reaction as well as the caramelisation reaction showed this dependence on pH value.

Selection of reactants

Based on the literature studies of [1, 2, 3, 4] it was decided to investigate a model based glucose and lysine. In references [1, 2] the authors specifically suggest glucose-lysine Maillard reactions to be part of the process causing browning in the lens of the eye. The authors use argpyrimidine in addition to lysine; I chose to use lysine alone, as this was a simpler model system to investigate – giving fewer free variables and thus a more clear and predictable behaviour. In addition, lysine is the amino acid giving the strongest browning of sugar [3, 4]. No other sugars and/or amino acid combinations were studied, as it was outside the scope of this project to investigate Maillard rections in general – the scope was merely to select a promising system and study this.

5.2 Evaluation of glycated lysine compounds

Different mixtures and means of producing coloured (browned) glucose-lysine mixtures were investigated, and the results have been compared. It was found that the mixtures do not react, or only very slowly, in ambient room temperature, whereas a heating speeds up the process considerably. Different pH values, incubation times, and incubation temperatures were evaluated.

5.2.1 Preparing the mixtures

In the Appendix D is presented a comprehensive recipe and details on how the glycated lysine was made. The concentration was from the beginning chosen to be 0.1 M in both glucose and lysine. As this gave a strong browned mixture without the need for excessive dilution, and as it was relatively easy to handle the required amounts of chemicals needed for this strength, this concentration was used as standard. Batches 1, 2 and 3 (see table 5.1) were prepared with different buffers to test the influence of pH value on the reaction.

Batch#	pH	Glucose	Lysine	Buffer
1	8.9	100mM	100mM	Borate pH 9
2	9.2-9.3	100mM	100mM	Water
3	7	100mM	100mM	Phosphate 1/15M pH 7

Table 5.1: *The constituents of the different, mixed test batches.*

The main tool for evaluation of the different samples were transmission measurements. Transmission measurements were carried out in a photospectrometer (Cary 3, Varian Australia). For the measurements a diluted sample (dilution dependent on the chromophore concentration of the sample – to get the absorbtion down to a measurable level) was measured against a water blank – both

in 10 mm pass length cuvettes. The measurements were reproducible within approximately plus/minus one percent.

5.2.2 Test for pH dependence

Glycated lysine mixtures from batches 1, 2, and 3 – see table 5.1 – were incubated at 65 C for 48 hours. Comparative transmission data for these five samples are shown in figure 5.1.

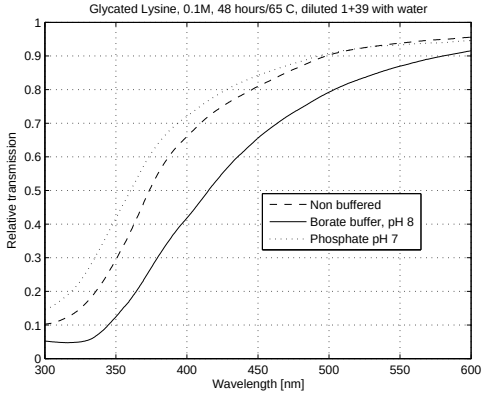

Figure 5.1: *Transmission of differently prepared glycated lysine mixtures, incubated 48 hours at 45 C. Samples were from batches "1" (borate buffered), "2" (non-buffered), and "3" (phosphate buffered).*

As seen from figure 5.1 the use of buffer influences heavily on the transmission spectra post incubation in a way similarly to found in literature [3] – the higher the pH value the stronger the browning. The pH value of the non-buffered solution was measured to around 9.2-9.3. In addition to influencing the chromophore yield/transmission spectra the pH value has a large influence on the fluorescence of the post reaction mixture [1].

Based on the concerns that the use of a pH environment different than in the lens of the eye could result in data of little or no interest to the problem at hand, it was chosen to focus investigations on mixtures buffered to around pH 7 – as the pH value in the lens of the eye.

5.2.3 Temperature dependence

In order to test the temperature dependence of the browning process samples of 0.1 M glycated lysine in 1/15 M phosphate buffer pH 7 were incubated for 48 hours at 45 C, 55 C, 65 C, and 75 C. As reaction speed increases with increasing temperature, and nothing foul was happening at the highest temperature tested, it was decided to use 75 C as the incubation temperature. The transmission plots for the four different temperatures are shown in figure 5.2.

[1] Private communications with Line Kessel, Department of Ophthalmology, Herlev Hospital

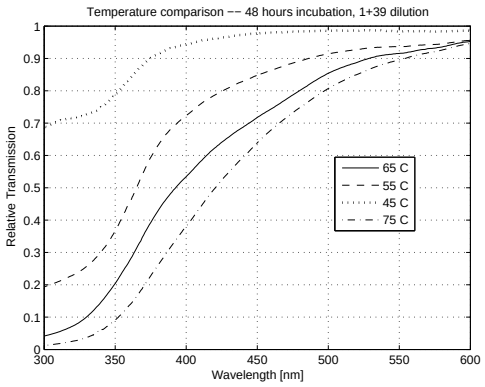

Figure 5.2: *Transmission of glycated lysine mixtures incubated at different temperatures; all samples incubated 48 hours and mixed of 0.1M glucose and lysine in 1/15M phosphate buffer pH 7.*

To further illustrate the dependence the transmission at specific wavelengths were measured and plotted against incubation temperature. Looking at the transmission plots in figure 5.2 multiple absorption peaks may be seen. Two kinks are seen on the transmission curves – most clearly on the 45 C sample, around 340 nm and around 375 nm. To cover both ends of the absorption spectrum 325 nm and 400 nm were selected for comparison – see figure 5.3.

From the figure it is noticeable that the browning have different dependence on incubation temperature for different wavelengths. The fits are overlaid to illustrate this behaviour. While the 325 nm absorption line is best fitted by a second order polynomial, a first order polynomial is enough to describe the 400 nm absorption line. Most likely two or more different reaction products having different absorption spectra and reaction kinetics are involved in the final colouring of the incubated mixture. At 48 hours and up to 75 C of incubation no tailing off of any of the absorption lines were seen. It was decided 75 C was a useable temperature for incubation, as no foul side effects were noted after 48 hours at this temperature, when compared to lower temperatures.

5.2.4 Incubation time

To find the dependence of incubation time on the resulting chromophore concentration a mixture of 0.1 M glucose and lysine mixed in phosphate buffer pH 7 were incubated at 75 C for 72 hours. Samples were taken from the incubated mixture after 24 and 48 hours. Transmission measurements of the samples were done against water blanks in UV macro cuvettes. The dilution of the samples to make the absorption measurable was 100 μL of sample plus 3900 μL of distilled water (40 times volume increase corresponding to 1+39 dilution). The resulting transmission curves are shown in figure 5.4.

The transmission curves in figure 5.4 for the samples incubated 48 and 72 hours are interesting in that they are exactly similar. Re-checking everything confirmed this. This should mean that the chromophore concentrations are the

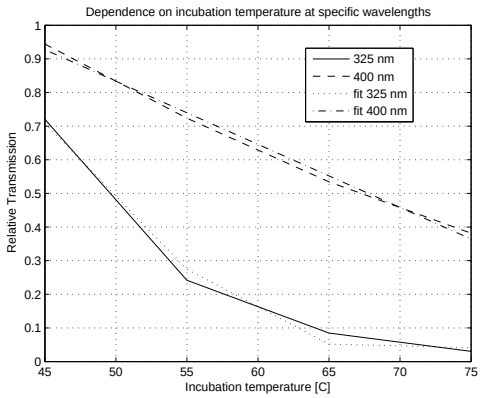

Figure 5.3: *Transmission of glycated lysine mixtures incubated at different temperatures at 325 nm and 400 nm. All samples were incubated 48 hours and was mixed to 0.1M strength in glucose and lysine in 1/15M phosphate buffer pH7. The data-fits illustrate the dependence on temperature. 325 nm fit is in second-order ($y = p_1 \cdot x^2 + p_2 \cdot x + k$), with parameters $p_1 = 0.0011$ and $p_2 = -0.1495$. 400 nm fit is in first-order ($y = p_1 \cdot x$), with parameter $p_1 = 0.0188$.*

same for the two samples. Which in turns means the reaction must have reached stability after less than 48 hours. Reaction speed is considerably higher at 75 C than at lower temperatures so reaching some equilibrium within 48 hours is likely. Features regarding rest sugar content are described in section 5.3.

5.2.5 Influence of non-reacted glucose and lysine

In order to evaluate the influence of non-reacted glucose and lysine in the incubated mixes, transmission spectra were recorded for the pure substances. These are shown in figure 5.5.

The figure shows that glucose has little absorption in the measured wavelength range; residual glucose does not influence on the transmission spectra for the browned mixtures. Lysine has some absorption in the short wavelength range; the mixture itself is also pale yellow so this is no surprise. The concentration in this measurement (100 mM) is much higher than in the measured (diluted) samples of the browned mixture. Residual non-reacted lysine probably does not contribute significantly to the absorption in the browned samples.

In section 5.4 are presented results for incubated pure glucose.

5.2.6 Selecting the model system incubation parameters

Based on the results from the experiments with varying incubation time, temperature and pH value, it was decided to use a 0.1 M glucose-lysine mixture in phosphate buffer pH 7 incubated for 48 hours at 75 C as the standard sample for the bleaching experiments. This gives a sample with a good chromophore

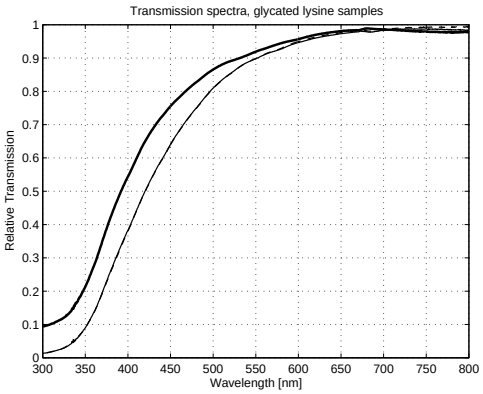

Figure 5.4: *Incubation time dependence on transmission for glycated lysine. Thick solid curve is incubated 24 hours, thin solid and thin dashed curves are for 48 and 72 hours respectively. Dilution is 1+39 with distilled water prior to measurement. The incubator temperature was 75 C.*

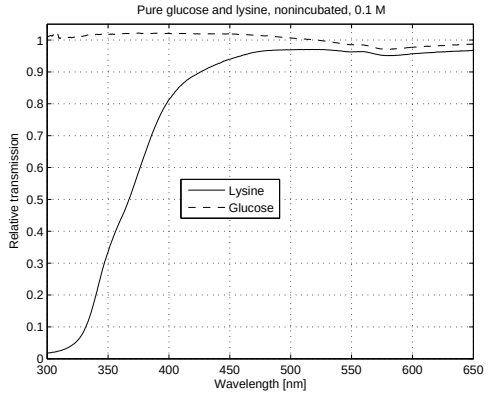

Figure 5.5: *Transmission measurements on pure glucose and lysine (0.1 M strength mixed in distilled H_2O).*

yield and a lack of spurious side effects. In the following section 5.3 the standard sample is analysed with respect to remaining glucose post incubation, together with samples incubated for 24 hours and 72 hours – for comparison.

5.3 Test for rest sugar content

The yield of the reaction depends on the concentration of reactants. Therefor measuring the rest sugar content should give an idea of how much glycated lysine had been formed, and if any slowing up of the reaction speed would be observable in this 72 hours test. The test material was 0.1 M glucose/lysine

strength mixed in phosphate buffer pH 7, and incubated for 72 hours at 75 C. Samples were taken from the mixture in the oven after 24 hours and 48 hours. To estimate the rest sugar content Glucose Hexokinase was utilised. A test kit meant for automatic testing was acquired (Glucose HK, ABX, Montpellier, France). This is commonly used in testing sugar levels in commercial testing equipment. As we do not have such equipment the procedure was modified to allow the use of our spectrophotometer (Cary3, Varian Pty.)The procedure for testing was as follows [2]:

First some Glucose HK is prepared. The test kit consists of a separate-room container containing substances 1 and 2. The preparation consists of mixing 1.2 measures of substance 1 with 4.6 measures of substance 2. The test kit is now ready to be used. The test measures the transmission of the test sample at 340 nm in a spectrophotometer. In the normal automatic apparatus for testing 2.5 μL sample is mixed with 10 μL water and 240 μL of mixed Glucose HK. As I used 1.5 mL volume cuvettes (PS UV semi-micro cuvettes, Bie&Berntsen, optical path length 1 cm) considerably larger portions had to be prepared for the transmission measurement. This was done by first mixing 50 μL of the sample to be tested with 200 μL of distilled water. 50 μL of this mix was subsequently mixed with 960 μL of Glucose HK in the semi-micro cuvette. The cuvette was placed in water kept at 37 (+/- 1) C for 6 minutes. Transmission was then measured at 340 nm in our spectrophotometer. The reason for using these volumes were that the smallest pipette available in our chemistry lab was a 50 μL micropipette. Volumes 100 μL and up were measured with a digital Finnpipette (Thermo Electron Corporation).

Then a scale was established. This was done by measuring a set of samples with a known sugar content (gauge samples). Glucose gauge samples with glucose concentrations of 4 mM, 6 mM, 8 mM, 10 mM, and 12.5 mM were measured. In addition a water gauge was also measured. Results from the measurements on the gauge samples are shown in table 5.2. As seen from the calculated absorptivities for the gauge samples the linearity improves with increasing glucose concentration, in the detectable range from 0.1 mM to 33.3 mM. Due to the exponential nature of the absorption law this is as expected, and a small error in the measurement will have a large influence on the calculated absorptivity for low concentrations of glucose. So the highest possible gauge giving a transmission value in the same order of magnitude as the glycated lysine samples should be used.

These samples were treated and measured in the same way as the glycated lysine samples. From these measurements a scale was made. The absorption follows Beers law:

$$\ln(I/I_0) = -\sigma_{mol} \cdot n \cdot l \tag{5.1}$$

Where I is the transmission, I_0 is the blank transmission, σ_{mol} is the molar absorptivity (unit $\mathrm{cm}^{-1}\mathrm{mM}^{-1}$), n is the molar concentration (in mM), and l is the optical path length (in cm). The glycated lysine samples were first tested undiluted. As this was found to be a too high glucose concentration to yield good results the samples were subsequently diluted. Different dilutions also

[2]The procedure was instructed to me by Susanne Christensen from Triolab, Brøndby, Denmark (the vendor) as especially modified to my needs and equipment. Therefor it may vary slightly from the factory specified procedure.

Gauge sample	Concentration	Transmission coefficient	Calculated absorptivity [$mM^{-1}cm^{-1}$]
Water	–	50.7%	–
Glucose	4 mM	30.1%	0.130
Glucose	6 mM	24.1%	0.124
Glucose	8 mM	17.1%	0.136
Glucose	10 mM	13.2%	0.135
Glucose	12.5 mM	9.3%	0.136

Table 5.2: *Gauge measurements – the glucose gauges for the rest glucose estimation measurements.*

allowed cross-checking of the results. Most samples, as well as the gauge samples, were measured twice in either same or two different dilutions in the initial measurement series. To increase statistical significance the measurements series – including the gauge measurements – were randomised. The measurements were done against air blank, hence the rather low transmission values. The measurement results are shown in table 5.3.

Sample	Concentration	Uncorrected	Filter factor	Corrected
Water gauge	–	50.7%	1	50.7%
GL 24 hours	1+2	7.2%	0.78	9.2%
GL 48 hours	1+2	12.1%	0.70	17.3%
GL 48 hours	1+2	12.3%	0.70	17.6%
GL 72 hours	1+2	13.5%	0.64	21.1%
GL 72 hours	1+3	19.9%	0.75	26.5%

Table 5.3: *Data for the filter factors for glycated lysine (GL).*

5.3.1 Filter factor

The filter factor is the inner filter effect in the samples. The glycated lysine compound is strongly absorbing in the UV range of the electromagnetic spectrum. It was therefore necessary to correct the data for the absorption due to glycated lysine chromophores. This was done by measuring the transmission of the glycated lysine samples at 340 nm in the same chromophore concentrations as used for the rest glucose measurements. The results are summarised in table 5.3. The corrected results in table 5.3 are calculated as the uncorrected transmission coefficient divided by the filter factor.

5.3.2 Setting the scale and results

From Beer's Law given above in equation 5.1 the molar absorptivity can be extracted. The blank transmission I_0 is here the transmission of the water gauge sample (against air blank). So I_0 is equal to 0.507 (average values are

used). Then for the 4 mM sample $I = 0.507 \cdot \exp(-\sigma_{mol} \cdot n \cdot l) = 0.301$ or $0.301/0.507 = 0.594 = \exp(-\sigma_{mol} \cdot 4\ mM \cdot 1\ cm)$. This gives for the molar absorptivity $\sigma_{mol} = -ln(0.594)/4 = 0.130\ mM^{-1}cm^{-1}$. This result may be checked with the result obtained for the 8 mM glucose gauge sample yielding $I/I_0 = 0.171/0.507 = 0.337 = \exp(-\sigma_{mol} \cdot 8\ mM \cdot 1\ cm)$, which in turn gives $\sigma_{mol} \cdot 8\ mM \cdot 1\ cm = -ln(0.337) = 1.09$ and from this $\sigma_{mol} = 1.09/8 = 0.136\ mM^{-1}cm^{-1}$.

The next step is applying the found molar absorptivities on the glycated lysine samples to extract the rest glucose concentrations. The results are calculated utilising Beer's Law as $I = 0.507 \cdot exp(-0.136\ mM^{-1}cm^{-1} \cdot 1\ cm \cdot n)$, which leads to $n = -ln(I/0.507)/0.136$. Taking as an example the sample incubated 24 hours and diluted 1+2 with water, the transmission was measured to 0.092 after correction for inner filter effect – see table 5.3. So $n = -ln(0.092/0.507)/0.136$, which gives $n = 12.5\ mM$ – in the diluted sample, so in the undiluted sample $3 \cdot 12.5\ mM = 37.5\ mM$. For the 72 hours sample the measurement with 1+2 dilution gives a concentration in the undiluted sample of $3 \cdot 5.3\ mM = 15.9\ mM$, and the 1+3 diluted sample measurement gives a concentration in the undiluted sample of $4 \cdot 3.8\ mM = 15.2\ mM$. The repetition accuracy is sufficient for giving estimates on the rest sugar content.

Results for glycated lysine samples are given in table 5.4. It may be argued it is better to use either a mean value for the absorptivity than using the values from the gauge measurement closest in transmission, or use the value 0.136 $mM^{-1}cm^{-1}$ from the gauge measurements with the highest concentration. The last argument based on the presumably higher significance in this more linear region. An average value based on all gauge measurements gives 0.132 $mM^{-1}cm^{-1}$. In table 5.4 all three methods are compared. Most significant absorptivity is 0.136 $mM^{-1}cm^{-1}$. For the samples incubated 24 and 48 hours the difference is insignificant. For the 72 hours sample the difference is around 10%. Subsequently, the result for 12.5 mM gauge sample was used, as this was considered to be most linear.

Sample Glycated Lysine	Dilution	Closest gauge	Average gauge	12.5 mM gauge	Concentration in undiluted sample
24 hours	1+2	12.5 mM	12.9 mM	12.5 mM	37.5 mM
48 hours	1+2	7.8 mM	8.1 mM	7.8 mM	23.4 mM
72 hours	1+2	7.1 mM	6.6 mM	6.4 mM	19.2 mM
72 hours	1+3	5.2 mM	4.9 mM	4.8 mM	19.2 mM

Table 5.4: *Comparison of rest glucose concentrations based on different values for the absorptivity – depending on the gauge used. Undiluted concentrations based on 12.5 mM gauge.*

As found in section 5.2.4 the browning had reached an equilibrium after around 48 hours of incubation – the spectra for 48 hours and 72 hours were found to be almost identical. Still, the rest glucose concentration kept dropping after the (assumed) equilibrium had been reached. This indicates that "something" was still happening to the rest glucose after browning had stopped. This could be some kind of polymerisation, either between the glycated lysine molecules

and the glucose molecules, or between the glucose molecules themselves, creating longer sugar molecules not responding to the glucose hexokinase reaction. Or possibly the Glucose HK test only measures for the D-isomer of glucose, and glucose may change to the L-isomer when heated. I had no means for testing these hypotheses.

5.4 Incubation of glucose

Glucose was incubated pure at 45 C, without any noticeable browning taking place within a timescale of a few days. But it could be possible that the reaction for pure glucose just is too slow, or not taking place at all at this temperature. To test this D-Glucose was mixed in phosphate buffer 1/15 M pH 7 to a concentration of 0.1 M. This was then put to incubate at 75 C. Samples were taken out after 0, 24, 48 and 72 hours. The samples were then measured for glucose content with the glucose hexokinase test, utilising the absorptivity value of 0.136 $mM^{-1}cm^{-1}$. The tests were performed as described previously, except to get the absorption down to a measurable level the samples were diluted 1+7 with distilled water prior to testing. Results from this test are shown in table 5.5.

Incubation time	Measured transmission	Calculated glucose concentration	Undiluted glucose concentration
Water blank	45.60%	–	–
0 hours	8.30%	12.5 mM	100 mM
24 hours	9.20%	11.8 mM	94.2 mM
48 hours	10.70%	10.7 mM	85.3 mM
72 hours	11.30%	10.3 mM	82.1 mM

Table 5.5: *Transmission values and glucose concentrations for incubated pure glucose samples.*

As seen there is a reduction in glucose concentration following incubation. In addition the samples turn increasingly yellow with increasing incubation time. Figure 5.6 shows transmission curves for 48 hour incubated pure glucose samples. From the figure it is seen that the absorption is much more peaked than for glycated lysine; two peaks – or dips in the transmission spectrum – are seen, one around 360 nm, and another, weaker, around 335 nm. In addition below 310 nm the transmission drops again. However, diluted to "bleaching-strength" – 1+29 with distilled water – the absorption becomes insignificant at the bleaching wavelengths 392 nm and 405 nm.

From this I will assume that the part of the absorption belonging to caramelised glucose is insignificant in the bleaching samples. In addition in the glycose-lysine mixture there is a strong competition for glucose, therefore it is unlikely the caramelisation of glucose would lead to a significant yield in chromophores as this reaction is the slowest – as seen from the experiments. From data in table 5.5 a 15% drop in rest sugar level after incubating for 48 hours was found. For the glucose-lysine mixtures the drop after similar incubation time is more than 76%, so the pure glucose reaction is slowest by a factor of 5. Still it may be partly responsible for the continued drop in sugar level after the chromophore

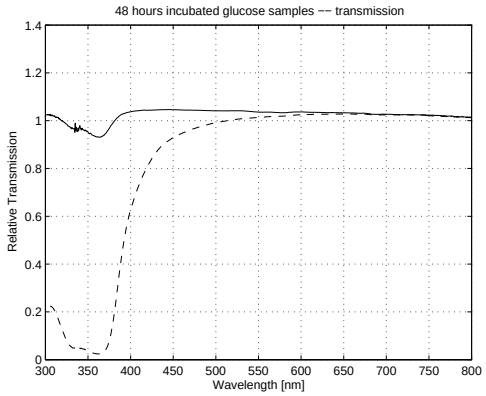

Figure 5.6: *48 hours incubated 0.1M glucose samples in phosphate buffer. Dashed line is undiluted, solid line is in 1+29 dilution. Higher than 1 transmission is not a measurement error, as the higher refractive index of the sugarised water gives lower reflection at water-cuvette interfaces than the pure-water blank.*

production after to the Maillard reaction seemingly has stopped.

5.5 Calculation of chromophore cross section σ_{abs} for the glycated lysine samples

To calculate the absorption cross section of the glycated lysine molecules, the found concentrations together with the found transmission values were used. A few assumptions have to be made to extract the cross section from these measurements, though these assumptions may be in contradiction with the results found in general. First of all it is not known what the exact outcome of the browning reaction is, as I had no means of checking this. Therefore there might be other reaction products, which may be absorbers as well. It was therefore assumed that the only chromophores in the incubated mixture were glycated lysine molecules. Second it was assumed each lysine molecule eats one and only one glucose molecule during the incubation. If this was not the case, or if any other reaction may happen to the glucose molecules in such a way they do not take part in the glucose hexokinase reaction, the estimated rest glucose concentration is wrong, and thus the concentration of glycated lysine molecules post reaction is also wrong, as the concentration of glycated lysine is based on the assumption that every reacted glucose molecule has been incorporated in one and only one glycated lysine molecule. Finally it is assumed no polymerisation has taken place; polymerisation might take place between glucose molecules alone, or between glycated lysine molecules, or between a mix of these two molecules. Polymerisation involving glucose molecules could change the yield of the glucose HK reaction, likewise polymerisation involving glycated lysine molecules could change the absorption properties of these in an unpredictable way.

So to recap, it was assumed that by measuring the rest glucose concentration the concentration of glycated lysine chromophores can be estimated as the "missing" amount of glucose. And the absorbers in the transmission measurement are only the glycated lysine molecules. In the light of the slightly suspicious results regarding the similar transmission curves for the 48 and 72 hours incubated samples and the drop in rest glucose concentration for the same two samples, these assumptions clearly do not hold completely. So to minimise the influence from any polymerisation or other glucose consuming process it was decided to use the 48 hours incubated sample for calculating the cross section as well as for for the bleaching.

With the notation used here stating the molar absorptivity per mM per cm, the absorptivity σ_{mol} is related to the absorption cross section σ_{abs} by the relation $\sigma_{mol} \cdot n\,[mM/L] = \sigma_{abs} \cdot n\,[molecules/cm^3]$, where n is the concentration. The absorption cross section of the glycated lysine molecule is the "size" of the molecular transition, which gives the transition probability for a given flux. In a 1 mM solution there is (Avogadro's number divided by 1000) molecules per litre or (Avogadro's number/1000)/1000 molecules per cubic cm. Avogadro's number is $6.02214199 \cdot 10^{23}$, so a 1 mM solution contains $6.02214199 \cdot 10^{20}$ molecules per litre, or $6.02214199 \cdot 10^{17}$ molecules per cm^3. As it was decided to use the 48 hours incubated sample the values for this were used. Also the 24 hours incubated sample was evaluated, as this might have a higher purity in chromophore content. The 48 hours incubated sample had a rest glucose content of 23.4 mM in the undiluted sample – refer to table 5.4. The chromophore concentration for this sample was then estimated under the assumptions mentioned above to be 100 mM (the initial concentration of glucose) minus 23.4 mM, giving a chromophore concentration of 76.6 mM. This corresponds to $76.6 \cdot 6.02214199 \cdot 10^{17}$ chromophores per cm^3, or $46.1 \cdot 10^{18} cm^{-3}$. The measurement series for the 24 and 48 hours incubated samples are shown in figure 5.4, where the samples were diluted 1+39 with distilled water prior to measurements. This means that the chromophore concentration is 1/40 of the concentration in the undiluted samples, or $(46.1 \cdot 10^{18})/40 = 11.5 \cdot 10^{17}\, cm^{-3}$. For the 24 hours incubated sample the rest glucose content was estimated to 37.5 mM in the undiluted sample. This gives a chromophore content of $100 - 37.5 = 62.5\, mM$, or $62.5 \cdot 6.022 \cdot 10^{17} = 37.6 \cdot 10^{18}$ cm^{-3} in the undiluted sample and $94.1 \cdot 10^{16}\, cm^{-3}$ in the sample used in the transmission measurement. The values on the y-axis on the transmission plot 5.4 is already I/I_0, as the transmission is measured against a water blank. As before Beer's Law equation 5.1 is applied:

$$\ln(I/I_0) = -\sigma_{abs} \cdot n \cdot l \Rightarrow \sigma = \frac{-ln(I/I_0)}{n \cdot l} \tag{5.2}$$

A "cross section plot" is shown in figure 5.7. The values of the estimated cross sections for the 24 hours and 48 hours incubated samples are comparable. The numerical differences are largest at the short wavelength end. Differences may be due to a combined effect of slight errors in the estimates of chromophore content, and the difference in glucose content, which may be influential either through the absorption in glucose, or the influence of the glucose on the chromophore cross section. If any polymerisation or other reaction has taken place between any of the components this may also lead to additional errors. In table 5.6 are shown the most interesting cross sections for the 48 hours sample.

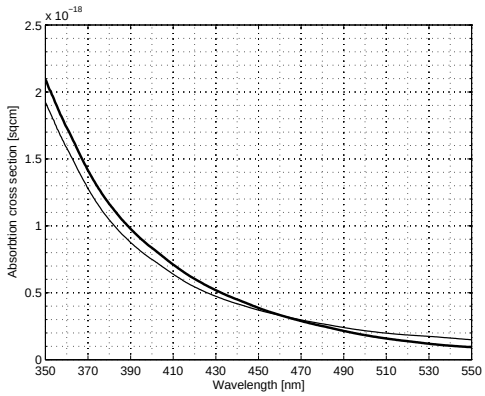

Figure 5.7: *Absorption cross sections for samples incubated 24 hours (thin line) and 48 hours (thick line).*

Wavelength	355 nm	392 nm	405 nm	785 nm	809 nm
σ_{abs} $[10^{-19}\,cm^2]$	19.1	9.46	7.85	0.138	0.150

Table 5.6: *Cross sections measured on the 48 hours incubated sample.*

As a test the calculated cross sections were used for calculating the transmission coefficients at specific wavelengths of a sample diluted 1+29 as used in the bleaching experiments. Calculated coefficients are in table 5.7 compared with measured transmission coefficients from a real sample with same dilution.

Wavelength	355 nm	392 nm	405 nm
Relative transmission, measured	6.5%	26.2%	33.7%
Relative transmission, from cross section	5.3%	23.4%	29.9%

Table 5.7: *Transmission for glycated lysine samples incuabted for 48 hours and diluted 1+29 with distilled. Compared to values calculated from measured glucose concentrations and transmission coefficients.*

The comparison in table 5.7 is quite important. When the quantum efficiency is calculated in section 6.1.4, the actual transmission coefficients measured on the bleached and control samples are used for calculating the chromophore concentrations before and after bleaching. The concentrations are used for calculating the quantum efficiency. For these calculations the initial glucose concentration is also used. So calculations for the quantum efficiency use values measured on different sets of samples, and therefore these values should be credible. The deviations between the measured and calculated values of about 10% were within what must be considered the "tolerable range" for such experiments. More comments on this in section 6.1.5.

Comparison with endogenous chromophore and commercial laser dye

Finding data for cross section for chromophores naturally occurring in the human body is not an easy task, as most references are concerned with emission and excitation spectra. Finally the most commonly investigated chromophores are connected with tissue, such as NADH, and tryptophan. For the latter, which is also found in the eye, reference [5] states the peak molar absorption coefficient to be 5.6 $mM^{-1}cm^{-1}$ at 278 nm, which may be recalculated into an absorption cross section of $9.3 \cdot 10^{-18}\, cm^2$[3]. A commercial laser dye such as the xanthene dye Rhodamine 6G has a peak absorption coefficient around 105 $mM^{-1}cm^{-1}$ at the absorption peak at 530 nm [6], corresponding to a cross section of $1.74 \cdot 10^{-16} cm^{-2}$.

5.6 Glycated lysine measurements

The glycated lysine was measured for SPE and TPE fluorescence. In addition TCSPC was performed. All this work was performed at Uppsala University, Department of Physical Chemistry, kindly made possible through the collaboration with Professor Lennart Johansson, Umeå University, Department of Biophysical Chemistry; and with help, guidance, equipment operation, good advises, and lunch break company provided by Dr. Emad Mukhtar and Ph.D. Student Linus Ryderfors.

5.6.1 Sample preparation

The samples were prepared as discussed in detail in the appendix section D, albeit with a slightly different mixture: In phosphate buffer pH 7 D-Glucose and L-Lysine were measured off to a strength of 0.2M (both chemicals) and mixed. The samples were incubated at 55 C for 72 hours. A plot of the relative transmission is show in figure 5.8, together with a plot for the relative transmission for a 0.1 M sample incubated at 75 C for 48 hours for comparison. The general shape of the absorption curves are alike, although the absorption is stronger for the 0.1M curve.

To use this mixture instead of the standard incubated at 75 C for 48 hours was not the optimal choice – especially when considering the reaction speed difference between absorption lines at 325 and 400 nm, as noted in section 5.2.3. However this mixture was ready at hand (as an experimental mixture) at the time of these fluorescence experiments, and due to circumstances this was then used for the measurements in Sweden.

In table 5.8 is a comparison of the absorption cross section for a standard 0.1 M, 48 hours, 75 C incubated sample, and for a sample used for the measurements in Sweden – at some distinct wavelengths. Looking at the absorption cross section rather than the relative transmission removes the dependence on final concentration (dilution). The glucose content after incubation was measured – utilising the method described in section 5.3 – to 35 mM in the samples used in Sweden. This gives a chromophore concentration for the diluted sample shown in figure 5.8 of $99.3 \cdot 10^{16} cm^{-3}$. The cross sections were found utilising

[3]Cross section values can only be directly compared if they are measured at the same wavelengths. At 278 nm the studied glycated lysine molecule has a much larger absorption than at around 400 nm, but my spectrophotometer does not measure well under 300 nm.

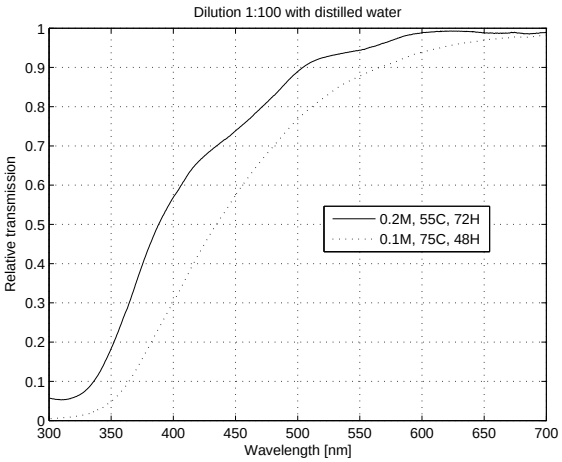

Figure 5.8: *Comparison of samples – 0.2M incubated 72 hours at 55 C, and 0.1M incubated 48 hours at 75 C.*

the method for calculating cross sections described in section 5.5, and the data used were the found chromophore concentrations and the relative transmission values.

Wavelength	355 nm	392 nm	405 nm	785 nm	809 nm
0.1M/48H/75C	19.1	9.46	7.85	0.138	0.150
0.2M/72H/55C	15.1	6.51	5.26	0.389	0.403

Table 5.8: *Comparison of the cross sections at some distinct wavelengths of the sample used in the Sweden measurements and of the standard 0.1M 48 hours, 75 C incubated sample. Cross sections are given as* σ_{abs} $[10^{-19}\,cm^2]$.

The comparison in table 5.8 shows that cross section values are in the same order of magnitude, and show the same wavelength dependence. However the values for the 0.1M sample incubated at 75 C are 25-50% higher in the blue end of the spectrum, while it is approximately 50% lower in the red end of the spectrum. It shows that a lower temperature and longer incubation does not produce the same result as when incubated for a shorter time but higher temperature. However, the results are similar enough to expect the trend of the recorded fluorescence spectra to be valid also for the "standard" samples – at least when considering the absorption cross sections.

5.6.2 Fluorescence spectra

SPE fluorescence spectra were measured in a spectrophotometer (SPEX Fluorolog). This instrument allows you to fix a desired emission wavelength, and scan the excitation (a so-called excitation spectrum), or fix the excitation wavelength and scan the emission (a so-called emission spectrum – also the most

commonly looked at[4]). The sample was diluted to about 0.5 in optical density[5] at 350 nm. In order to be able to compare with recorded data taken from human lenses, an array of emission and excitation wavelengths were used. For emission spectra 335, 350, 360nm, and 400nm excitation was used. For excitation spectra the measured emission lines were 420nm and 470nm. Peak values from excitation and emission recordings are not comparable.

SPE fluorescence spectra

Curves for emission are plotted in figure 5.9, and curves for excitation are plotted in figure 5.10. For comparison curves for cataractous lenses from are shown in figure 5.11 (emission), and figure 5.12 (excitation) – adapted from [8].

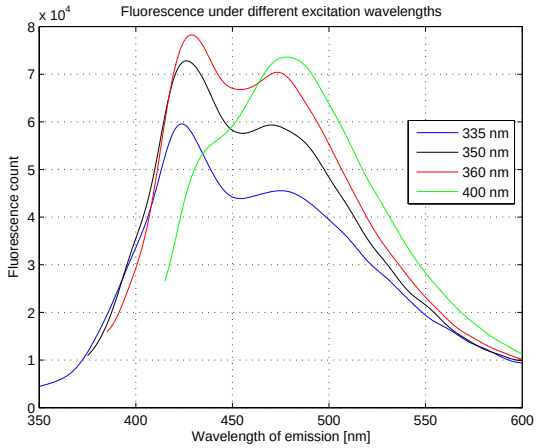

Figure 5.9: *SPE fluorescence emission spectra for glycated lysine. Smoothed data, smoothing window 15 points.*

A direct comparison between figures 5.9 and 5.11 shows some interesting details. First of all, for the spectra of the lens there is a sharp peak in fluorescence around 425 nm. In addition there is a smaller peak – a hump – around 480-500 nm. On the emission spectra of glycated lysine the same trend is seen, a peak in fluorescence around 425 nm as well as a fluorescence peak around 480 nm. The difference is that the relative strengths of the emission peaks for the glycated lysine are different. At an excitation wavelength of 400 nm the fluorescence line at 480 nm dominate in glycated lysine, and is quite pronounced even at shorter excitation wavelengths. So though the glycated lysine and lens spectra are not exactly similar they still contain common features.

Comparing figures 5.10 and 5.12 for the excitation spectra it is again seen that the spectra are of same kind, though not identical in relative excitation line strengths. On figure 5.12 is vaguely seen two excitation peaks, one around 340 nm and one around 380 nm – last one for 470 nm emission only. On figure 5.10

[4]It is generally assumed the emission spectrum is largely independent on the excitation wavelength, as long as the latter is "short enough" [1].

[5]Optical density is given as $\log(1/T)$, where T is the relative transmission.

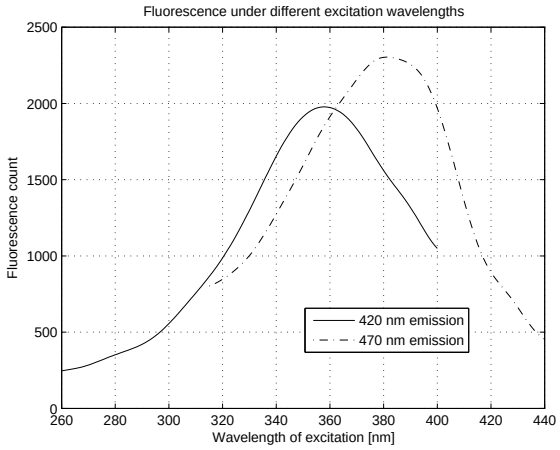

Figure 5.10: *SPE spectra for glycated lysine. Smoothed data, smoothing window 15 points.*

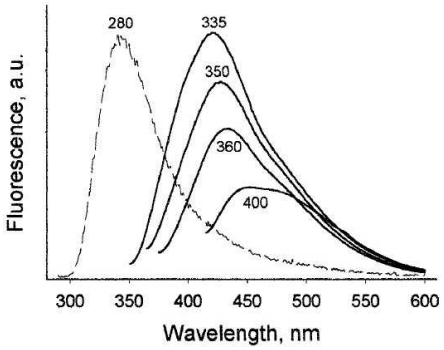

Figure 5.11: *Emission spectra for a typical cataractous lens. Dashed line is tryptophan fluorescence and can be ignored in studies of cataract. Figure adapted from reference [8].*

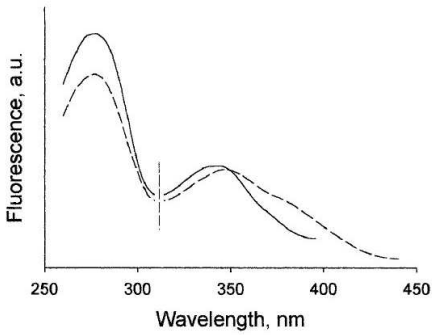

Figure 5.12: *Excitation spectra for a cataractous lens. Solid line is 420 nm emission, dashed 470 nm. The left part of the spectra up to the vertical line is due to tryptophan fluorescence. Figure adapted from reference [8].*

is seen two peaks – at 355 nm and at 385 nm. The individual excitation lines seem related to the chosen emission wavelength for glycated lysine, whereas for the human lens both excitation peaks shows up at 470 nm emission.

5.7 TPE

TPE fluorescence measurements are rapidly gaining use in investigations in the microbiological field. Fluorescence based methods are already one of the main tools for analysis of chemical, biological, biochemical and biophysical reactions, environments and structures [1]. Fluorescence microscopy is widely used for

analysis of especially biological samples. TPE fluorescence has been used in fluorescence microscopy for about 15 years by now [9, 10]. The advantages over traditional confocal fluorescence microscopy are related to high penetration of the fundamental light – low absorption especially in tissue, low photodamage/photobleaching even when excitation in the UV region is required – due to the absence of UV exposure in non-sampled sample regions, and high precision – excitation only takes place in a very small volume making high 3D resolution possible, and finally good separation between excitation and emission wavelengths. All these features are especially useable when used in microscopy studies of living tissue [11]. In addition the microscope may also be used for making very precise cuts [10, 12].

The biggest difference between SPE and TPE fluorescence is that where SPE fluorescence is linear dependent on the excitation, TPE fluorescence depends on the square of the excitation field.

TPE bleaching is the ultimate goal of this projects. Therefor it is of importance and interest to measure the fluorescence spectra under TPE, and compare these to SPE spectra. The question is, if the spectra are similar under the different kinds of excitation – single- and two-photon. The difference in excitation can be visualised by a transition diagram – see figure 5.13.

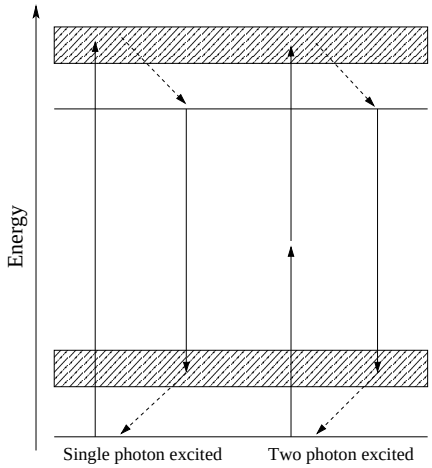

Figure 5.13: *Transition diagram – or so-called Jabłoński diagram. The initial and excited energy level are the same for both SPE and TPE. Broad bands illustrate broad energy bands. Dashed, inclined arrows indicate non-emissive transitions. In real systems the final ground and excited states are not single lines as illustrated here but merely the lower energy edge of the bands involved in the transitions.*

Strictly speaking the fluorescence is independent on excitation, but the absorption process is not. Two photon absorption has different selection rules than single photon absorption. The latter requires the ground and final state to be of opposite parity as an absorbed photon necessarily must change the angular momentum by +/- 1. Two-photon absorption implies change of angular momentum of +/-2 or 0, so different final states should in theory be reached [13]. However there are so many absorption states in these (complex) molecules studied leading to the same fluorescence emission that no difference due to excitation may be seen. It is only of importance when treating individual atomic states (such as thin atomic vapours). Similar fluorescence spectra for SPE and TPE should thus be expected [7].

An example of a way to derive a simple, approximate expression for the two-photon absorption cross section is given in section 7.1.1. Although the treatment presented in that section is elegant more than scientifically correct (for a start

it ignores parity), it gives a good, intuitive picture of the process behind two-photon absorption, and gives useable estimates. I will not treat multi-photon processes any further theoretically in this report.

5.7.1 TPE fluorescence spectra

To compare SPE and TPE fluorescence a spectrum of TPE fluorescence was recorded. This is shown in figure 5.14, where it is plotted together with a SPE excited spectrum from a Spex Fluorolog.

The used set-up for the recording was an ad hoc construction. The cuvette containing the sample was placed up against the entrance slit of a computer driven grating monochromator. No additional collection or focussing of the fluorescent light was performed. A PMT detected the exit signal from the monochromator. The laser (250 kHz, 350 mW average power, 150 fs pulse width) was focused with an f = 50 mm lens into the sample. In order to avoid super-continuum generation a neutral density filter-wheel was utilised to adjust the laser power to the highest possible.

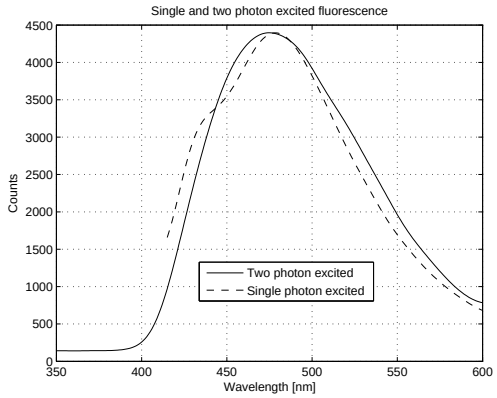

Figure 5.14: *The plot shows SPE (400 nm) and TPE (800 nm) fluorescence from glycated lysine samples. The spectra were smoothed and normalised to same peak value. The strength of TPE is seen here, where it is possible to measure the fluorescence down to below the effective excitation wavelength for TPE, while SPE is cut off at 415 nm to avoid cross talk.*

As the fluorescence signal was very weak it was necessary to use a relative high chromophore concentration in the sample during TPE, as compared to the Fluorolog measurement, leading to a large inner filter effect. This probably is why the peak from the SPE curve around 435 nm is not showing up on the TPE curve. Better TPE measurements should be obtainable in a dedicated set-up – such as a customised Spex Fluorolog. Except for the slight lack of details the spectra are similar.

5.8 TCSPC measurements on glycated lysine

TCSPC was performed on glycated lysine. With TCSPC it is possible to measure decay times for fluorescent transitions. It the used set-up the excitation source was an amplified Ti:Sapphire laser, doubled to 400 nm. Average power 40 mW and pulse lenght $\sim$ 200 fs. The detection system consisted of a photomultiplier arranged normal to the excitation direction. Due to high system sensitivity a highly dilute sample was used.

The glycated lysine relaxation proved to be broadly distributed in time, so an exponential distribution method was applied to analyse the data [6]. This lead to the results shown in figure 5.15. The broad distribution of the exponentials is due to a large spread in decay times. This indicates that for the chromophore(-s) there is also a broad distribution of fluorescence transitions.

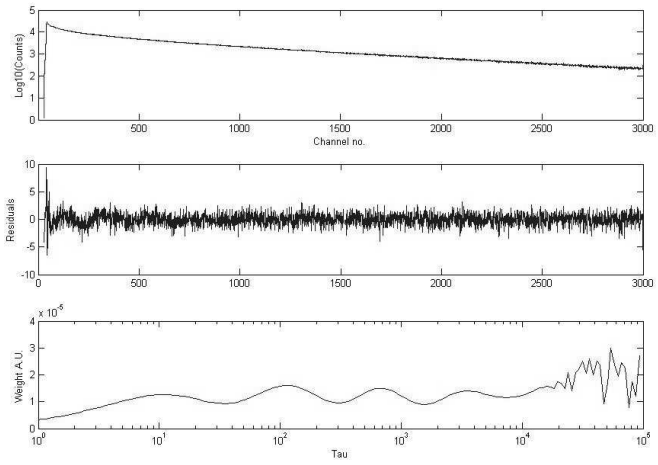

Figure 5.15: *TCSPC on glycated lysine sample. Time bin – the channel width – was 50 ps per channel. Tau – the decay time – is time given in units of the channel width – 50 ps.*

If the sample had up to 3-4 exponentials in its decay the analysis should have shown a few, distinct peaks in the decay time distribution. As this is not the case – and as the utilised set-up gave valid results for test-samples, the glycated lysine decay can not be described by less than 4-5 exponentials.

It is hard to make a conclusion from this; either multiple, distinct chromophores exist, or each chromophore has several possible fluorescent transitions – indicating large, complex molecules. Later in this report is assumed only a single chromophore is present – to be able to make calculations on sample/chromophore behaviour. In the section dealing with bleaching it is found that one chromophore is not sufficient to describe the found data, which is supported by the results found in this TCSPC measurement.

[6] Matlab program for calculation of fluorescence decay from TCSPC data. © J.L. Mortensen, Technical University of Darmstadt.

Published TCSPC measurements on lens samples [8] have shown a multi-exponential decay with decay times in the nanosecond range. What is found in the above measurements are similar to this, although I found a more complicated behaviour. In all cases its not possible to say anything exact for the fluorescence time behaviour of the glycated lysine based on the analysed results.

5.9 Summary on model system

The conclusion to be drawn from the measurements on glycated lysine is that it exhibits some of the same characteristics as real lenses. As lenses contain a wide variety of chemical compounds the difference is to be expected. Still the same characteristics could indicate that some of the compounds in the lens may be in family with glycated lysine. Which in turns means glycated lysine is a useable assay for the possible bleaching of cataract.

In addition SPE and TPE spectra were recorded of glycated lysine. The spectra proved to be identical within the limits set by the ad hoc nature of the TPE experiment.

TCSPC measurement indicated that multiple fluorescence lines exist. Published measurements on lens samples [8] have shown a multi-exponential decay with decay times in the nanosecond range. Measurements presented here shows same behaviour for glycated lysine.

Bibliography

[1] S.K. Grandhee, and V.M. Monnier, "Mechanism of Formation of the Maillard Protein Cross-link Pentosidine – Glucose, Fructose, and Ascorbate as Pentosidine Precursor"; J. Biol. Chem., vol. 266, pp. 11649-11653; 1991

[2] D.G. Dyer, J.A. Blackledge, S.R. Thorpe, and J.W. Baynes, "Formation of pentosidine during nonenzymatic browning of proteins by glucose. Identification of glucose and other carbohydrates as possible precursors of pentosidine in vivo"; J. Biol. Chem., vol. 266, pp. 11654-11660; 1991

[3] E.H. Ajandouz, and A. Puigserver, "Nonenzymatic Browning Reaction of Essential Amino Acids: Effect of pH on Caramelization and Maillard Reaction Kinetics"; J. Agric. Food Chem., vol. 47, pp. 1786-1793; 1999

[4] E.H. Ajandouz, L.S. Tchiakpe, F. Dalle Ore, A. Benajiba, and A. Puigserver, "Effects of pH on Caramelization and Maillard Reaction Kinetics in Fructose-Lysine Model Systems"; J. Food Science: Food Chem. and Toxicol., vol. 66, pp. 926-931; 2001

[5] R. Richards-Kortum, and E. Sevick-Muraca, "Quantitative Optical Spectroscopy for Tissue Diagnosis"; Annu. Rev. Phys. Chem.; vol. 47, pp. 555-606; 1996

[6] U. Brackmann, *Lambdachrome® Laser Dyes – Data Sheets* (Lambda Physik, Germany; 1999)

[7] J.R. Lakowicz, *Principles of Fluorescence Spectroscopy* (Kluwer Academic/Plenum Publishers, 1999)

[8] L. Kessel, S. Kalinin, R. Nagaraj, M. Larsen, and L. B.-Å. Johansson, "Time-resolved and Steady-state Fluorescence Spectroscopic Studies of the Human Lens with Comparison to Argpyrimidine, Pentosidine and 3-OH Kynurenine", Photochem. and Photobiol., vol. 76, pp. 549-554, 2002

[9] W. Denk, J.H. Strickler, and W.W. Webb, "Two-Photon Laser Scanning Fluorescence Microscopy"; Science, vol. 3.248, pp. 73-76; 1990

[10] K. König, "Multiphoton microscopy in life sciences"; J. Microscopy, vol. 200, pp. 83-104; 2000

[11] K. König, P.T.C. So, W.W. Mantulin, and E. Gratton, "Cellular response to near-infrared femtosecond laser pulses in two-photon microscopes"; Optics Lett., vol. 22, pp. 135-136; 2005

[12] K. König, I. Riemann, P. Fischer, and K.-J. Halbhuber, "Intracellular nanosurgery with near infrared femtosecond laser pulses"; Cellular and Molecular Biology, vol. 45, pp. 195-202; 1999

[13] R. Loudon, *The Quantum Theory of Light* Second Edition (Oxford University Press, 1983)

Chapter 6

Bleaching by UVA

So you'd like to save the world
I'd really like to help you
I'd really like to be you for a while
is that all right
and I could call it ultraviolet radiation

Lloyd Cole.
So you'd like to save the world
American songwriter (1961 –)

The main purpose of the frequency doubled Ti:Sapphire laser was bleaching of glycated lysine compounds. The setup for bleaching utilised the frequency doubled Ti:Sapphire laser purpose-built in our lab. This laser is described in details in chapter 3.

Based on previous results it was decided only to look at glycated lysine as a model molecule. In addition to the blue laser, another new tool was introduced for these bleaching experiments – the glucose hexokinase test for rest glucose concentration. This was needed for estimating the chromophore content in the browned samples.

This chapter presents results from bleaching of glycated lysine.

- Section 6.1 on page 73 present method and results for SPE bleaching. The purpose-built SHG UV laser was used for the bleaching. Based on the bleaching results the quantum efficiency for bleaching was calculated.
- Section 6.2 on page 84 briefly discusses the obtained results compared to published results by other groups on bleaching of human lenses.
- Section 6.3 summarises the chapter.

6.1 Bleach Bleach Bleach!

As the whole project was originally based on looking into possibilities for "bleaching" cataract in human eyes utilising femtosecond NIR lasers, the interesting wavelengths for single-photon bleaching are in this respect around 400 nm. 600-1000 nm is the window of lowest absorption in tissue, therefore the femtosecond

laser for the eye treatment should be around this wavelength for two-photon bleaching, hence for single photon bleaching it should be around half that. Thus I have been looking mainly at the two wavelengths 392 nm and 405 nm. The interesting here is whether there would be a difference in quantum efficiencies for bleaching between these wavelengths (the absorption is different with some amount). The laser gives high power and narrow line width, so utilising a laser it is possible to bleach macroscopic samples and still have full control of wavelength.

6.1.1 Measurement set-up

The laser generated blue light in two directions. After the first of the blue outputs was placed a blue filter to filter away any NIR radiation, after this was placed a power-metre (Melles Griot 13PEM001). The power-metre was connected to a LabView program for automatic data collection. The power-metre output was sampled every 2 seconds and the data stored. This was considered necessary as the laser had previously demonstrated periodical instability with loss of output power. So to accurately estimate the actual total flux of blue light passed through the glycated lysine sample the laser was monitored throughout the entire bleaching run. After the other output the sample was placed. No additional focussing of the output was necessary, as the blue beam after the out coupler was around 2 mm in diameter. This was an appropriate size for the bleaching. Right after the sample a mirror was placed (reflection coefficient for 392 nm around 94 %) to double pass the blue beam through the sample. The set-up is shown in figure 6.1.

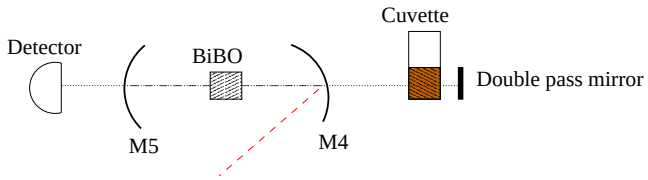

Figure 6.1: *Set-up for bleaching.*

6.1.2 Sample preparation for bleaching

The mixture for bleaching was prepared by taking 100 μL of glycated lysine – 0.1 M glucose and lysine buffered with phosphate pH 7 incubated at 75 C for 48 hours – and dilute it with 2900 μL of distilled water – a 1+29 dilution. The transmission coefficient of this mix was measured to be 23.2% at 392 nm.The absorption cross section estimated above can be cross checked with this result; the undiluted sample 48 hours incubated had an assessed chromophore concentration of $46.1 \cdot 10^{18}$ molecules per cm^3, which for this used 1+29 dilution gives a chromophore concentration of $15.4 \cdot 10^{17}$ molecules per cm^3. With the absorption cross section estimated above in section 5.5 to be $9.46 \cdot 10^{-19}\, cm^2$ at 392 nm the normalised transmission should be 23.3%. The negligible error of the estimate clearly shows the strength of this method for calculating the cross section. For bleaching 1000-1500 μL of sample was placed in a UV plastic cuvette sealed

with laboratory wrap (waxed plastic film). A control sample was prepared in the same way as the bleached sample, and kept next to the bleaching set-up in a dark place. This way it has been exposed to the same processing, environment and ambient temperature as the bleached sample to minimise the influence of the handling and storage processes on the result.

6.1.3 Cuvette loss

Some additional measurements were done to estimate the absorption and reflection of the blue light caused by the cuvette itself. The refractive index of the used cuvette type was approximately 1.4-1.5 (for most high density plastics, such as PMMA or HD-PS) giving a reflection from each air-cuvette surface of about 3-4%. Water has a refractive index of about 1.35 (at around 400 nm) giving a reflection at the sample-cuvette interfaces of about 0.2%, which can be considered negligible. Measuring the transmission through an empty cuvette and a cuvette filled with distilled water, both against air blanks, gives the transmission values shown in table 6.1. In addition a quartz cuvette filled with distilled water was also measured. This to check the water and plastic cuvettes for any absorption peaks, as the quartz used is known not to absorb light in the utilised wavelength region; in addition it's refractive index is around 1.46 in the blue region. (cuvette type Hellma QS, material SUPRASIL synthetic quartz).

Cuvette	392 nm	405 nm
Plastic Empty (HD-PS)	88.3%	88.3%
Plastic Water filled (HD-PS)	93.7%	93.7%
Semi-micro Water filled (PMMA)	88.8%	88.8%
Fused Quartz water filled	93.7%	93.7%

Table 6.1: *Transmission values for combinations of cuvettes, water, and wavelengths.*

From the data in table 6.1 it may be concluded that water has negligible absorption at the wavelengths in question, and that the refractive index for the plastic used for the cuvettes was about 1.46 – as the quartz cuvettes. This gives the correction factor to be used when calculating the amount of blue light to reach the sample to be bleached; the refractive index of the sample can be considered identical to that of water, which means for first pass of the blue light (100%-93.7%)/2 = 3.15% $\sim$ 3% should be subtracted; while for second pass an additional two times 3% should be subtracted.

The semi-micro cuvettes were made of PMMA. The transmission for these (water filled) proved to be practically flat from 380 to 410 nm at 88.8%. The slightly lower transmission as when compared to the macro cuvettes is due to higher index of the new cuvettes (of optical grade PMMA) causing larger reflection losses at the interfaces. A loss of (100%-88.8%)/2 $\sim$ 5.5% was assumed at each air-cuvette-water interface.

6.1.4 Calculation of bleaching quantum efficiency

Calculating the bleaching quantum efficiency is not entirely trivial. What is known is the initial amounts of chromophores in the sample, the initial absorbed blue flux and the chromophore amount after the bleaching has stopped, derived from the absorption after the bleaching. From these data the quantum efficiency of the bleaching is estimated. The amount of absorption events is proportional to the photon flux. So the easiest is to start from the absorption, and the problem can be treated analogue to the decay for radioactive nuclei ensembles. That is, $\partial(n(t))/\partial t = -(Abs(t)) \cdot P \cdot \zeta$, where $n(t)$ is the (time dependent) concentration of chromophores at time t, $Abs(t)$ is the (time dependent) absorption at time t, $P(t)$ is the amount of (blue) photons passing through the sample per time unit at time t, and ζ is the quantum efficiency for bleaching, which is assumed to be a material parameter and thus time independent. ζ gives the probability of one absorbed photon leading to a bleaching event; the reciprocal value of the quantum efficiency is the average number of absorption events per chromophore before it is bleached. Now the bleaching rate is an easy expression, but the expression for the chromophore concentration as function of time $(n(t))$ may not be. I did not manage to derive a analytical expression in a reasonable time. Others who have considered bleaching have typically been looking at the bleaching in the actual region with flux passing through [1, 2]. The problem at hand is more complicated, as the bleached volume is coupled to and in balance with a chromophore reservoir. To avoid having to resort to artificial "fluxes" filling the entire sample area, it was decided to implement a numerical solution. This is only useable under the assumption that the bleaching follows the rate given above, going towards zero for time going towards infinity. Multiple exponentials for the bleaching or a finite concentration of chromophores are not considered. The first is less important as the time dynamics are not studied, only the long time/permanent bleaching effect. Multiple chromophores would give a multiple exponentials behaviour, but to be able to get realistic results in my rather simple laboratory set-up single-exponential bleaching was assumed. The second assumption, finite concentration of chromophores is zero, may be uncorrect, but this is difficult to asses properly without letting bleaching time actually go towards infinity.

A small program was implemented in Fortran to do the calculations. The program first guesses on an initial value for the bleaching quantum efficiency, based on an assumption of constant absorption throughout the bleaching run. This value is then used in an iteration routine. The routine first calculates the concentration of chromophores after bleaching based on the concentration pre bleaching and the guessed quantum efficiency – time stepping with steps size of 1 second, for each step calculating the bleached amount of chromophores and from this updating the amount left, thereby updating the absorption. The result from the time stepping is then compared to the measured end value of the chromophore concentration, the value of the quantum efficiency updated, and the time stepping loop run again. After about 4 to 6 iterations a precision of 10^{-6} (ncalc-nmeas<nmeas$\cdot 10^{-6}$) is reached. Running the program takes less than a few seconds (g95 compiler without optimisation on a 1.8GHz Pentium-4M). A commented version of the program code may be found in the appendix chapter F. The program takes double passing of the blue light including reflection losses into account.

6.1.5 Bleaching results

The bleaching experiments were performed at 392 nm and 405 nm. The chronological order followed the development of the laser set-up, first 392 nm and later 405 nm. Below are the individual experiments explained. Bleaching quantum efficiencies are shown for all experiments in table 6.3. Some transmission plots before and after bleaching may be seen in figures 6.2 and 6.3.

- **392 nm – 1st.** Bleaching time was 120 minutes. The blue power from the laser was in average 23.76 mW for the first hour of bleaching and 23.61 mW for the second, after correction for filter transmission (blue filter in front of the power-metre). An average of 23.67 mW for both hours was used in subsequent calculations. Fluctuations in the blue power were only of short time scale character/spikes, and negligible – amplitude around 5% of average value. Macro cuvette and 1 ml sample volume was used. This experiment run differentiated itself from the others in that the samples were diluted 1+2 with phosphate buffer pH 7 instead of water before transmission measurements, which were against 1+2 water/buffer blank. Therefor the cross section calculated for water diluted samples does not hold, and the cross section for this particular sample[1] was calculated from the transmission of the control sample assuming the chromophore concentration was as previously calculated for a 1+29 water diluted sample ($15.4 \cdot 10^{17}\, cm^{-3}$). Transmission of samples diluted with phosphated buffer were 66.1% and 80.1% for unbleached/bleached respectively, corresponding to chromophore concentrations of $15.4 \cdot 10^{17}\, cm^{-3}$ (assumed) and $8.22 \cdot 10^{17}\, cm^{-3}$ (in the samples prior to dilution for transmission measurements). Cross section in the transmission measurements was estimated to $8.07 \cdot 10^{-19}\, cm^2$ (due to the use of phosphate buffer), while cross section during the bleaching was taken as the normal $9.46 \cdot 10^{-19}\, cm^2$ found previously (as the dilutant here was pure water) – both at 392 nm. The initial absorption of the sample before bleaching was 76.8% and the absorption in the cuvette just after bleaching can be estimated to 54%, corresponding to the drop in the chromophore content of about 47% following bleaching. The result for the quantum efficiency is found to be $2.60 \cdot 10^{-3}$ from this first 392 nm bleaching experiment.

- **392 nm – 2nd.** Bleaching time 120 minutes. Average power 24.6 mW. Cuvette type utilised was semi-micro cuvettes, hence 1.5 mL of sample was bleached. The transmission for the non-bleached control sample was found to be 27.2%, which was higher than the expected transmission of 23.2% for this dilution. This means either the cross section or the concentration of chromophores had changed slightly. Assuming the chromophore concentration had not changed, the cross section was estimated to be $8.45 \cdot 10^{-19}\, cm^2$. Or a deviation from previously found result of $9.46 \cdot 10^{-19}\, cm^2$ of about 11%. Instead assuming unchanged cross section for absorption the chromophore concentration may, from the measured transmission value and using $9.46 \cdot 10^{-19}\, cm^2$ as the cross section, be estimated to $13.8 \cdot 10^{17} cm^{-3}$, a deviation from the from the glucose hexokinase test found concentration of $15.4 \cdot 10^{17} cm^{-3}$ of about 10%. The

[1] For the transmission measurement only. The cross section is pH dependent, and during the bleaching the cross section was as previously found.

data in upper half of table 6.2 are estimates based on unchanged (initial) chromophore concentration. The quantum efficiency for bleaching for this experiment was under these assumptions calculated to be $3.10 \cdot 10^{-3}$. Compared to the value found under the first bleaching experiment this value is +23.1% higher. Had I instead used the assumption that rather the chromophore concentration than the absorption cross section had changed, the initial concentration would be $13.8 \cdot 10^{17} cm^{-3}$, and final concentration then $8.65 \cdot 10^{17} cm^{-3}$ (data table 6.2 lower half). This would give a bleaching efficiency of $2.80 \cdot 10^{-3}$. This value deviates from the value calculated from the first 392 nm bleaching by +7.7%. Considering the inherent uncertainties in these bleaching experiments the change in absorption is not significant enough to degrade the validity of the experiment.

- **405 nm – 1st.** Bleaching time was 120 minutes. Average blue power for the experiment was 15.6 mW for the first hour and 15.1 mW for the second (corrected for blue filter transmission of 0.75), giving an average of 15.4 mW. At $1.49 \cdot 10^{18} cm^{-3}$ (corresponding to 67.7% transmission) the value for the chromophore concentration in the control sample matches the value used in calculating the absorption cross section. Post bleaching chromophore concentration was found to $1.00 \cdot 10^{18} cm^{-3}$ from a transmission of 76.9% after 1+2 dilution. An absorption cross section of $7.85 \cdot 10^{-19} cm^2$ was used. Quantum efficiency was calculated to $2.71 \cdot 10^{-3}$.

- **405 nm – 2nd.** 120 minutes of bleaching. This experiment utilised the semi-micro cuvette and 1.5 mL of sample. Average power was 22.1 mW for the first hour, and 21.3 mW for the second – both after filter correction; an average for both hours of 21.7 mW was used. Utilising the $7.85 \cdot 10^{-19} cm^2$ cross section an undiluted control sample transmission of 33.9% at 405 nm gave a chromophore concentration of $1.38 \cdot 10^{18} cm^{-3}$. For the bleached sample the transmission at 405 nm of 45.3% gave a chromophore concentration of $1.01 \cdot 10^{18} cm^{-3}$. Quantum efficiency was calculated to $2.29 \cdot 10^{-3}$.

- **405 nm – 3rd.** 120 minutes of bleaching. Average power for this experiment was 15.9 mW for the first hour and 15.1 mW for the second – after filter correction. Close enough for a 15.5 mW average to be used. Transmission at 405 nm for the control and bleached samples respectively after 1+2 dilution of the samples were 70.7% and 79.3%. Utilising the $7.85 \cdot 10^{-19} cm^2$ cross section at 405 nm chromophore concentrations were found to be $13.3 \cdot 10^{17} cm^{-3}$ for the control and $8.9 \cdot 10^{17} cm^{-3}$ for the bleached. Quantum efficiency was calculated to $2.52 \cdot 10^{-3}$.

Bleaching quantum efficiencies

Table 6.3 summarises the calculated quantum efficiencies. As seen the efficiencies are higher at 392 nm than at 405 nm. Average values gives $2.70 \cdot 10^{-3}$ at 405 nm and $2.51 \cdot 10^{-3}$ at 392 nm. The difference is not large, 392 nm being about 7.6% more efficient than 405 nm. Ignoring the potential outlier of the second 405 nm experiment the difference would be down to 3%, which is insignificant with the present data set. For the 392 nm experiment 2 the value based on

Sample	Transmission at 392 nm	Chromophore concentration	Cross section
Control	27.2%	$15.4 \cdot 10^{17}\, cm^{-3}$	$8.45 \cdot 10^{-19}\, cm^2$
Bleached	44.1%	$9.69 \cdot 10^{17}\, cm^{-3}$	—
Control	27.2%	$13.8 \cdot 10^{17}\, cm^{-3}$	$9.46 \cdot 10^{-19}\, cm^2$
Bleached	44.1%	$8.65 \cdot 10^{17}\, cm^{-3}$	—

Table 6.2: *Data for the second round of bleaching at 392 nm. Upper half: Cross section used was calculated from absorption measurement under the assumption that the chromophore concentration had not changed from the previously found initial value. Lower half: Assuming the chromophore concentration – rather than the cross section – had changed, values are instead calculated based on chromophore concentration found via the previously calculated absorption cross section.*

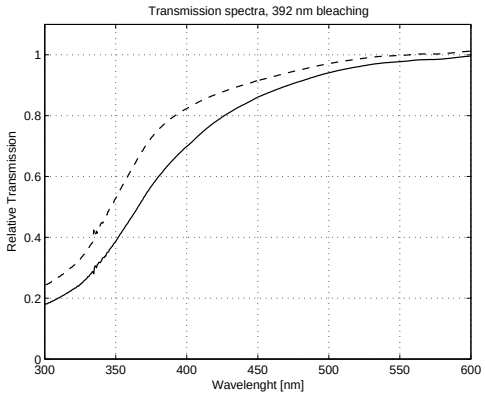

Figure 6.2: *Bleaching experiment 392 nm – 1st. Bleached sample (dashed line) and non-bleached control (solid line).*

unchanged cross section is used – refer to the discussion for the experiment above.

These found values may be compared with those found in literature. In the literature to my knowledge only laser dyes have been investigated, so for comparison Rhodamine may be used. For Rhodamine 6G fixed in a matrix reference [1] gives an (isotrope) bleaching quantum efficiency ranging from $7.1 \cdot 10^{-7}$ (PMMA matrix) to $3.3 \cdot 10^{-6}$ (epoxy resin matrix). Reference [2] find for fluid samples quantum efficiencies ranging from $5 \cdot 10^{-7}$ (dissolved in ethanol) to $8.3 \cdot 10^{-6}$ (dissolved in water containing a deaggregating agent). The strong dependence of host material on the quantum efficiency indicates the bleaching is probably a due to excited state reactions with or involving the host material or impurities/gasses therein.

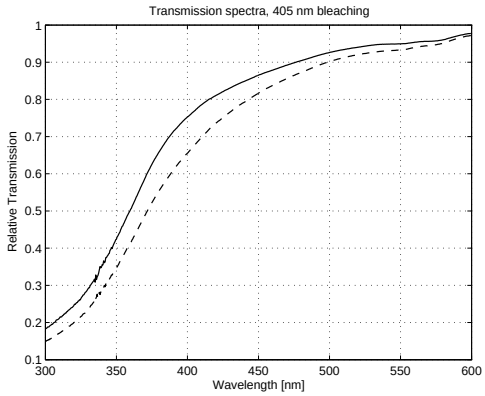

Figure 6.3: *Bleaching experiment 405 nm – 1st. Bleached sample (dashed line) and non-bleached control (solid line).*

Wavelenght	Number	Quantum efficiency
392 nm	1	$2.60 \cdot 10^{-3}$
392 nm	2	$2.80 \cdot 10^{-3}$
392 nm	Average	$2.70 \cdot 10^{-3}$
405 nm	1	$2.71 \cdot 10^{-3}$
405 nm	2	$2.29 \cdot 10^{-3}$
405 nm	3	$2.52 \cdot 10^{-3}$
405 nm	Average	$2.51 \cdot 10^{-3}$

Table 6.3: *Quantum efficiencies for bleaching.*

Differential absorption bleaching

The differential absorption bleaching can be said to be the wavelength dependent change in absorption following bleaching. As seen from figures 6.2 and 6.3 the change in transmission is wavelength dependent. To view better this dependency the relative transmission changes for the individual measurements are shown in figure 6.4.

In figure 6.4 the logarithmic values of the transmission coefficients are taken prior to dividing the control sample curve with the bleached sample curve. This directly gives the relative chromophore concentration before and after bleaching – $n_{control}/n_{bleached}$. All curves were normalised to a peak value of one, to eliminate baseline shifts and remove dependence on absolute bleaching. However this means it is not possible to directly compare the individual curves with each other, except for the position of the peak value. From the figure the clear tendency is the peaking of the highly wavelength dependent drop in transmission centred around 370-405 nm. The peak drop in absorption is centred at the bleaching wavelength. Though this initially may seem erroneous it matches if the assumption is made that more than one chromophore is involved in the absorption process (in fact, a continuous distribution of wavelength-individual absorbers is needed throughout the absorbing wavelength region). This does

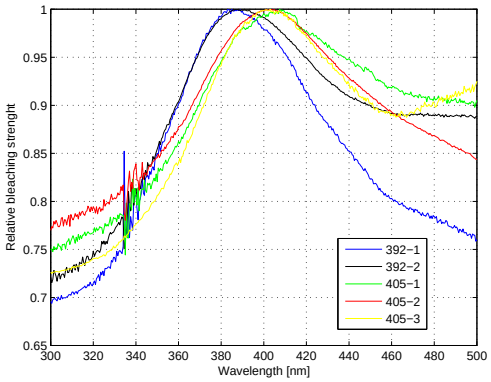

Figure 6.4: *Wavelength dependent change in transmission.*

seem to correspond well with the results from TCSPC measurements – section 5.8 page 69, where the results could be interpreted as a broad distribution of absorbers. The clearly peaked differential transmission may be interpreted as multiple absorbers exist in the samples. Either way, it is proved that the absorbing compounds may be bleached. The use of phosphate buffer as dilutant prior to transmission measurements for the 392-1 sample clearly has had a large effect on the long wavelength transmission.

Dropping chromophore concentrations

As seen from the bleaching experiments above there was a general trend of lower sample chromophore concentrations in the control samples than previously measured. It is possible that the concentration did in fact change over time due to polymerisation or other processes despite the samples being stored at 5 C. Samples mixed 1+29 ready for bleaching were not stored longer than a week and generally just a few days before being used. The browned glycated lysine for these samples was from the same incubated batch, and 1+29 mixed dilutions were measured just after mixing to check for correct dilution. As differences between measured values on the control samples and the values from the initial cross section estimations were not much above 10%, the control and bleached samples having suffered same fate, and considering the uncertainties and assumptions involved in general, it was decided that the estimated values for the quantum efficiencies could be used.

Note on transmission measurements

Following the bleaching runs the transmission of the samples – bleached as well as control samples – were measured in our Cary 3 spectrophotometer. Two different approaches were used depending on what cuvette had been used for the bleaching. If macro cuvettes were used, the sample volume was 1 ml and the sample was diluted with distilled water 1+2 (1 part sample and 2 parts water) prior to measurements. Found concentrations given above were multiplied by three to account for this dilution, so to make it possible to compare them to

previous values. Semi-micro cuvettes were used with 1.5 ml of sample, and these were not diluted prior to transmission measurements. It was found that due to the sample holders in the spectrophotometer the results were dependent on how the semi-micro cuvettes were positioned in the holders. This proved difficult to do consistently, and thus the exact results for these cuvettes tended to be difficult to repeat. Despite the problems associated with using this type of cuvette in the spectrophotometer an advantage was that samples could be measured without further dilution, reducing the risk of errors in the dilution process. Thus both types of cuvettes have their advantages and disadvantages.

6.1.6 Fluorescence spectra after bleaching

As a final test it was tried to take fluorescence spectra excited at 392 nm on the bleached and control samples. A dedicated set-up for fluorescence measurements was not available, so a simple set-up was bodged together in the lab utilising a fibre-coupled spectrometer (Avantes AvaSpec 2048). Resulting recorded curves are shown in figure 6.5. The many individual peaks ("grass") are not a feature of the fluorescence, which is smooth. It is varying dark noise from the individual detector pixels in the spectrometer showing up strongly due to an integration time of several seconds, for which this type of spectrometer is not well suited. Bleaching caused $\sim$ 20% drop in peak fluorescence. The drop in chromophore concentration as estimated was around 37% for the same samples, so the correlation is not 100%. Then again, the inner filter effect will also be lower for the bleached sample, so this will counterbalance the discrepancy a bit. Without better equipment though, it is not possible to state if there is a 1-to-1 correlation between bleaching and drop in fluorescence, but clearly there is a trend.

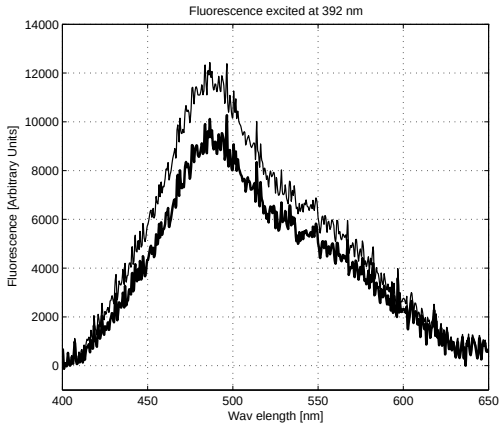

Figure 6.5: *Fluorescence spectra under 392 nm excitation. Before (thick line) and after bleaching (thin line).*

6.1.7 Bleaching of pure glucose at 392 nm

With the 392 nm set-up bleaching was tried on a incubated pure glucose samples. A sample were made from the 72 hours incubated glucose, diluted with distilled water 1+1. Sample volume was 1350 μL in a semi-micro cuvette. In figure 6.6 is shown transmission before and after bleaching, measured against a water blank.

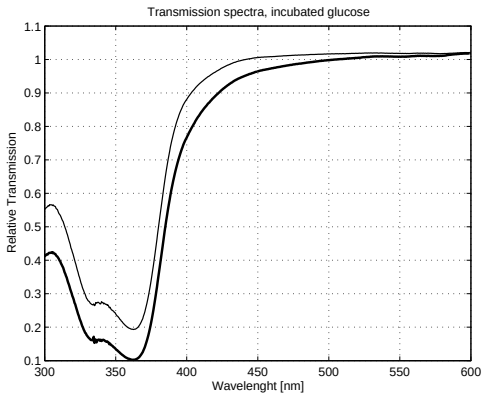

Figure 6.6: *0.1 M pure glucose incubated 72 hours, before (thick line) and after bleaching (thin line).*

The drop in transmission is significant, especially around the absorption peaks. This sample was previously found to have a rest glucose content of 82.1 mM. The chromophore concentration is more difficult to guess, as I have no idea whether the chromophores consist of one (broken down) glucose molecule, or are composed of two (or more – but two should be a faster reaction than multiple) glucose molecules. Assuming the chromophores consist of two glucose molecules, the chromophore content should be (100 mM - 82.1 mM)/2 = 9 mM. In the dilution used the chromophore concentration is thus (guessed to be) 4.5 mM, or $4.5 \cdot 6.02214199 \cdot 10^{17} = 27.1 \cdot 10^{17}$ molecules per cm^3. Transmission at 392 nm is measured to be 66.6%. This yields the data for absorption cross sections at 392 nm to $1.50 \cdot 10^{-19} cm^2$. This may be compared with same value for the glycated lysine, $9.46 \cdot 10^{-19} cm^2$. Bleaching was 90 minutes at an average 392 nm power of 21.9 mW. Post bleaching the transmission is found to be 80.0%. Utilising the just found value for the absorption cross section this corresponds to a chromophore concentration of $14.9 \cdot 10^{17} cm^{-3}$. Running these data through the quantum efficiency evaluation program gives a quantum efficiency for bleaching of $17.5 \cdot 10^{-3}$, or a value 6.5 times higher than for the glycated lysine chromophores.

It is thus possible the bleaching results have been influenced by bleaching of browned pure glucose, but considering the relative low yield of this reaction – browning of pure glucose – the initial absorption due to these chromophores in the sample was likely too low to have a significant influence on the results of the experiments.

6.2 Bleaching on human eyes

Previously results have been published regarding the SPE bleaching of real, whole lenses as well as homogenates of these [3, 4]. In reference [3] the authors expose whole lenses to UVA radiation for up to 24 hours. Their set-up consisted of a 1000 W Hg/Xe lamp filtered through a Copper Sulfate filter and a 338 nm short wavelength cut-off filter. The used type of lamp has very powerful emission lines at 365 nm, 405 nm and 436 nm; it is unclear if all lines were passed through the filters. This is likely though, as copper sulfate filters cut-off around 450 nm and upwards. It is not without importance where their cut-off lied, as indeed also 405 nm – and possibly even 436 nm – will contribute to the bleaching. The lenses irradiated were subjected to 900 Joule hour^{-1} cm^{-2}. Recalculating this it corresponds to 250 mW cm^{-2} – a serious dose of UV light. Their results showed almost complete bleaching of lenses after 24 hours bleaching time; already after a few hours bleaching is clearly seen. Most interestingly they find the differential absorption to improve in a spectral shape like the one presented here (figure 6.4), but peaking around 355 nm – not far from the 365 nm emission line of their lamp. The dependence of peak differential absorption on bleaching wavelength they find look very similar to the one found in this report. The authors in reference [3] find the fluorescence dropping post bleaching. In contrast to this the authors of reference [4] find that fluorescence does not change following irradiation of whole lenses with UVA light, despite they too find pronounced bleaching.

In essence previously published results show characteristics similar to what is found for glycated lysine in this project, indicating glycated lysine may be used as a study molecule – a model system – for cataract.

6.3 Summary on bleaching

Average bleaching quantum efficiencies were found to be $2.51 \cdot 10^{-3}$ at 405 nm and $2.70 \cdot 10^{-3}$ at 392 nm. Measured data for absorption cross sections and transmission measurements pre-/post-bleaching were fed to a numerical iteration routine, which extracted the bleaching quantum efficiencies.

The found wavelength dependence of the bleaching indicates more than one chromophore was present in the glycated lysine. This is in agreement with results found for the TCSPC measurements in section 5.8 page 69. For the quantum efficiency calculations were assumed only one chromophore present as multiple chromophores can not be included in the simple numerical model I used. However, unless the bleaching quantum efficiencies for the individual chromophores are significantly different, the model still gives a useable estimate.

For comparison estimated bleaching efficiency for pure glucose, browned through incubation, was found to be $17.5 \cdot 10^{-3}$.

Fluorescence was found to be lower post bleaching.

Presented results by other research groups were discussed, and it was found that UVA bleaching of human cataractous lenses yield results much alike what has been obtained in this project.

This method of bleaching efficiency measurements utilised in the present chapter could easily be used for measuring bleaching in other (liquid) samples; this could be useful for assessing bleaching of dyes for instance.

Bibliography

[1] I.P. Kaminow, L.W. Stultz, E.S. Chandross, and C.A. Pryde, "Photobleaching of Organic Laser Dyes in Solid Matrices"; Applied Optics, vol. 11, pp. 1563-1567; 1972

[2] E.P. Ippen, C.W. Shank, and A. Diennes, "Rapid photobleaching of organic laser dyes in continuously operated devices"; IEEE J. Quant. Electron., vol. QE7, pp. 178-9; 1971

[3] B.J. Ortwerth, V. Chemoganskiy, and P.R. Olesen, "Studies on Singlet Oxygen Formation and UVA Light-mediated Photobleaching of the Yellow Chromophores in Human Lenses"; Exp. Eye Res., vol. 74, pp. 217-229; 2002

[4] L. Kessel, S. Kalinin, V. Soroka, M. Larsen, and L.B.-Å. Johansson, "Impact of UVR-A on whole human lenses, supernatants of buffered human lens homogenates, and purified argpyrimidine and 3-OH-kynurenine"; Acta Ophthalmol. Scand, vol. 83, pp. 221-227; 2005

Chapter 7

Bleaching – two-photon

> The great tragedy of Science – the slaying of a beautiful hypothesis by an ugly fact.
>
> Thomas H. Huxley.
> *English biologist (1825-1895)*

The long term scope of this ongoing research project is bleaching of cataractous human lenses by a TPE procedure. However, financing to buy equipment for this purpose was not made available during the course of the project. It is possible to build a femtosecond laser from basic components, but this idea was not found feasible as is would take not only an excessive amount of time, but also the research value of spending time building a femtosecond laser would not be significant. Finally, the laser is only a small part of the set-up required for actually making TPE bleaching. In addition sensitive measurement equipment is needed, and most importantly a beam delivery set-up. In this chapter is presented a discussion of the feasibility of using TPE bleaching on human cataract based on the results obtained for the model system and SPE bleaching hereon.

The experiments done regarding TPE were all performed at other research labs, whenever there was a possibility of borrowing some. This meant that a dedicated set-up could not be built. Equipment and laboratories were borrowed at/from the following persons and research institutions, whom I would hereby like to thank for letting me use their time, money, patience, and equipment: Ph.D. Student Jonas Beermann, Department of Physics and Nanotechnology, University of Aalborg, Denmark; Professor Michael Giles, Klipsch School of Electrical and Computer Engineering, New Mexico State University, New Mexico, USA; Department of Physics, University of New Mexico, New Mexico, USA; Professor Emad Mukhtar, Department of Physical Chemistry, University of Uppsala, Sweden; The Bioimaging Centre, Department of Plant Biology, Royal Veterinarian and Agricultural University, Denmark; Research Centre COM, Technical University of Denmark; Dr. Claus Sternberg, BioCentrum, Technical University of Denmark; Danish Technological Institute, Denmark.

- In section 7.1 is presented a discussion of a semi-empirical estimation of the two-photon absorption cross section. Results from the investigation of cross sections for glycated lysine is used to evaluate the TPE cross section.

- Section 7.2 found on page 90 presents an estimate on the applicability of TPE bleaching on an in-vivo system (lens); utilising the estimate for cross section presented in the previous section and bleaching characteristics found in previous chapters.
- Finally section 7.3 summarises the chapter.

7.1 TPE

Fluorescence spectroscopy is one of the main tools for analysis of chemical, biological, biochemical and biophysical reactions and environments [1]. Two photon fluorescence has been used in fluorescence microscopy for about 15 years by now [2, 3]. The advantages over traditional confocal fluorescence microscopy are related to the high penetration of the fundamental light – low absorption especially in tissue, low photodamage/photobleaching even when excitation in the UV region is required – due to the absence of UV exposure in non-sampled sample regions, and high precision as excitation only takes place in a small volume making high 3D resolution possible, and finally good separation between excitation and emission wavelengths. All these features are especially useable when used in microscopy studies of living tissue [4]. In addition the microscope may also be used for making very precise cuts [5, 3].

The biggest difference between SPE and TPE fluorescence is that SPE fluorescence is linear dependent on the excitation, where TPE fluorescence depends on the square of the excitation field.

7.1.1 Two photon absorption cross section

In general the two-photon absorption cross section is difficult to measure, as the fluorescence output depends on the laser parameters such as pulse length, average power, and repetition rate. Most methods are based directly comparing generated TPE fluorescence to SPE fluorescence, as first proposed in reference [6]. Especially pulse length may be difficult to determine for many applications as ultra short pulses suffer from dispersion stretching in most medias. Which means the pulse length measured at the laser output may not be valid in the sample after the pulse has passed multiple optical components (and indeed the sample itself may add to the stretching). Calibrating against other nonlinear signals such as Hyper Rayleigh Scattering may reduce or remove the need for knowing details about temporal shape of the excitation pulse [7].

Some estimate may be based on the single photon absorption cross section. Most sources investigating two-photon absorption cross sections [8, 9, 10, 11] present a picture in which two-photon absorption cross section may be described by a cascaded process. From the picture given in reference [10]:

- First the molecule's electron cloud is disturbed by a passing photon. The molecule is then brought into an intermediate – or transitional – state of an energy above the initial level corresponding to the absorbed photon energy. If nothing further happens the molecule then re-emits the photon at the same energy with a short time lag (in bulk materials this is what can be described as the index of refraction). It is here important to notice that **no** stable or meta-stable energy level is needed for the process to take

place. The "cross section" for this process is proportional to the electronic size of the orbital involved in the process, which is in the order of the peak (single photon) absorption cross section for this transition (this absorption band) ($\sigma_{SPA\,max}$) and the flight time of the photon through the molecule (W_{mol}/c, W_{mol} being the size of the orbital disturbed, c is the speed of light). The latter giving the time scale on which this disturbance lives – the lifetime of the transitional state. The magnitude of this transitional cross section is then given as:

$$\sigma_{transitional} = \sigma_{SPA\,max} \cdot \frac{W_{mol}}{3 \cdot c} \tag{7.1}$$

Where division by three is from averaging over random molecule orientations.

- Following this disturbance there is now a chance to excite the molecule to an energy state above the initial level of energy $h(\nu_1 + \nu_2)$ if another photon (of energy $h\nu_2$) arrives and interacts with the molecule before it returns to its ground state. The cross section σ_{SPA} for this part process is proportional to the (single photon) absorption cross section into the final state level for the absorption of two photons of energy $h\nu_1 + h\nu_2$. This is in the general case not equal to $\sigma_{SPA\,max}$.

For the cascaded process a two-photon absorption cross section is given by:

$$\sigma_{2P} = \sigma_{SPA} \cdot \sigma_{transitional} = \sigma_{SPA} \cdot \sigma_{SPA\,max} \cdot \frac{W_{mol}}{3 \cdot c} \tag{7.2}$$

Where equation 7.1 has been used. Strictly speaking two distinct absorption processes takes place, where the first influences the result and the probability of the second – photons taken out of the beam by the first process are not available for the second process. But the absorption of the laser beam is for all normal cases so weak the photon flux is approximately the same throughout the cascaded absorption process. Thus the flux following the cascaded process may be evaluated as [10]:

$$I(L) = I_0 - I_0^2 \cdot 2 \cdot \sigma_{2P} \cdot n \cdot L = I_0 - I_0^2 \cdot 2 \cdot \sigma_{SPA} \cdot \sigma_{SPA\,max} \cdot \frac{W_{mol}}{3 \cdot c} \cdot n \cdot L \tag{7.3}$$

Where n is the chromophore concentration in the sample, L is the length of the interaction region, and the multiplication factor of two arises from two photons taken out for every cascaded excitation process. I_0 is the initial flux into the sample.

A more quantum mechanical treatment reaches a similar expression – see reference [11] for an example. The advantage of the treatment given above is that although it is somewhat hand-waving, it is based on known values, and may therefore with relative ease be evaluated to give useable estimates.

7.1.2 Evaluating the TPE cross section

Using equation 7.3 the cross section may be estimated. Following the lines of reference [9] W_{mol} may be taken as 0.2 nm. The measured absorption cross

Wavelength fundamental	785 nm	810 nm
σ_{2P} [m^{4}s]	$6.08 \cdot 10^{-63}$	$5.04 \cdot 10^{-63}$

Table 7.1: *Two-photon cross sections at 785 nm and 810 nm, calculated utilising data found in section 5.5 and equation 7.3.*

sections for glycated lysine, as presented in section 5.5, are now used. In figure 5.4 the transmission curve seemingly kinks around 330 nm, which may be taken as the peak point of the absorption band addressed. Of course this is only a guess, as more than one absorption band may be available – these molecules may be quite complicated. At 330 nm the transmission cross section may be calculated using the procedure described in section 5.5 to $28.9 \cdot 10^{-23} m^2$. From table 5.6 cross sections at 392 nm and 405 nm can be found to $9.46 \cdot 10^{-23} m^2$ and $7.85 \cdot 10^{-23} m^2$, respectively. For σ_{2P} this gives the results shown in table 7.1.

The cross sections are very small. The flux of the laser therefore needs to be comparable large in order to generate any noticeable fluorescence or bleaching. For a comparison, and to check the method used here, the two-photon absorption cross section for Rhodamine 6G has previously been found to be in the range of $1.4 - 5 \cdot 10^{-58} m^4$s [7] (at around, but not necessarily exactly at, 1060 nm) [1] utilising different experimental techniques. Using equation 7.3 the cross section for Rhodamine 6G in ethanol may be estimated to $0.676 \cdot 10^{-58} m^4$s. Thus my used semi-empirical method underestimates the cross section by a factor of about five[2]. Still, considering the number of assumptions and estimates made in general regarding the two-photon absorption/bleaching I consider this a useable estimate.

7.2 Photobleaching in the eye – an estimate

It is not possible to calculate the TPE bleaching without knowing the optical set-up or parameters for the laser. But if some – reasonable – assumptions are made, it is possible to give some – reasonable – estimate over the bleaching. The laser parameters should be set after what a maximum acceptable thermal load of the eye may be. Shooting laser beams into the eye is generally not acceptable so the thermal load should be kept low. Taking the laser beam as a train of mode-locked pulses it is for a start sufficient to look at the effect of an individual pulse. The parameters for the pulse are peak power and duration. Above a threshold pulse power optical breakdown may be the resulting effect, leading to local cavity formation and "streak" line formation in the tissue. This is actually used in certain experimental treatments of presbyopia[3] to create minute cavities in the lens to increase the flexibility of it [13]. In that paper the authors utilise

[1] I have divided data by two as this reference presents cross sections for photon absorption, which have factor of two incorporated. However, for many of the older works, it is not clear whether this factor was incorporated or not, thus there is the possibility that (some of) the values given in [7] may be off by a factor of 2

[2] Not all authors [12] are happy about the method presented in reference [10], as I have used here.

[3] Presbyopia, the age-related loss of accommodation-ability of the lens of the eye due to the loss of elasticity of the lens.

an optical system with a 75 mm focal length giving a focal spot diameter of 5 μm. A shorter focal length is probably not practical when a scanner system has to be employed to scan the spot inside the lens. The authors achieve strong bubble formation and lasting photodisruption of the lens tissue at 1μJ pulses with a pulse duration of 150 fs as delivered by the laser system. Likely the pulses at the actual focal point are slightly longer due to dispersion effects in the optics and the eye. For the assumption the pulse length may be set to 200 fs. In reference [14] an example of pulse energy in non-destructive TPE microscopy in corneal tissue is given at 0.13 nJ per pulse at 170 fs oscillator pulse duration (10 mW average power at 76 MHz repetition rate). In this reference a focal spot diameter of about 1 μm is used [4]. This gives a focal spot area 25 times smaller than for the eye scanner in reference [13], which indicates that for a practical focal spot in the lens at 5 μm a 25 times higher energy may "safely" be used. In addition under similar focal and laser conditions by own experience[5] up to ten times higher pulse energy (100 mW average at 76 MHz repetition rate) is useable without cooking the tissue (thermal overload being the problem rather than optical breakdown) if the laser is scanned "reasonably quickly". So as an estimate a pulse energy for a practical system may be $250 \cdot 0.13nJ = 32.5nJ$. This is still 30 times less than used in reference [13] for bubble formation and photo-disruption. Assuming a top hat pulse shape (realistic if the laser beam is delivered by a multi-mode fiber), the flux for 32.5 nJ 200 fs 785 nm pulses with area $A_{spot} = \pi \cdot (2.5\ \mu m)^2 = 19.6\ \mu m^2$ can be evaluated assuming square pulses (spatially as well as temporally) to:

$$I_0 = \frac{32.5\ nJ \cdot 785\ nm}{h \cdot c} \cdot \frac{1}{200\ fs} \cdot \frac{1}{19.6\ \mu m^2} = 3.27 \cdot 10^{34}\, m^{-2} s^{-1} \tag{7.4}$$

The focal spot length corresponds approximately to the confocal parameter l_{spot}:

$$l_{spot} = \frac{A_{spot}}{\lambda} = \frac{\pi \cdot (2.5\mu m)^2}{785nm} = 25\mu m \tag{7.5}$$

Chromophore concentration in cataractous lenses

To estimate bleaching in a real life cataractous lens it is necessary to estimate the chromophore concentration and absorption and bleaching cross sections in such a lens. For a grade II cataract the light transmission may be 50% compared to a non-cataractous lens [15]. Assuming this transmission drop is solely due to a browning of the lens and not intra-nuclear scattering sites (as cataract comes in many shapes this assumption should hold for some cases) the chromophore concentration may be assessed if it is assumed the chromophore absorption cross section found for glycated lysine compounds also holds for chromophores in the lens. This is questionable as the chemical and physical environments are different in the lens. Still for an estimate this may be useful enough. The optical

[4] Assuming diffraction limited spot size obtained by a water immersion microscope objective with numerical aperture 1.2 – as in the reference. Spot size $\approx 2.44 \cdot \lambda \cdot D_{working}/d_{aperture}$, where $D_{working}$ is the working distance of about 0.28 mm, and $d_{aperture}$ is the aperture of the objective estimated as $d_{aperture} \approx 2 \cdot D_{working} \cdot N.A./n_{water}$.

[5] As I used at the FIBMT, St. Ingbert, Germany, for microscopy on (ex-vivo) pig corneal and lens tissues.

pathway through the central region of the lens is approximately 5 mm, but it may be assumed the cataractous region is limited to the nucleus – about 3 mm in length. Assuming a 50 % drop in light transmission can be interpreted as a 50 % drop in the transmission at 550 nm where the sensitivity of the eye is highest (for photopic – daylight – vision) the needed chromophore concentration to reach this absorption may be assessed. Following the lines of section 5.5 the cross section of absorption for 550 nm for 48 hours incubated glycated lysine is estimated to $\sigma_{550\ nm} = 0.183 \cdot 10^{-18}\, cm^2$. To achieve 50% transmission at a path length of 3 mm the needed concentration $n_{T50\%}$ may be calculated using equation 5.1 page 56 to $n_{T50\%} = 12.6{\cdot}10^{18}\, cm^{-3}$. As glycated lysine is the model system, cross sections for this are used to estimate the chromophore content in the lens.

Estimate of realistic in-vivo bleaching

An estimate of the practicality of in-vivo bleaching of lenses by TPE bleaching may now be based on the found/estimated parameters for absorption cross section, concentration, and bleaching quantum efficiency. As it would be unrealistic to bleach all chromophores the question is, what a necessary bleaching would be for vision improvement. It may be sufficient just to increase the light transmission in a "tunnel" through the optical centre line of the lens. This tunnel or tube may for the example be 3 mm in diameter and extend 3 mm through the nucleus , with the transmission at 550 nm restored to 75%. Calculated as above this transmission corresponds to a chromophore concentration of $n_{T75\%} = 5.24 \cdot 10^{18}\, cm^{-3}$. Splitting the region to be bleached up in tubes of diameter 5 μm and length 25 μm gives for the transversal "resolution":

$$\left(\frac{1.5 \cdot 10^{-3}\ m^2}{2.5 \cdot 10^{-6}\ m^2}\right)^2 = 360 \cdot 10^3 \tag{7.6}$$

Above is given the transversal number of bleaching "pixels" for the desired channel. In the longitudinal direction there is (3 mm/25 μm)= 120. Thus the final number of 3-dimensional volume pixels (sometimes known as "voxels") is about $43.2 \cdot 10^6$. It may now be estimated how long bleaching time each voxel needs before the required drop in absorption is reached. This may be estimated from equation 7.3 – only using the part representing the loss in flux (second term right hand side), multiplied with the area to get the photon loss per second, and multiplied with the pulse length to get the photon loss per pulse. This time it should be remembered that for each two absorbed photons only one excitation event takes place. So for the excitation[6], inserting numbers from above, $I_0 = 3.27 \cdot 10^{34}\, m^2 s^{-1}$, $\sigma_{2P} = 6.08 \cdot 10^{-63}\, m^4 s$ (at 785 nm fundamental), $A = 19.6\ \mu m^2$, $L = 25\ \mu m$, $t_{pulse} = 200\ fs$, the initial excitation events (for $n_{initial} = n_{T50\%} = 12.6 \cdot 10^{18}\, cm^{-3}$) can be found to be

$$\frac{n_{excited,\ ini}}{per\ pulse} = n_{initial} \cdot I_0^2 \cdot \sigma_{2P} \cdot A \cdot L \cdot t_{pulse} \approx 8000 \tag{7.7}$$

As a comparison, in the bleaching tests I used approximately 15 mW absorbed power at 392 nm – corresponding to $29.6 \cdot 10^{15}$ absorbed photons per

[6]This covers into all reachable states – may they lead to fluorescence, bleaching, phosphorescence, or just non-emitting relaxation.

second. For a pulse duration of 200 fs this would lead to ≈ 6000 excitation events (one absorption is the same as one excitation in this case). Finally the excitation events per pulse should be multiplied with the quantum efficiency of the bleaching. Thus the change in concentration Δn in a voxel may be calculated as:

$$\frac{\Delta n}{per\ pulse} = \left(\frac{n_{excited}}{per\ pulse}\right) \cdot \zeta_{785\ nm} \tag{7.8}$$

Where $\zeta_{785\ nm} = 2.70 \cdot 10^{-3}$ is the bleaching quantum efficiency at 392 nm excitation. For the initial bleaching this gives ≈ 22 bleached chromophores per pulse.

For time integrated bleaching of a voxel equation 7.8, with 7.7 inserted, may be used:

$$n(C_p) \cdot A \cdot L = n_{initial} \cdot A \cdot L - \sum_p (n(C_p) \cdot I_0^2 \cdot \sigma_{2P} \cdot A \cdot L \cdot t_{pulse} \cdot \zeta_{785\ nm}) \tag{7.9}$$

With C_p as the pulse counter – summation is over all previous pulses up to p. Multiplication of the concentrations n by the voxel volume $A \cdot L$ is to take into account the limited amount of chromophores in the sample. Inserting the initial and final chromophore concentrations $n_{initial} = n_{T50\%} = 12.6 \cdot 10^{18}\, cm^{-3}$ and $n_{final} = n_{T75\%} = 5.24 \cdot 10^{18}\, cm^{-3}$, the required pulses needed to achieve the final transmission may be calculated easily numerically along the lines used in the single photon bleaching experiments – section 6.1.4 page 76. Just instead of iteratively finding the quantum efficiency, the bleaching time is found. An assumption is that it is possible to use the bleaching quantum efficiency for 392 nm excitation for TPE-bleaching. This does seem reasonable as the energy delivered to the molecule is the same under the two different excitation models. The required number of pulses per voxel to reach the desired 75% transmission may be evaluated to be:

$$\begin{aligned} C_{p,\ end} &= 2.49 \cdot 10^8 \\ \Rightarrow \quad & 8.09 Joules \end{aligned}$$

A repetition rate of typical mode-locked oscillators is up to $100 \cdot 10^6\, s^{-1}$ the exposure time in seconds can be estimated to $T_{Exposure} = 2.49$ seconds per voxel. This is reasonably quick, but considering the amount of voxel needed to be bleached in order to get a macroscopic effect (estimated above to be around 43 millions), it would take in the order of three and a half years ($107.5 \cdot 10^6$ seconds) for bleaching the proposed region. Thus it does not seem realistic to bleach the cataractous lens with TPE bleaching. Had UV light at 392 nm been used for bleaching the bleaching time for a comparable amount of chromophores (assuming 3 mm by 3 mm cube to be bleached with chromophore concentration as for the TPE bleaching above, incident power 15 mW at the lens) the bleaching time would be around 24000 seconds – or 400 minutes. More worryingly is the amount of energy – 8.09 J – required for bleaching each voxel. By far the largest amount of the energy is *not* absorbed in the lens, but in the retina/RPE. Utilising a laser with 100 MHz repetition rate for a bleaching time of 2.49 seconds

per voxel this would lead to an average laser power into the eye of approximately 3.25 W. This is far too much to be acceptable; even if the defocussing of the laser spot on the retina does not lead to spot burns the heating of the retina would still be unacceptable.

7.2.1 Photo-bleaching by TPE

The major problem regarding experimental TPE bleaching is the low macroscopic bleaching rate – as shown above. This either calls for a very small sample size if the entire sample is bleached. Or some method of fixating the chromophores so a small region may be bleached in a larger sample. Both methods were briefly investigated in the course of the project.

Small sample volumes

In order to use liquid sample the volume of the bleached sample had to be small. In liquid samples the chromophore concentration is bleached for the entire sample as the chromophores diffuse around the sample quickly. To keep absorption relatively high the concentration can not be too low. Thus the number of chromophores in the sample has to be kept low by using a small sample volume. This was tried by drilling holes of 2 mm diameter in a 1.5 millimetre thick copper plate and fill these holes with liquid sample. Both ends were then sealed with glass cover slips. The bleaching was tried at Teknologisk Institut, Høje Taastrup, Denmark, in their amplified femtosecond laser system. The results were negative as the samples could not be kept free from bubble formation at the glass seals, which quickly led to thermal destruction of the samples.

Another approach was by forming small cavities in a silicone based sealant between glass cover slips and fill these with sample. This method was tried utilising a femtosecond oscillator at the COM Centre, Technical University of Denmark. This method did not provide any significant bleaching results. Probably due to the sample volume being too large to allow any bleaching to be detected. Smaller sample volumes could not be mounted this way.

Fixing samples

To be able to bleach just a small area in a larger sample it is necessary to stop the diffusion of chromophores. In the lens of the eye this is not a problem as the chromophores are bound to the protein chains, which lie in a highly fixed hexagonal structure. A number of methods were considered for fixating the samples, briefly described below:

- Mixing the liquid samples with a gelling agent. Two gelling agents were tested for this purpose, household porcine collagen based gelling agent (as may be purchased in any food store) and a gel powder usually used for making gels of growth media (for bacteriological growth). Porcine gelling agent ("Husblas", Coop, Denmark) was found to give a watery gel with poor stability. Subsequently, a commercial laboratory gelling agent ("Phytagel", Sigma-Aldrich, Germany) was tested. This gave a hard, dry-feeling gel. Drops of sample with this gel powder added were placed between microscope slides before solidification. The glass slides were then

pressed lightly together to create a gelled slab of about a millimetre in thickness. Bleaching experiments were performed on such samples in a femtosecond LSM at the Royal Veterinarian and Agricultural University, Frederiksberg, Denmark. It was found that the diffusion rate in this gel was still too high to allow TPE bleaching to be "written". Even under UV bleaching, which is much more efficient than TPE bleaching, the bleached area ($\sim$ a square of few hundred μm side length) would disappear after few seconds due to in-diffusion of chromophores from surrounding non-bleached areas.

- Casting the chromophores in a polymer matrix. For microbiological or histological microscope studies samples are routinely fixed in a polyamide matrix. It was tried to make a polymer sample by staining polyamide with the glycated lysine. As the components going into polyamide are highly neurotoxic and carcinogenic the polyamide samples were kindly processed at the BioCentrum, Technical University of Denmark, by Associate Professor Claus Sternberg. Subsequently, TPE bleaching was tried at the femtosecond LSM facility at the same department. Diffusion in this matrix was found to be too high to give any permanent bleaching.

- Drying the chromophores. Not tested.

- Using a model system where the browned components are bound to fixed sites. An idea for this was directly browning the porcine gel mentioned above by incubating them with lysine as for the glucose. It turned out it was not possible to obtain a stable gel after incubation. In the appendix chapter E is presented results on investigations of gels and browned porcine collagen.

No TPE bleaching was successfully performed. This proves how difficult it is to perform TPE bleaching of macroscopic samples. To perform initial TPE bleaching in the laboratory the best solution will be to create a more stable sample with no diffusion of chromophores and bleach this in a femtosecond LSM. The femtosecond LSM has the advantage of simultaneously being able to induce bleaching while monitoring the progress via its built in fluorescence detectors. Further research on sample preparation should be investigated.

7.3 Summary on TPE bleaching

TPE bleaching was evaluated empirically based on results obtained for glycated lysine. TPE cross section and bleaching were evaluated, estimate for bleaching time was given based on assumptions of initial and final chromophore concentration and the volume of the eye. It was shown that under the given assumptions the lens in the eye may be bleached by TPE but it would require longer time than is practical in a clinical treatment. Some factors may improve on this, the two-photon absorption cross section is for a start estimated rather conservatively. Still as discussed in the text the estimation method used on other chromophores yield results differing from measurement results only with an order of magnitude. To successfully utilise TPE bleaching in a clinical environment much larger increase in bleaching speed would be needed. Alternatively

the bleached volume should be smaller, or the targeted increase in transmission should be relaxed. Possibly multiple femtosecond beams could be employed simultaneously, but there should be established a safe limit for thermal load on the eye to avoid damages if more power is sent in.

TPE bleaching of model samples in liquid and jellified form were tested but found to be unsuccessful due to diffusion.

Bibliography

[1] J.R. Lakowicz, *Principles of Fluorescence Spectroscopy* (Kluwer Academic/Plenum Publishers, 1999)

[2] W. Denk, J.H. Strickler, and W.W. Webb, "Two-Photon Laser Scanning Fluorescence Microscopy"; Science, vol. 3.248, pp. 73-76; 1990

[3] K. König, "Multiphoton microscopy in life sciences"; J. Microscopy, vol. 200, pp. 83-104; 2000

[4] K. König, P.T.C. So, W.W. Mantulin, and E. Gratton, "Cellular response to near-infrared femtosecond laser pulses in two-photon microscopes"; Optics Lett., vol. 22, pp. 135-136; 2005

[5] K. König, I. Riemann, P. Fischer, and K.-J. Halbhuber, "Intracellular nanosurgery with near infrared femtosecond laser pulses"; Cellular and Molecular Biology, vol. 45, pp. 195-202; 1999

[6] J.P. Hermann, and J. Ducuing, "Absolute measurement of two-photon cross sections"; Phys. Rev. A, vol. 5, pp. 2557-2568; 1972

[7] P. Kaatz, and D.P. Shelton, "Two-photon fluorescence cross-section measurements calibrated with hyper-Rayleigh scattering"; J. Opt. Soc. Am. B, vol. 16, pp. 998-1006; 1999

[8] D. Kleinman, "Laser and Two-Photon Processes"; Phys. Rev., vol. 175, pp. 87-88; 1962

[9] D.J. Bradley, M.H.R. Hutchinson, and H. Koetser, "Interactions of picosecond laser pulses with organic molecules II. Two-photon absorbtion cross sections"; Proc. R. Soc. Lond. A, vol. 329, pp. 105-119, 1972

[10] F.P. Schäfer, W. Schmidt, "Geometrical Model and Experimental Verification of Two-Photon Absorption in Organic Dye Solutions"; IEEE J. Quant. Elect., vol. 2, pp. 357-360; 1966

[11] R. Loudon, *The Quantum Theory of Light* Second Edition (Oxford University Press, 1983)

[12] J.P. Hermann, and J. Ducuing, "Dispersion of the two-photon cross section in rhodamine dyes"; Op. Comm., vol. 6, pp. 101-105; 1972

[13] T. Ripken, A. Heisterkamp, U. Oberheide, R.R. Krueger, E. Luetkefels, W. Drommer, W. Ertmer, and H. Lubatschowski, "First in-vivo studies of presbyopia treatment with ultrashort laserpulses"; Proc. SPIE – OSA Biomed. Optics., vol. 5142, 137-145; 2003

[14] A.T. Yeh, N. Nassif, A. Zoumi, and B. Tromberg, "Selective corneal imaging using combined second-harmonic generation and two-photon excited fluorescence"; Op. Lett., vol. 27, pp. 2082-2084; 2002

[15] K. Nishimoto, K. Sasaki, "In vivo light scattering intensity in the lens versus in vitro spectral transmission in the nuclear region"; Ophthalmic Res., vol. 27, pp. 1-11, 1995

Chapter 8

Conclusion

> Results! Why, man, I have gotten a lot of results. I know several thousand things that won't work.
>
> Thomas A. Edison.
> *American inventor (1847-1931)*

This thesis has covered both sides of applied optics – the optical side and the applied side. The optical side dealt with setting up a solid-state laser system for generation of blue-to-UV light. The application side dealt with bleaching of a cataract assay. I will summarise the most important results here.

BiBO for SHG of Ti:Sapphire laser

For making the necessary blue-to-UVA light a frequency doubled Ti:Sapphire was utilised. For the nonlinear crystal it was chosen to use the novel crystal material BiB_3O_6. Two crystals were acquired – one for doubling 785 nm, and the other for doubling of 808 nm. The most important results:

- Doubling of 785 nm utilising a 3 mm long BiBO crystal gave a maximum blue output of 53 mW. Doubling of 810 nm utilising a 5 mm long crystal gave a maximum blue output of 100 mW.
- Tunability for the 3 mm long crystal was found to be approximately 8 nm.
- Temperature dependence was found to be low.

Model system for cataract and bleaching

A model system for cataract was investigated. Based on published results it was chosen to utilise glycated lysine for the purpose. Glycated lysine was manufactured and investigated. Excitation and emission spectra were recorded. TPE emission spectrum was compared with SPE emission spectrum. Bleaching of the chromophore was tried utilising the frequency-doubled Ti:Sapphire laser. The possibility for bleaching utilising a two-photon process was discussed, in vitro and in vivo. Main results:

- Glycated lysine was found to give emission and excitation spectra comparable to spectra from human cataractous lenses and to spectra for suspected candidates for the yellowing chromophores. Glucation of lysine was found to give a higher yield at neutral than at higher pH values.
- TPE fluorescence spectra were found to be comparable to SPE spectra.
- Bleaching of glycated lysine was found to have a quantum efficiency of $2.70 \cdot 10^{-3}$ at 392 nm and a slightly lower quantum efficiency at 405 nm of $2.70 \cdot 10^{-3}$.
- Fluorescence was found to be reduced following bleaching.
- Utilising found data for SPE absorption cross section and SPE bleaching quantum efficiency, a semi-empirical model for TPE absorption, and estimating the necessary bleaching of a cataractous lens before vision is improved, it was found that the required time for bleaching a lens in vivo would be in the order of three and a half years. This is a conservative estimate, but it may still be used as a hint at the time required.

8.0.1 Future work

Based on the results found new experiments may be suggested. One thing that was not tested for, was the long term stability of the bleached samples. The bleached samples stayed bleached on a time scale of a few days when stored cold, but one experiment that could be done is a re-incubation of bleached samples. This should prove if the bleaching is permanent. Care must be taken to ensure any subsequent browning is not caused by residual, non-reacted glucose and lysine in the bleached samples. This may be done by using samples having been incubated sufficiently long to ensure all glucose and lysine has reacted before bleaching. A further check would be to measure the rest glucose level after bleaching.

Although the bleaching experiments in this work have all shown same trend regarding bleaching and quantum efficiency, more bleaching experiments should be performed. If possible bleaching should be tried for substantial longer time – i.e. up to a day; with control of transmission at regular intervals. This would reveal if the bleaching saturates or continues towards zero absorption.

As the clinical implementation utilises a two-photon process for bleaching this should be investigated. It will be necessary to first make a model system where the chromophores are quite tightly bound. Any diffusion will quickly make TPE bleaching undetectable in a larger sample due to the small bleached volume.

Finally, and this is paramount, the bleaching should be tried on real, cataractous lenses. Real eyes have been bleached by a single photon process by others, but to the best of my knowledge it has never been tried with monochromatic light. Only with monochromatic light parameters such as wavelength dependence and quantum efficiency for the bleaching may be estimated. If the quantum efficiency turns out to be as low – or lower – for real lenses as for glycated lysine, it is questionable if the concept is practically useable in a clinical environment.

8.1 Final remarks and comments

This project was established in order to investigate the possibility of utilising femtosecond laser pulses to bleach cataract in the human lens. Although it was never managed to perform TPE bleaching important results regarding this have still been obtained. As an assay glycated lysine was investigated, and it was found this is an easy system to work with. In addition it shows many of the same characteristics also seen with cataract. Results obtained for cross section and bleaching quantum efficiency indicate it might be difficult to perform the desired procedure in a clinical environment – mostly because of the long time required. Several assumptions were made, and the conclusion should been viewed in light of this. Many factors may prove to be different for a real lens – such as absorption cross section and bleaching quantum efficiency. This can only be discovered by experiments on real human lenses. Still, in light of the found results research efforts on utilising ultra short pulse lasers in ophthalmology should be directed towards possibilities of using these lasers for surgical or investigative procedures. For both purposes much the same equipment will be needed as for bleaching of cataract. And when such equipment is implemented work on bleaching may easily be brought to life again.

Several novel and interesting results were obtained in the field of intracavity SHG in a Ti:Sapphire laser system. With further work it should be straight forward to make a compact UVA solid-state laser system utilising Ti:Sapphire as laser medium and BiBO as the nonlinear medium.

Although stressful at times – when we repeatedly failed to get funds for much desired equipment, when I tried to understand ophthalmology, and when things in the lab for weeks went nowhere – it was always a joy to work with this project. It gave me a unique chance to deal not only with the laser side of biomedical optics but also the application of it. And I believe this has given me an insight into both worlds – physical as well as biomedical – that few experience as Ph.D. students. I hope this is reflected in the presented work, and it is my hope the results obtained may be of benefit to others in this field.

Appendix A

Matrices

The best way to model a laser resonator is by using ABCD-matrices (a general introduction into this subject may be found in laser text books such as [1, 2]). Take a ray somewhere in the – rotationally symmetric – laser system. This may be described fully by its off-axis position x, and its inclination x'. Then look at another given point in the cavity. The same ray transformed through the cavity to a new point will have the parameters y and y'. The transformation that links x,x' to y,y' may be conveniently described by a matrix of dimension (2,2):

$$\begin{bmatrix} x \\ x' \end{bmatrix} = \begin{bmatrix} A & B \\ C & D \end{bmatrix} \cdot \begin{bmatrix} y \\ y' \end{bmatrix} \tag{A.1}$$

The transformation matrix is also commonly know as an ABCD-matrix. It turns out the same transformation matrix also works for transforming the q factor of Gaussian beams [1]. In this section matrices not commonly found in the litterature are derived.

A.0.1 Oblique incidence on mirrors

When the incidence on components transforming the beam front is not normal but oblique, the system is no longer rotationally symmetric. Instead the two cases – in the plane of folding and perpendicular to that plane – must be treated separately. For non-flat mirrors under normal incidence the ABCD-matrix is given as:

$$\begin{bmatrix} 1 & 0 \\ \frac{2}{R} & 1 \end{bmatrix}_{flat} \tag{A.2}$$

Now the equation A.2 given above is modified in the case of incidence away from the mirror normal. The curvature of the component in the vertical case must be modified by ***multiplication*** with $\cos\theta$, where θ is the angle between the direction of the incident beam and the normal of the mirror in the point of incidence; for the horizontal case, horizontal being here the plane of folding, the curvature is modified this time by ***division*** with $\cos\theta$ [1]. The resulting matrices

[1] As instructed to me by Peter Tidemand-Lichtenberg. This is one of those facts "everybody knows´´, but is difficult to find in the litterature.

are:

$$\left[\begin{array}{cc} 1 & 0 \\ \frac{2}{R}\cdot\frac{1}{\cos\theta} & 1 \end{array}\right]_{mirrorH} \quad \& \quad \left[\begin{array}{cc} 1 & 0 \\ \frac{2}{R}\cdot\cos\theta & 1 \end{array}\right]_{mirrorV} \tag{A.3}$$

Oblique incidence on lenses

The thin lens is described by the ABCD-matrix:

$$\left[\begin{array}{cc} A & B \\ C & D \end{array}\right]_{thin\,lens} = \left[\begin{array}{cc} 1 & 0 \\ \frac{-1}{f} & 1 \end{array}\right] \tag{A.4}$$

Where f is the focal length of the thin lens.

The oblique incidence on lenses gives rise to the same modifications as for the case of oblique incidence on mirrors. Thus the matrices are:

$$\left[\begin{array}{cc} 1 & 0 \\ \frac{-1}{f}\cdot\frac{1}{\cos\theta} & 1 \end{array}\right]_{lensH} \quad \& \quad \left[\begin{array}{cc} 1 & 0 \\ \frac{-1}{f}\cdot\cos\theta & 1 \end{array}\right]_{lensV} \tag{A.5}$$

A.1 The oblique slab

In many resonator types a non-mirror component that is not normal to the slab but oblique may be found. The derivation of its generic ABCD-matrix is not covered nor is the matrix given in most – if any – textbooks treating laser resonators. I shall her present a derivation of the ABCD-matrix (for a Gaussian beam) for a parallel-sided dielectric slab.

A.1.1 Diffraction at slab interface – Huygens construction

For my purpose I look only at parallel sided slabs, which reduces the complexity of the system matrix for the slab. For verification of all used trigonometric formulas and equations a hand book like [3] has been consulted. The geometry for the oblique incidence on a slab of dielectric material is shown in figure A.1.

Discontinuity of beam waist

On figure A.1 the incident beam comes from left and hits the slab with the angle θ_1 between the propagation direction of the incident beam and the normal of the slab. First to be determined is the projection of the incident beam waist on the interface. Now the angle θ_i is given as $90^o - \theta_1$ and it may be found:

$$\sin\theta_i = \frac{W_1}{W_i} \tag{A.6}$$

$$\Rightarrow W_i = \frac{W_1}{\sin\theta_i} = \frac{W_1}{\sin(90^o - \theta_1)} \tag{A.7}$$

$$\Rightarrow W_i = \frac{W_1}{\cos\theta_1} \tag{A.8}$$

From the just found W_i it is now possible to find the projected beam size just cross the interface. This is W_2 in figure A.1.
W_2 may be found as:

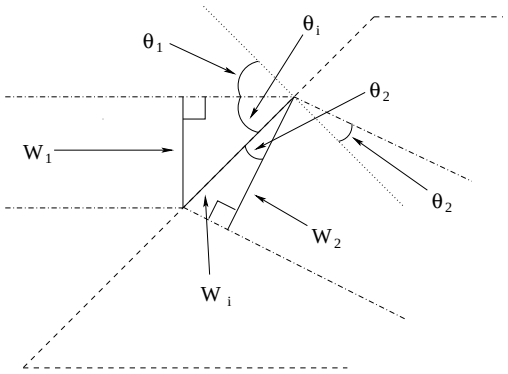

Figure A.1: *Incidence on slab – the geometry. Incident beam with spot size W_1 comes from left. Beams are dash-dotted, the slab is dashed.*

$$W_2 = W_i \cdot \cos\theta_2 \tag{A.9}$$

$$\Rightarrow W_2 = W_1 \frac{\cos\theta_2}{\cos\theta_1} \tag{A.10}$$

θ_2 is itself a function of θ_1 (see equation A.11) and the refractive indexes of the surrounding media and the slab. To make all equations and matrices dealing with the angles of incidence and internal angles so simple as possible, I have used the incidence and internal angles in cosine-equations. This is the most convenient form. θ_2 – the internal angle – is not explicitly known. But using Snell's law we can obtain:

$$n_2 \sin\theta_2 = n_1 \sin\theta_1 \Rightarrow \cos\theta_2 = \sqrt{1 - \left(\frac{n_1}{n_2}\right)^2 \sin^2\theta_1} \tag{A.11}$$

$$\cos\theta_1 = \sqrt{1 - \sin^2\theta_1} \tag{A.12}$$

Where n_1 is the refractive index of the surrounding medium (from where the beam enters the slab), while n_2 is the refractive index of the slab.

The beam spot experiences a discontinuous change, which must be incorporated into the ABCD-matrix. The beam is determined by the lateral position of the individual "rays" forming the beam (in a strange mixed ray-Gaussian picture), and the coefficient of change at the interface is given as W_2/W_1, and thus the discontinuity change goes into the A-coefficient of the matrix as:

$$A = \frac{\cos\theta_2}{\cos\theta_1} \tag{A.13}$$

Change in curvature of beam, horizontal plane

As the beam passes the interface the curvature of the wavefront changes. Here a pseudo-paraxial approximation is used. That is not to consider the full equations for Gaussian beams across interfaces but to look at a planar beam, which has an infinitesima change in incidence angle, leading to an infinitesimal change in the refracted angle. From Snell's law:

$$\sin\theta_2 = \frac{n_1}{n_2}\sin\theta_1 \tag{A.14}$$

$$\Rightarrow \theta_2 = \arcsin\left(\frac{n_1}{n_2}\sin\theta_1\right) \tag{A.15}$$

Consider a small change $\Delta\theta_1$ of the incident ray around the incidence angle θ_1. The resulting change in θ_2 is given as $\Delta\theta_2 = \Delta\theta_1 \cdot (\partial\theta_2/\partial\theta_1)$; where $\partial\theta_2/\partial\theta_1$ is given as:

$$\frac{\partial\theta_2}{\partial\theta_1} = \frac{\partial}{\partial\theta_1}\arcsin\left(\frac{n_1}{n_2}\sin\theta_1\right) \tag{A.16}$$

$$\Rightarrow \frac{\partial\theta_2}{\partial\theta_1} = \frac{1}{\left(1-\left(\frac{n_1}{n_2}\right)^2\sin^2\theta_1\right)^{\frac{1}{2}}}\frac{\partial}{\partial\theta_1}\left(\frac{n_1}{n_2}\sin\theta_1\right) \tag{A.17}$$

Where in equation A.17 it has been used that:

$$\frac{\partial}{\partial x}\arcsin u = \frac{1}{\sqrt{1-u^2}}\frac{\partial u}{\partial x} \tag{A.18}$$

The last derivative of equation A.17 gives:

$$\frac{\partial}{\partial\theta_1}\left(\frac{n_1}{n_2}\sin\theta_1\right) = \frac{n_1}{n_2}\cos\theta_1 \tag{A.19}$$

Equation A.17 with the result from equation A.19 substituted may now be simplified using the relation in equation A.11. The resulting equation for the discontinuity in beam curvature is then:

$$\frac{\partial\theta_2}{\partial\theta_1} = \frac{n_1}{n_2}\frac{\cos\theta_1}{\cos\theta_2} \tag{A.20}$$

This result goes in as the D-coefficient of the ABCD matrix of the interface. The result is the following ABCD matrix for the interface going from the surrounding media into the oblique dielectric slab:

$$\begin{bmatrix} A & B \\ C & D \end{bmatrix}_{inH} = \begin{bmatrix} \frac{\cos\theta_2}{\cos\theta_1} & 0 \\ 0 & \frac{n_1}{n_2}\cdot\frac{\cos\theta_1}{\cos\theta_2} \end{bmatrix} \tag{A.21}$$

The vertical case of interface discontinuity

When the folding plane of the cavity is the horizontal plane, then in the vertical plane the angle of incidence is 0^o, and thus the internal angle is zero as well, and all cosines equate to 1. So for the vertical plane there is no discontinuity in beam spot size, and no discontinuity in curvature due to the incident angle

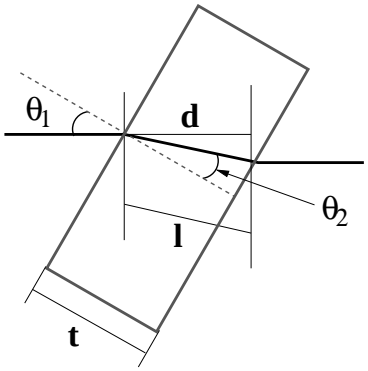

Figure A.2: *Different lengths to be considered in the slab. θ_1 is the incident angle normal to the slab interface. θ_2 is the internal angle in the slab. d is the distance the beam is closer to the next component along the optical axis after passing the slab. l is the length of the path the beam takes inside the slab. t is the slab thickness from interface to interface.*

(but still due to the difference in refractive index). The matrix for the vertical case:

$$\begin{bmatrix} A & B \\ C & D \end{bmatrix}_{inV} = \begin{bmatrix} 1 & 0 \\ 0 & \frac{n_1}{n_2} \end{bmatrix} \tag{A.22}$$

A.1.2 Out of the slab

The interface crossing going form the slab back into the surrounding medium may be treated in the same way as crossing from the medium into the slab. As only parallel sided slabs are treated here, the only difference is swapping medias in the ABCD-matrix. All incidence and exit angles are swapped as compared to before, now the incidence angle is θ_2 and the exit angle is θ_1. This gives the following ABCD-matrix:

$$\begin{bmatrix} A & B \\ C & D \end{bmatrix}_{outH} = \begin{bmatrix} \frac{\cos\theta_1}{\cos\theta_2} & 0 \\ 0 & \frac{n_2}{n_1} \cdot \frac{\cos\theta_2}{\cos\theta_1} \end{bmatrix} \tag{A.23}$$

Vertical plane case for interfaces matrices

The vertical plane is not the folding plane, and therefore the interface matrix is the same as for normal incidence:

$$\begin{bmatrix} A & B \\ C & D \end{bmatrix}_{outV} = \begin{bmatrix} 1 & 0 \\ 0 & \frac{n_2}{n_1} \end{bmatrix} \tag{A.24}$$

A.1.3 Travelling through the slab

Before the system matrix for the dielectric slab can be derived, we still need to consider the traversing of the Gaussian beam through the thickness of the slab itself. Three different lengths may be considered when looking at the slab in the resonator – see figure A.2.

The most interesting length here is the actual path length the beam travels in the slab. This length is given as l in figure A.2. l can be found as:

$$l = \frac{t}{\cos\theta_2} \tag{A.25}$$

Where t is the thickness of the slab (along its normal). The equivalent resonator-length d is the distance the beam is to the next component after propagation through the slab. This can be found to be:

$$d = l \cdot \cos(\theta_1 - \theta_2) \tag{A.26}$$

$$\Rightarrow d = t \cdot \frac{\cos(\theta_1 - \theta_2)}{\cos\theta_2} \tag{A.27}$$

Where equation A.25 was used. Often the length of the beam path inside the oblique component is given rather than the length of the slab or crystal (as it is normally assumed to be positioned in the Brewster angle, this length is unambiguous); this is the length shown as l in figure A.2. Thus the B-coefficient of the ABCD-matrix for propagation through the slab medium is simply:

$$\begin{bmatrix} A & B \\ C & D \end{bmatrix}_{through} = \begin{bmatrix} 1 & l \\ 0 & 1 \end{bmatrix} \tag{A.28}$$

Only thing to remember is to modify the given length as according to equation A.25 in case the length is given as t in figure A.2.

Vertical case for slab propagation

The ABCD-matrix for propagation through the slab is the same for the vertical as for the horizontal case, as the propagation distance is the same. So this matrix is unchanged and equal to equation A.28.

A.1.4 The slab – ABCD-matrix, horizontal

Now the final ABCD-matrix for the oblique slab may be written. It simply consists of a matrix multiplication of the three matrices presented above, in the order into the slab times the slab times out of the slab (matrix multiplication, so in reverse order):

$$\begin{bmatrix} \frac{\cos\theta_1}{\cos\theta_2} & 0 \\ 0 & \frac{n_2}{n_1} \cdot \frac{\cos\theta_2}{\cos\theta_1} \end{bmatrix}_{out\ H} \cdot \begin{bmatrix} 1 & l \\ 0 & 1 \end{bmatrix}_{through} \cdot \begin{bmatrix} \frac{\cos\theta_2}{\cos\theta_1} & 0 \\ 0 & \frac{n_1}{n_2} \cdot \frac{\cos\theta_1}{\cos\theta_2} \end{bmatrix}_{in\ H}$$
$$= \begin{bmatrix} 1 & \frac{n_1}{n_2} \cdot \frac{\cos^2\theta_1}{\cos^2\theta_2} \cdot l \\ 0 & 1 \end{bmatrix}_{slab\ H} \tag{A.29}$$

This matrix may now be put in to the model for the laser.

And the total slab matrix for the vertical case

For the vertical case the same multiplication is performed, but this time using the ABCD-matrices for the vertical orientation. That is, for in and out of the slab – the interfaces – one has to use the matrices given in equations A.22 and A.24; the matrix for the slab propagation is unchanged. In the end for the vertical case one ends up with:

$$\begin{bmatrix} A & B \\ C & D \end{bmatrix}_{slab\ V} = \begin{bmatrix} 1 & \frac{n_1}{n_2} \cdot l \\ 0 & 1 \end{bmatrix}_{slab\ V} \tag{A.30}$$

So the vertical case is somewhat simpler, but of course must be used to evaluate the laser cavity in the vertical non-folding plane. This matrix may now be put into the laser model as well.

A.1.5 Lensing in the crystal

That is, just "insert" a (weak) thin lens in the crystal. The lens is given by equation A.4, and this is now included in the general case of a slab with oblique incidence on it. As lensing effects in crystals normally are weak the thin-lens approximation should give good estimates for most cases[2].

Horizontal case

The matrix for horizontal case of the slab including this lens is calculated as [out of slab(A.23)]*[half propagation length]*[lens(A.4)]*[half propagation length]*[into slab(A.21)]; where [half propagation length] is analogue to the matrix for propagation through the slab (equation A.28), but with the B-coefficient divided by 2 ($B = l/2$). The [lens] matrix is the one just introduced.
This gives the following matrix for the slab+lens:

$$\begin{bmatrix} A & B \\ C & D \end{bmatrix}_{slab+lens\ H} = \begin{bmatrix} 1 - \frac{l}{2 \cdot f} & \frac{n_1 \cdot \cos^2 \theta_1}{n_2 \cdot \cos^2 \theta_2} \left(l - \frac{l^2}{4f} \right) \\ -\frac{\cos^2 \theta_2 \cdot n_2}{\cdot \cos^2 \theta_1 n_1} \cdot \frac{1}{f} & 1 - \frac{l}{2 \cdot f} \end{bmatrix} \tag{A.31}$$

This may now be inserted into the laser model instead of the normal slab matrix without lens.

Vertical case

For the vertical case of the oblique slab with lens, the equations for the vertical passing of interfaces are used, equations A.22 and A.24. This leads to the following matrix:

$$\begin{bmatrix} A & B \\ C & D \end{bmatrix}_{slab+lens\ V} = \begin{bmatrix} 1 - \frac{l}{2 \cdot f} & \frac{n_1}{n_2} \left(l - \frac{l^2}{4f} \right) \\ -\frac{n_2}{f \cdot n_1} & 1 - \frac{l}{2 \cdot f} \end{bmatrix} \tag{A.32}$$

[2] For cases where the lensing is a desired effect – such as for Kerr-induced mode-locking – a full (numerical) GRIN-lens model should be used.

Bibliography

[1] T. Skettrup, *Laserteknik* 5. udg. (Polyteknisk Forlag, 1993)

[2] A. Yariv *Optical Electronics* Fourth Edition (Saunders College Publishing/HBJ, 1991)

[3] M.R. Spiegel, *Schaum's Outlines Mathematical Handbook of Formulas and Tables* (McGraw-Hill, 1968)

Appendix B

Theoretical SHG estimates

To give an estimate over the possible obtainable blue output for the chosen crystals some light theoretical analysis was performed.

B.1 Theoretical model for SHG

The SHG output was calculated along the lines given in references [1, 2, 3]. In reference [3] the following formula is given for calculating the generated SHG output:

$$P_{2\omega} = K \cdot P_{\omega}^2 \tag{B.1}$$

$$K = \frac{2 \cdot \omega^2 \cdot d^2}{\pi \cdot \epsilon_0 \cdot c^3 \cdot n^3} \cdot \frac{L^2}{w_0^2} \cdot h(B, \xi) \tag{B.2}$$

Where $P_{2\omega}$ is the generated SHG power at frequency 2ω, P_{ω} is the fundamental field at frequency ω, d is the effective nonlinear coefficient, L is the crystal length, ϵ_0 is the free space permittivity, c is the free space speed of light, n is the refractive index of the crystal (assumed to be approximately equal for fundamental and second harmonic field), and finally w_0 is the fundamental field beam waist radius inside the BiBO crystal. The equations B.2 and B.2 are slightly modified under the assumption of perfect phase match. In addition the factor $h(B, \xi)$ is included as used in reference [2] to allow for non-perfect focussing conditions. Finally a factor of 2 was multiplied on, to account for generation in both directions.

$h(B, \xi)$ is read visually from a table (as found in [2]), where the variables B and ξ are calculated as:

$$B = 0.5 \cdot \rho \left(\frac{2\pi \cdot n \cdot L}{\lambda} \right)^{0.5} \tag{B.3}$$

$$\xi = \frac{\lambda \cdot L}{2\pi \cdot n \cdot w_0^2} \tag{B.4}$$

Where – in addition to the already mentioned variables – λ is the fundamental wavelength, and ρ is the walk-off angle. The above equations may now be utilised for estimating the possible blue SHG output.

λ	785 nm	810 nm
ρ	61 mrad	58 mrad
L	3 mm	5 mm
n	1.85	1.85
w_0	25 μm	25 μm
d_eff	3.75 pm/V	3.70 pm/V
B	6.42	7.78
ξ	0.32	0.56
$h(B,\xi)$	≈ 0.08	≈ 0.08
P_ω	33 W	33 W
K	$7.9 \cdot 10^{-5} W^{-1}$	$20.0 \cdot 10^{-5} W^{-1}$
$P_{2\omega}$	85 mW	217 mW

Table B.1: *Data used in and results for theoretical estimate on obtainable blue output power for the SHG in BiBO crystals. The circulating field is a rough estimate based on values measured through mirror M1.*

B.2 Theoretical results for SHG

In table B.1 are shown used variables and results obtained when applying equations B.2 and B.2 together with found values for $h(B,\xi)$ on the SHG in the BiBO set-up.

The values for $h(B,\xi)$ are taken as equal for the two different crystals, as B is slightly bigger for the 810 nm SHG outbalancing ξ being a little smaller. The value for the intracavity field is based on what was found during the power-slope measurement for the 785 nm SHG case. For the 810 nm case it was difficult to come with a good estimate as the mirror transmission (for 810 nm) was close to zero. The longer crystal for 810 nm SHG should give higher nonlinear conversion efficiency, but with the lower mirror transmission the resulting loss for the NIR field should be much the same at both wavelengths. The large difference in conversion efficiency K is basically down to the 810 nm crystal being longer. Some issues have not been addressed in these theoretical estimates; first of all the line width of the fundamental fields were not exactly delta functions, but quite broad – around 0.69 nm. This influences the results in a negative way, especially for the longer crystal. The correction factor (G-factor) due to the IR line width may be calculated utilising a proprietary software program [1]; for the 3 mm crystal is found a G-factor of 0.97, while the 5 mm crystal gives a G-factor of 0.93. Taking the G-factor into account the theoretical values are 82 mW and 201 mW at 392 nm and 405 nm respectively. I have not included the G-factor in the K-coefficients, as this is determined by the IR line width, and not a feature due to the BiBO crystals. For a comparison with actual measured values and a discussion, see section 3.3.3 page 31.

[1] Inhouse development; © J.L. Mortensen, Department of Physics, Technical University of Denmark

Bibliography

[1] GD. Boyd, and D.A. Kleinmann, "Parametric interaction of focussed Gaussian light beams"; J. Appl. Phys., vol. 39, pp. 3597-3639; 1968

[2] P.M. Petersen, and T. Skettrup, *Ulineær optik* 1. udgave (Polyteknisk Forlag, 1994)

[3] I. Shoji, T. Kondo, A. Kitamoto, M. Shirane, and R. Ito, "Absolute scale of second-order nonlinear-optical coefficients"; J. Opt. Soc. Am. B, vol. 14, pp. 2268-2294; 1997

Appendix C

Eye pictures and lens scans

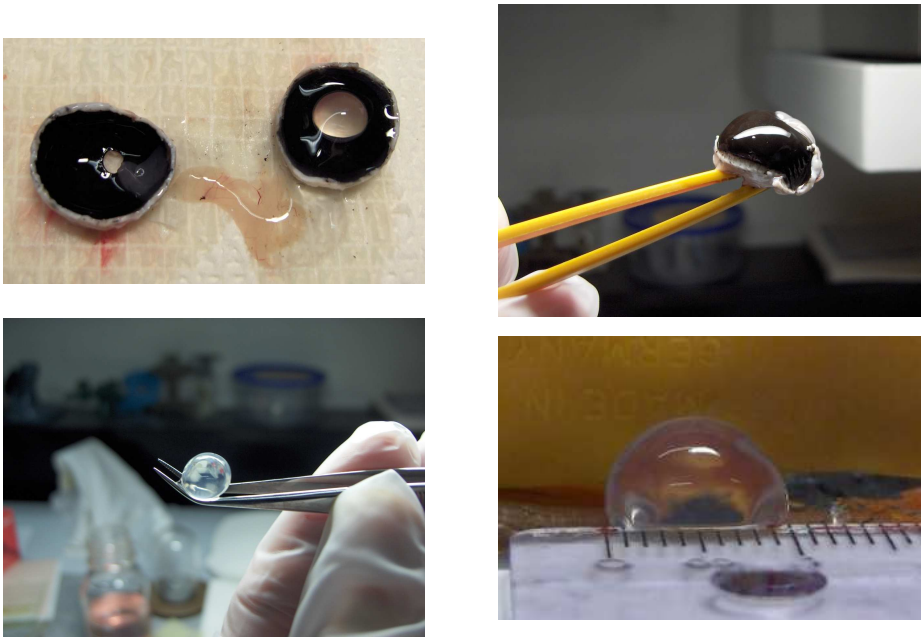

Figure C.1: *Some additional pictures of a dissected pigs eye. See discussion in section 4.2 page 42.* **Top left:** *An eye cut in halves. Posterior part left: The hole where the optical nerve enters the eye is seen on the posterior part, slightly offset from the optical axis towards the nose side. The thickness of the sclera is clearly seen. It is about 1-2 mm thick. The retina is the grey sheet between the halves. It seems more attached to the vitreous body (the gel-like substance on the tissue paper), than to the RPE. Anterior part right: The lens is still in place and its clarity can be seen. From an eye cut in half like this the lens may be easily removed by grabbing around and behind it with a pair of tweezers and gently pulling it free.* **Top right:** *The RPE.* **Bottom left:** *The lens seen in light. It has started to get hazy, which it does quickly after being extracted from the protective surroundings of the eye.* **Bottom right:** *The lens seen from the side. It is lens-shaped but gravity flattens it.*

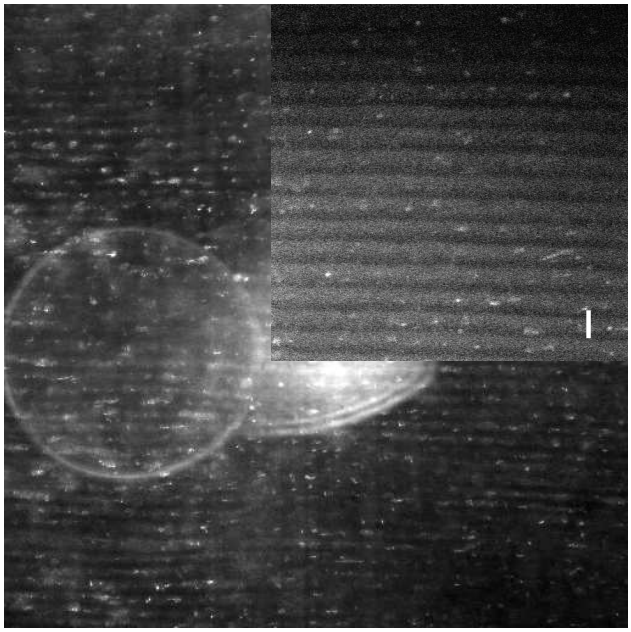

Figure C.2: *Images of lens fibres. The large picture is in reflection mode, while the insert is fluorescence mode. Depth is about 100 μm into the lens. The side length on the large image is 350 μm while the white bar on the inserted image is approximately 10 μm. The large circular reflections seen in the reflection image were internal reflections in the microscope that could not be removed. Laser wavelength was 760 nm.*

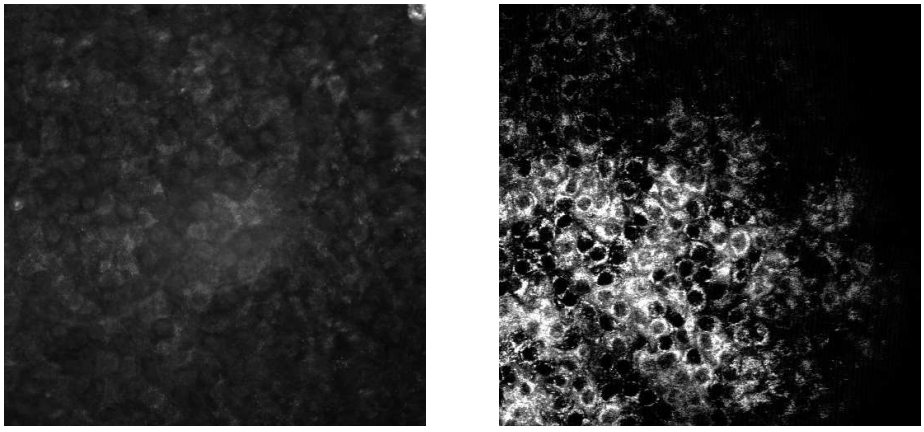

Figure C.3: *Images of the lens epithelium. See discussion in section 4.2.1 on page 43.* **Left:** *A reflection image of the lens epithelium. Laser wavelength is 760 nm. The cells are clearly very different from the deeper lens fibres – much more cell like. The contours of the cells are clearly seen but details in the cells are not distinguishable.* **Right:** *Fluorescence image of the same area as left image. Fluorescence is seen to be strong from the intra-cellular fluid, while the nuclei of the cells do not give any fluorescence signal at all. Compared to the left picture this image shows the strength of fluorescence imaging – details in the cells are showing up nicely (the intra-cellular fluid being clearly distinguishable from the nuclei).*

Appendix D

Preparation of glycated lysine

D-Glucose (Sigma-Aldrich G8270) and L-Lysine (Sigma-Aldrich L5501) were acquired together with sterilised water, borate buffer pH 9, and phosphate buffer 1/15 M pH 7 (all Bie-Berntsen).

As only small amounts of the sample is used per experiment, it is easiest to make a base solution and from this make the final samples.

10 ml base solution may be made as 0.5 M in strength in both components in the following way. 9.5 ml of the chosen buffer (borate, water or phosphate) in a glass jar. The molar weight of D-Glucose is 180.02 g/mole and 146.19 g/mole for L-Lysine, so 0.90 g of D-Glucose is measured off and added to the buffer under relaxed stirring and heating at 50 C to ease dissolution. To this is added 0.73 g of L-Lysine. When both components are completely dissolved the solution is transferred to a cylindrical 10 cc measurement glass, and additional buffer is added until the volume is exactly 10 ml. This is the base solution, and it may now be poured into a container of choice (Blue-cap bottle, baked at 138 C for 4 hours for sterilisation) for storage. The solution may be stored cold (5 C) for prolonged periods as the reaction is negligible a little below room temperature.

To make a 0.1 M glucose/lysine solution 1 part of base solution and 4 parts of buffer are added in a suitable, oven proof container – such as a bluecap bottle. This may now be incubated at the desired time and temperature.

The finished, browned solution is optically very dense, and depending on the purpose of it, it is in general necessary to dilute it further before the measurement/experiment. For this distilled water was generally used.

Appendix E

Gels and browned porcine collagen

In this appendix chapter results are presented regarding browning of porcine collagen, and regarding the possible use of gelling agents for creating a gel with low enough diffusion to allow two-photon excited bleaching of gel samples.

E.1 Browned porcine collagen "Husblas"

To make a stable gel-like model one possibility could be to attempt to brown an already gelling protein-based agent. One such is a household gelling agent sold under the name of "Husblas" (Coop, Denmark). It is based on porcine boiled-off carcasses and hides, and mainly contains collagen. In this section is presented additional results obtained on browning of "Husblas". More comments are given in section 7.2.1 page 94.

E.1.1 Preparation of samples and results

Mixing of 2 grams of Husblas swollen with distilled water, 1 gram of D-Glucose with 10 ml of (borate) buffer – pH 9. Initial testing showed that reaction speed was considerably higher using borate buffer pH 9 rather than phosphate buffer pH 7. After preparation the sample was placed in the oven at 65 C. After incubation for 24 hours the temperature was increased to 75 C to speed up the reaction. After 10 days at 75 C the temperature was turned down to 45 C, in order to slow the reaction down. Hereafter no further change was seen for the samples. After the browning had taken place, the samples could not gellify on their own, the consistency was fully liquid even at 5 C.

A comparison between glucated lysine and the prepared glucated porcine collagen is shown in figure E.1. As seen in the comparison the transmission spectra of glucated lysine and glucated husblas are very comparable. As expected, as likely the reactions are closely similar – in husblas likely glucose reacts with amino acid – such as lysine – residues creating same (intermediate) reaction products as the glucated lysine. Encouraged by this a stronger (in husblas) mixture was made to see if this would gellify post incubation. For this purpose 2.5 grams of D-Glucose was mixed in 50 ml borate buffer pH 9 with

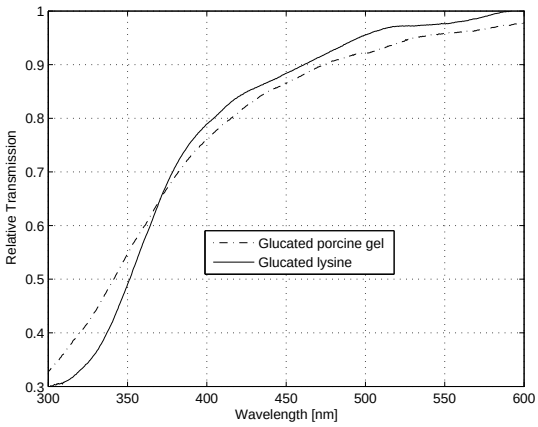

Figure E.1: *Glucated porcine gel, diluted 1+99 before measurement. For comparison is shown standard glucated lysine, this particular sample 0.2 M/0.2M glucose/lysine incubated at 55 C for 72 hours, diluted 1+99 before measurement. It is thus seen that the spectra are quite alike.*

5 grams of (dry) porcine collagen gel. This was incubated for 8 days at 75 C. The sample turned nicely dark brown, but could post incubation not form gel at room temperature. Either the heated incubation or the reaction responsible for the browning in addition also destroys the ability to form gel.

E.1.2 Summary on browned porcine gel

It was shown that of porcine collagen-based gelling agent by incubating with sugar at elevated temperatures produced transmission spectra similar to spectra of glucated lysine. Unfortunately even at high concentrations of husblas it was not able to gellify following incubation and browning. No further investigation was done.

E.2 Gelling of samples

To make a lasting macroscopic two-photon bleaching of a sample it was necessary either to bleach a very long time or a very small volume, due to the slow process of TPE bleaching. One method of limiting the amount of chromophores is to fix them, to inhibit diffusion. Thereby the bleached area could stand out from the non-bleached surrounding. This mainly for using as a technology demonstrator. Testing a household porcine collagen-based gelling agent ("Husblas", Coop, Denmark) and a gelling agent for making microbiological substrates ("Phytagel", Sigma-Aldrich, Germany) it was found the latter produced the hardest, "dryest" gel. A sample was prepared by heating a few millilitres of glucated lysine and under rapid stirring mixing in a few mg of Phytagel (the manufacturer recommends to use $\sim$ 10 g/l). A few drops of this was transferred to a microscope slide, and another slide was place over it and the slides pressed lightly together. The gel solidified almost immediately when taken off heating. A layer of $\sim$ 0.6 mm in thickness was created. This was subsequently bleached by SPE bleaching. A femtosecond laser doubled to 400 nm was used for the bleaching. A mechanical stage scanned the laser along a line of $\sim$ 9 mm. The UV power was 40 mW and scan time was 105 minutes. The resulting bleaching is shown in figure E.2.

Figure E.2: *Bleaching of gellified sample. The bleached area is visible on the centre-right of the image. The 400 nm beam for bleaching was approximately 1 mm in diameter, and the scanned length was 9 mm. On the sample the bleached area is approximately 2 mm wide and 10 mm long, the widening of the area is due to diffusion of the chromophores. The scanning was done in the afternoon, and next morning the diffusion had completely wiped out the bleached area.*

The bleached area is vaguely visible, in effect a much larger area is bleached than just where the beam is scanning due to diffusion. Diffusion rapidly wipes out any traces of visible bleaching. This effectively shows that if any bleaching of a macroscopic area is to be visualised the chromophores need to have very low diffusion – especially with TPE bleaching.

Appendix F

Code

```
PROGRAM bleaching

IMPLICIT NONE

REAL,PARAMETER :: C0 = 27.1e17          !chromophores in the sample initially, cm^-3
REAL,PARAMETER :: Cend = 14.9e17        !chromophores in the sample after bleaching,
                                        !calculated by measured absorption before/after, cm^-3
REAL,PARAMETER :: Power0 = 21.9e-3      !power before first interface, WITH correction
                                        !for blue pass filter (0.75), in W (J/s)
REAL,PARAMETER :: Absrho = 1.50e-19     !cross section for absorption in the sample, cm^-2
REAL,PARAMETER :: vol = 1.35            !bleached sample volume in cm^3
REAL,PARAMETER :: Lenght = 1.0          !cuvette path length, in cm
REAL,PARAMETER :: Mirror = 0.94         !reflection coefficient of 2nd passing mirror
REAL,PARAMETER :: Lambda = 392e-9       !wavelength in m to calculate photon numbers
INTEGER,PARAMETER :: Time = 90          !exposure time in minutes
REAL,PARAMETER :: InterLoss = 0.055     !Estimate for reflection loss at AIR->CUVETTE
                                        !interfaces, 0.03 for macro 0.055 for semi-micro
REAL,PARAMETER :: h = 6.626068e-34      !plancks constant, m^2*kg/s
REAL,PARAMETER :: Light0 = 299792458.0  !speed of light, m/s

INTEGER :: x, i, select, steps,y

REAL :: absco,C,Pin,Iloss,abs1st,Cold
REAL :: abs2nd,bleach,abstot
REAL :: k,kold,ktemp            !k is the quantum efficiency for bleaching, to be guessed


steps = Time*60                         !Steps is the stepping, same as exposure time in seconds

Pin = (Power0)*(Lambda/(h*Light0))*(1.0-Interloss)      !Photon flow at cuvette sample interface
print *,'Pin', Pin

Iloss = (1.0-Interloss)*Mirror*(1.0-Interloss)              !Loss for 2nd passing light
k = ((C0-Cend)*vol)/((1-exp(-Lenght*Absrho*C0))*Pin*steps)  !Initial guess for quantum efficiency

print *, 'k guess', k
print *, 'abs ini', 1-exp(-Lenght*Absrho*C0)

kold = 0.0
ktemp = k
select = 6              !Default case is exit

i=1
```

```
DO                                  !Driver routine, contains time stepping loop
                                    !and updates of quantum efficiency
    C=C0

    DO x=1,steps                                !Time stepping loop

        absco = 1-exp(-Lenght*Absrho*C)         !The absorption in a single pass

        abs1st = Pin*absco                      !Absorbed flux in 1st pass
        abs2nd = (Pin-abs1st)*Iloss*absco       !Absorbed flux in 2nd pass
        abstot = abs1st+abs2nd                  !Absorbed total flux

        bleach = abstot*k/vol                   !The bleached chomophores
        C = C-bleach                            !Updating non-bleached chromophore amount

    END DO

print *, 'k=',k,'','C=',C

    IF (ABS(C-Cend).LT.((1.0/1000000.0)*Cend)) EXIT !If precision reached -> exit

    IF ((C-Cend).LT.(0.0)) select=1     !C < target, quantum efficiency too big
    IF ((C-Cend).GT.(0.0)) select=3     !C > target, quantum efficiency too small

    SELECT CASE (select)                        !Select case

        CASE(1)
        k=k-(ABS((C-Cend)/(Cold-C))*ABS(k-kold))    !Reduce quantum efficiency

        CASE(3)
        k=k+(ABS((C-Cend)/(Cold-C))*ABS(k-kold))    !Increase quantum efficiency

        CASE(6)                                     !In case of failure then exit
        print *, 'failed'
        EXIT

    END SELECT

    Cold=C              !Update Cold (previous C value)
    kold=ktemp          !Update kold (previous quantum efficiency value)
    ktemp=k

    i = i+1                 !update counter

    IF (i==50)  EXIT        !Check counter, to avoid runaway loop

END DO

print *, 'k',k
print *, 'kold',kold
print *, 'C',C
print *, 'C-Cend',C-Cend
print *, 'ABS(C-Cend)/Cend',ABS(C-Cend)/Cend
print *, 'iterations',i
print *, 'abs end',(1-exp(-Lenght*Absrho*C))

STOP

END PROGRAM bleaching
```

Appendix G

Articles and conference submissions

In total five papers were produced on results obtained in the course of this project. These include three conference contribution and one article covering results regarding the use of BiBO as non-linear medium for intra-cavity doubling of Ti:Sapphire lasers. In addition one conference contribution was produced based on results and ideas in the field of intra-ocular fluorescence detection. Hereunder brief description of the papers and abstracts presented. Figures in abstracts have not been included here. Posters (for poster presentation), and articles (for journal submissions) are enclosed at the end of the report.

Journal submissions

- **Tunable intra-cavity SHG of CW Ti:Sapphire lasers around 785 nm and 810 nm in BiBO-crystals**
  M. Thorhauge, J.L. Mortensen, P. Tidemand-Lichtenberg, P. Buchhave
  Optics Express, Vol. 14, pp. 2283-2288, 2006

  Abstract: Phase match curves as well as sensitivity to angular and wavelength misalignment for second-harmonic generation of 785 nm and 810 nm respectively in BiB_3O_6 crystal was calculated. Measurements were done for intra-cavity CW SHG in a Ti:Sapphire laser. The BiBO crystal was found to be excellent for this application. Temperature dependance was found to be low for both crystals, while power stability was good. Maximum blue output was found to be 53 mW at 392 nm and 100 mW at 405 nm; corresponding to pump-to-blue optical conversion efficiencies of 0.96% and 1.82% respectively.
  (Full article enclosed after the end of this thesis.)

Conference contributions

- **Measurement of two-photon excited fluorescens from Glycated Lysine compounds**
  M. Thorhauge, M. Larsen, L. Kessel, P. Tidemand-Lichtenberg, L. B.-Å. Johansson, et.al.
  SPO 2004, paper BO14, October 30, Kiev, Ukraine, October 28-31, 2004

Abstract: Two-photon excitation fluorescence (TPEF) offers several advantages compared to single-photon excitation when dealing with biological samples. Phototoxicity is lowered, penetration depth in tissue may be better, and resolution may be higher. One place where utilising two-photon excited fluorescence may be of interest is in the human eye. As the body ages several processes may take place in the lens of the eye, which may degrade its visual performance. One of the most widespread conditions amongst elder people is an accumulation of brown fluorophores in the lens – known as Cataract. In order to get a better understanding of the development of Cataract, it is of interest to be able to map the fluorescence from the lens in vivo with good resolution in all three dimensions. In order to evaluate assays useable designing and testing a system capable of 3D mapping of the fluorescence of the eye, we have studied two-photon excited fluorescence from Glycated Lysine compounds. These compounds are quite similar to the browning products found in human lens, and thus may be used as an efficient and realistic assay. We have measured TPEF spectra and compared these with single-photon spectra. An estimate over quantum efficiency of the process is given. In addition, we have compared with fluorescence spectra from cataractous human lenses.

- **Intracavity doubling of CW Ti:Sapphire laser to 392.5 nm using BiBO-crystal**
  P. Tidemand-Lichtenberg, M. Thorhauge, J.L. Mortensen, P. Buchhave
  CLEO/Europe-EQEC 2005, poster CD-25-MON, June 12, Munich, Germany, June 12-17, 2005

  Abstract: We present results on novel intracavity doubling of CW Ti:Sapphire laser to 392.5 nm utilising BiBO non-linear crystal. Maximum blue power of 6mW at 5W 532nm pump is achieved. Means to improve this are discussed.
  (Full abstract and presented poster enclosed after the end of this report.)

- **Intracavity frequency doubling of CW Ti:Sapphire laser utilising BiBO nonlinear crystal**
  M. Thorhauge, J.L. Mortensen, P. Tidemand-Lichtenberg, P. Buchhave, J.R. Rasmussen
  ASSP 2006, poster MB19, January 3, Incline Village, Nevada, USA, January 29- February 1, 2006

  Abstract: Utilising BiBO nonlinear crystal frequency doubling a Ti:Sapphire CW laser gave 100 mW at 405 nm and 53 mW at 392 nm. Stability proved excellent without servo control. Broad tunability was shown around 392 nm.
  (Full conference submission enclosed after the end of this thesis.)

- **100 mW of blue light at 405 nm from intracavity doubling of CW Ti:Sapphire laser utilising BiBO-crystal**
  M. Thorhauge, J.L. Mortensen, P. Tidemand-Lichtenberg, P. Buchhave, J.R. Rasmussen
  Poster presentation Photonics Europe 2006
  Solid State Lasers and Amplifiers II, Ed. A. Sennaroglu, Proceedings of the SPIE, Vol. 6190, pp. 117-127, 2006

  Abstract: Utilising BiBO non-linear crystal frequency-doubling a Ti:Sapphire CW laser gave 100.4 mW at 405 nm. Stability proved excellent without servo control of the cavity. Temperature dependence was non-critical.
  (Full conference submission enclosed after the end of this thesis.)